5-2017

Characterizing Light Output Variations from Solid State Lighting Due to High Frequency Electromagnetic Interference

Gaurav Singh
Clemson University, gauravs@clemson.edu

Characterizing light output variations from solid state lighting due to high frequency electromagnetic interference

---

A Dissertation
Presented to
the Graduate School of
Clemson University

In Partial Fulfillment
of the Requirements for the Degree
Doctor of Philosophy
Electrical Engineering

---

by
Gaurav Singh
May 2016

Accepted by:
Dr. Edward R. Collins Jr., Committee Chair
Dr. Elham Makram
Dr. Richard Groff
Dr. Pierluigi Pisu
Dr. Math H. J. Bollen (Honorary)

Abstract

Consumer electronic devices employing active power electronic switching have been increasingly used in the last decade. With the rise in number of these devices, the emission of harmonic currents by these devices has changed both in magnitude and character. The effects of harmonic frequencies up to 2000 Hz on various electrical and electronic devices has been the subject of considerable scrutiny over the past decade. However, newer consumer devices employ switched mode power electronic circuits that switch in the multiple kilohertz range. The emission from these devices, along with power line communication, are sources of high frequency currents in the range of 2 to 150 kHz. As a result, there has been an appreciable rise in the amount of conducted emission in the frequency range 2 to 150 kHz.

One of the important outcomes of rising emission in this frequency range is that there have been reported cases of interference with various consumer electronic devices. Among the devices in which interference has been reported are the new generation of solid state LED lamps which have become popular in the last 3-5 years. Considerable research has been done in the past about the effects of light flicker and the modulation of light output from incandescent lamps, on human beings. However, the utilization of power electronic converters changes this paradigm considerably. Unlike incandescent bulbs, where low frequency modulation of input voltage resulted in visible flicker, observations and reports have shown that LED lamps may be susceptible to flicker from frequencies above the 2 kHz mark. As a result, old methods of predicting flicker and studying it may no longer be applicable.

This thesis attempts to shorten this gap in knowledge by exploring the topic of LED flicker due to high frequency distortion, and the factors that affect it. This was achieved by exposing LED lamps of various sizes and from various manufacturers, to realistic voltage distortion signals, recorded in the power system. Signals with high-frequency distortion superimposed on to the fundamental,

were used. The test set-up used, allowed for the testing of light equipment with various types and levels of distortion at different points on wave. For the first time, experimental results showed that not only does high frequency voltage distortion cause changes in average value of light output and the modulation of light output, but that this change depends upon the point-on-wave at which the high frequency distortion appears. The mathematical tool of cross-correlation was proposed to quantify the effect of point-on-wave of high frequency distortion on light output. The utilization of this tool showed that LED lamps are susceptible to distortion appearing near the peak or near the zero crossing of the input voltage.

In order to understand the dependence of LED flicker on the topology of the LED driver, five LED driver development boards available commercially were also subjected to the above mentioned high frequency voltage distortion. The results showed that light flicker from LED lamps is not necessarily a by-product of LED driver topology. The utilization of discontinuous conduction mode of operation and an isolation transformer in the LED driver is not sufficient to disconnect the LED load from input voltage variations. LED drivers of the same topology can behave completely different, likely due to the control methodology employed by each manufacturer.

Finally, a simulation model of a popular LED driver solution: a flyback DC-DC converter with primary side regulation was developed to verify the experimental results and perform root cause analysis for the observed phenomena. Changes in control methodology and circuit design were suggested to overcome this flicker problem and evidence of the degradation of circuit components due to excess heat generated by high frequency distortion was shown.

Dedication

This work is dedicated to my parents and my sister. Your unwavering support and belief in me is the reason this moment came to fruition. As I take this step, I realize that it was never about me, but always about your lifelong sacrifices.

Acknowledgments

The majority of this work was funded by the Swedish Energy Agency. The financial support is greatly appreciated. Many thanks to Luleå University of Technology, Sweden for allowing me this once in a lifetime opportunity to explore the beautiful nation of Sweden and for the warm hospitality extended to me throughout my stay.

A project of this magnitude always has more than a few active parts. My sincerest thanks to Sarah Rönnberg and Anders Larsson. In you, I found two understanding mentors and amazing friends. Thank you for teaching me the virtues of patience during research. The lab experiments could not have been possible without Mikael Byström's expertise and direction.

Friends always form the support system when one is away from home. This work was carried out on two continents and I have had the privilege of getting to know some truly amazing people. My friends from Clemson, Shawn Ballenger, Harkaran Grewal and Matt Pepper have been my support system and my family since the day I arrived in Clemson six years ago. My stay in Sweden provided me the good fortune of getting to explore a new culture. Special thanks to John Laury, Manuel Alvarez, Daphne Schwanz and Anu Tiilikainen for being the shining light in a sometimes dark period of my life. Djordje Popovic and Benedikt Neyses: words cannot describe how much I love and appreciate you. Thank you for being there when I needed you the most. I may not be the best human being but I can surely say I have the best friends.

Finally, the biggest debt of gratitude is owed to two special human beings. Dr. Randy Collins has been nothing short of a father figure to me. Thank you for putting your faith in me and giving me the opportunities that you did. Many thanks to Dr. Math Bollen for teaching me what professionalism in engineering is all about. You two are my biggest influences and I owe this all to you. Hopefully, one day I will be able to become half as good an engineer as you are.

Table of Contents

Title Page . . . . . **i**

Abstract . . . . . **ii**

Dedication . . . . . **iv**

Acknowledgments . . . . . **v**

List of Tables . . . . . **viii**

List of Figures . . . . . **ix**

1 Introduction **1**
1.1 Supraharmonics 1
1.2 Solid state lighting 3
1.3 Supraharmonics and LED lamps 4

2 Existing immunity standards **9**
2.1 IEC $61000-4-19$ 9
2.2 Limitations of the standard 14
2.3 Other proposed immunity limits 15
2.4 Methodology used in the thesis 18

3 Field Measurements on LED lamps **20**
3.1 Measurement Technique 20
3.2 Measurement Results 23
3.3 Measurement Sites 27
3.4 Measurement at site 6 with light immunity problem 40
3.5 Conclusions from measurements 47

4 Interference with LED lamps **48**
4.1 High frequency distortion 48
4.2 Experimental setup and measurement apparatus 51
4.3 Illuminance measurements 53
4.4 Results of light measurement 54
4.5 Effects on LED lamp input current 65
4.6 LED lamps and Photometric flicker 67
4.7 Interference with dimmers 77

5 Factors that affect interference **80**
5.1 Point-on-wave of high frequency distortion 80
5.2 Importance of the cross-correlation operator 93

5.3 Impact of converter topology 94
5.4 Discussion of experiments 99

6 Simulation results 101
6.1 The theory of LED drivers 102
6.2 The Flyback converter 104
6.3 Flyback converter implementation and control 109
6.4 Software simulation of a Flyback converter with PSR 112
6.5 Simulation Results 115

7 Conclusions and Discussion 125
7.1 Main findings and discussion 125
7.2 Future work 127

Appendices 128
A Relevant data of LED lamps tested 129
B Nameplate data of LED drivers tested 130
C Load used with LED driver boards 131

Bibliography 132

List of Tables

2.1 Prescribed test voltage levels for differential mode testing 11

3.1 Parameters from voltage waveform 44

4.1 Average light output from lamp 8 in the three operating conditions 58
4.2 Modulation of light output in the three operating conditions 61
4.3 Effect of high frequency distortion on the average light output 66

List of Figures

1.1 High frequency current measured at three individual CFLs 2
1.2 Input voltage (left) and input current (right) at the terminals of an LED lamp . . . 5

2.1 Voltage test levels prescribed by IEC $61000-4-19$ [1]. 12
2.2 Test method 1. 12
2.3 Test method 2. 13
2.4 Schematic layout of the CDN. 14
2.5 Voltage characteristics for narrow-band signals 17
2.6 Emission limits for broadband signals 18

3.1 Voltage (blue) and current (green) waveforms drawn by lamp A 24
3.2 Voltage (blue) and current (green) waveforms drawn by lamp B 25
3.3 Voltage (blue) and current (green) waveforms drawn by lamp C 26
3.4 Voltage (blue) and current (green) waveforms drawn by lamp D 27
3.5 Current waveform (upper) and filtered current waveform (lower) for lamp A 28
3.6 Current waveform (upper) and filtered current waveform (lower) for lamp B 29
3.7 Current waveform (upper) and filtered current waveform (lower) for lamp C 30
3.8 Current waveform (upper) and filtered current waveform (lower) for lamp D 31
3.9 Harmonic spectra of the current waveform of each lamp up to 9 kHz. 32
3.10 Resulting spectra of the current waveform between $9-150$ kHz for each lamp 32
3.11 Voltage and current waveforms from lamp 1 at sites $1-5$ 33
3.12 Current waveform and filtered current waveform from each site with Lamp A 34
3.13 Spectrogram of the current drawn by Lamp A at the different sites. 36
3.14 Voltage spectra variation over time from 2 to 150 kHz 37
3.15 99% value of the background distortion at the four different sites 37
3.16 Average value of the background distortion at the four different sites 38
3.17 Variation in VTHD (upper) and ITHD (lower) over the 31 hour period 39
3.18 Harmonic spectra of the voltage (left) and current (right) 40
3.19 Voltage (upper) and current (lower) spectra over time 41
3.20 Voltage (upper) and current (lower) spectra over time 42
3.21 Schematic layout of the electrical system in the office building. 43
3.22 Voltage waveform at the connection point of a fluorescent lamp 44
3.23 Harmonic spectra before (blue) and after (red) busbar R1 was disconnected 45
3.24 Voltage and current waveform at bus-bar when running on backup generator 46

4.1 High frequency distortion test signal 1 (top) 49
4.2 High frequency distortion test signal 2 50
4.3 Laboratory setup for testing light equipment 52
4.4 Illuminance plotted against time for a 100 W incandescent lamp 55
4.5 Illuminance plotted against time for lamp 8 56
4.6 Illuminance plotted against time for lamp 24 57

4.7 Illuminance plotted against time for lamp 27 . . . 58
4.8 Spectrum of light output for lamp 8, lamp 24, lamp 27 and 100 W incandescent . . . 59
4.9 Spectrum of light output from lamp 8 in three cases . . . 59
4.10 Spectrum of light output from lamp 24 in three cases . . . 60
4.11 Spectrum of light output from lamp 27 in three cases . . . 60
4.12 Light output recorded over 30 s for lamp 8 . . . 62
4.13 Average light output recorded over 30 s for lamp 8 . . . 62
4.14 Light output recorded over 30 s for lamp 24 . . . 63
4.15 Average light output recorded over 30 s for lamp 24 . . . 63
4.16 Light output recorded over 30 s for lamp 27 . . . 64
4.17 Average light output recorded over 30 s for lamp 27 . . . 64
4.18 Input current plotted as a function of time for LED lamp 24 . . . 67
4.19 Single cycle of light output from lamp 24 . . . 70
4.20 Percent flicker and flicker index from lamp 8 . . . 71
4.21 Percent flicker and flicker index from lamp 24 . . . 71
4.22 LED lamp output light RF plotted as a function of input current THD . . . 74
4.23 LED lamp 2 output light RF plotted as a function of input current THD . . . 75
4.24 LED lamp 3 output light RF plotted as a function of input current THD . . . 76
4.25 LED lamp 4 output light RF plotted as a function of input current THD . . . 77
4.26 Schematic layout of a typical triac dimmer. . . . 78
4.27 LED input voltage with dimmer present in the circuit . . . 79

5.1 Voltage and current signal recorded at the terminals of a smart energy meter . . . 82
5.2 Quantification of point-on-wave . . . 84
5.3 Light modulation (top) and average light output (bottom) from lamp 8 . . . 86
5.4 One cycle of source voltage, LED input current and light output for lamp 24 . . . 87
5.5 Variation of light output, as a function of the point-on-wave for lamp 8 . . . 88
5.6 Variation of light output, as a function of the point-on-wave for lamp 31 . . . 89
5.7 Variation of light output, as a function of the point-on-wave for lamp 19 . . . 91
5.8 Variation of light output, as a function of the point-on-wave for lamp 27 . . . 92
5.9 LED lamp current plotted against input voltage . . . 93
5.10 Average light output and light modulation for LED driver board 1 . . . 95
5.11 Average light output and light modulation for LED driver board 3 . . . 96
5.12 Average light output and light modulation for LED driver board 4 . . . 97
5.13 Input voltage and output current for LED driver board 5 . . . 97
5.14 Output current for LED driver board 3 . . . 98
5.15 Output current for LED driver board 4 . . . 99
5.16 Output current for LED driver board 5 . . . 100

6.1 Block diagram of an LED driver . . . 102
6.2 Source voltage and input current waveforms for 4 lamps . . . 102
6.3 Basic diagram of a Flyback converter . . . 105
6.4 Primary and secondary currents in DCM . . . 107
6.5 Block diagram of flyback converter with PSR . . . 110
6.6 Input and Output signal values from a PSR implementation. . . . 113
6.7 Schematic layout of PSpice simulation . . . 114
6.8 Flowchart for PWM mechanism in simulation . . . 115
6.9 Output current from the simulated LED driver . . . 116
6.10 Light output from lamp 8 under different voltage conditions . . . 117
6.11 Primary and secondary currents from simulation . . . 118
6.12 Spectrum of primary currents from simulation . . . 119

6.13 Spectrum of secondary currents from simulation 119
6.14 Rectified voltage from simulation 121
6.15 Instantaneous power dissipated in the capacitor from simulation 122

Chapter 1

Introduction

During the past decade, consumer electronic devices employing active power electronic switching (as compared to "passive switching" mainly in diode rectifiers) have become commonplace. As power electronic circuits continue to evolve, the frequencies being emitted by these devices have increased as well. While passive rectifier front ends are responsible for generating frequency distortion in the lower frequency range up to 2 kHz, newer active power conditioning circuits cause distortion in the multiple kilohertz range [2–4].

1.1 Supraharmonics

Extensive measurements done on common household equipment over the last decade show that many devices on the market inject emission in the frequency range 2 to 150 kHz (also referred to as 'Supraharmonics' in literature) [2, 3, 5–9]. This emission contains remnants from the switching of power-electronic converters and short-duration oscillations that occur around the zero-crossing of the current waveform. Switched mode power electronic devices, operating at switching frequencies in this frequency region are ubiquitous, being present in devices such as computer power supplies, LED lamps and battery chargers. The increasing popularity of electric vehicles threatens to only increase emission in this frequency range in the future when their chargers utilize high frequency power electronic converters. In addition to the emission from end-user equipment, the frequency band above 2 kHz is also used for signaling purposes (power line communication) [10]. Measurements as well as simulations have shown that the total emission from an installation, for frequencies above

a few kilohertz, can be much less in magnitude than the sum of the emission from the individual devices [6]. Emission between 2 and 150 kHz tends to flow in between neighboring devices to a much greater extent than emission at lower frequencies [11]. This is illustrated in Figure 1.1 where the current spectra measured at three individual Compact Fluoroscent Lamps (CFL) are shown (upper right, lower left and lower right) together with a measurement of the combined current taken by all three lamps (upper left) measured at the delivery point to the house [11].

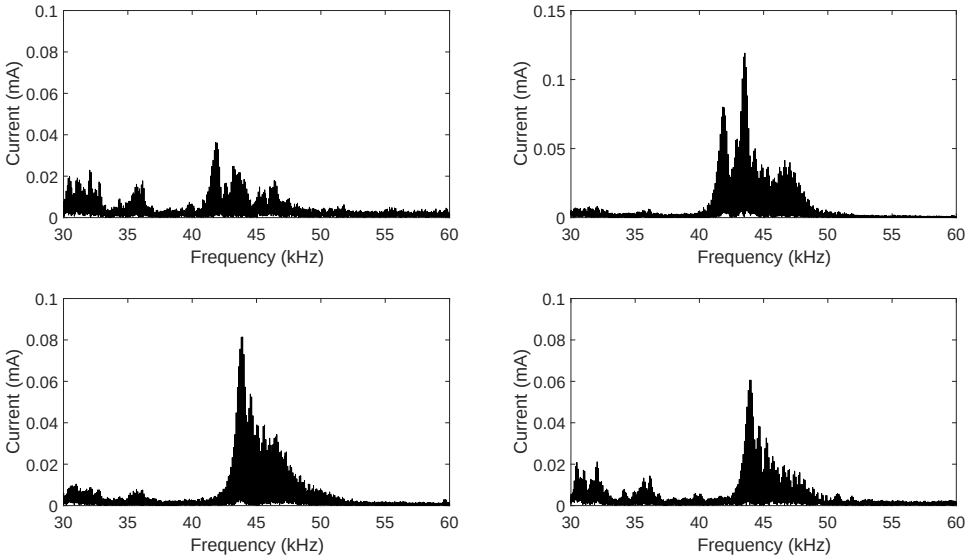

Figure 1.1: High frequency current measured at three individual CFLs (upper right, lower left and lower right) and the combined current taken by all three lamps (upper left). Fundamental current drawn by each lamp was approximately 52 mA. Total current drawn by the combination was 156 mA [6]

The switching frequency of the lamps lies in the range 40 kHz and 50 kHz. As more lamps are added the absolute amplitude (in milliAmpere) of the components between 40 kHz and 50 kHz at the delivery point drops. At the same time the amplitude of the high frequency current measured at each individual lamp increases. This shows that propagation of emission in this frequency range is significantly different compared to propagation of the emission below 2 kHz. How the emission will propagate will depend on both the grid impedance and the impedance of neighboring devices. In low-voltage installations, the capacitance and inductance of those devices is also expected to play an important role and resonances are likely to have a significant impact as shown in [12] where a resonance between a TV and a photovoltaic (PV) inverter is discussed. Connecting or disconnecting,

or even moving a single device to a different outlet, can change the resonant frequency and therewith the propagation and magnitude of the emission.

One of the important outcomes of rising voltage distortion in the frequency range 2 to 150 kHz is that there have been reported cases of interference with other consumer electronic devices, including the newer generation of solid state LED lamps, with reported cases of lamp failure and flicker [13].

1.2 Solid state lighting

According to the International Energy Agency (IEA), lighting accounts for about 20% of the energy consumption in the world (approximately 7 EJ in 2013). The traditional incandescent lamp converts only about 5% of the input electrical energy into light. One of the recommendations of the IEA in this regard, to achieve energy efficiency in lighting is to switch over to energy efficient lighting 'as soon as technically feasible and economically viable'. This need to achieve higher energy efficiency has led to tighter regulations being imposed on incandescent lamps all over the world. In the United States, the state of California will phase out the use of these lamps by 2018 and in the states of Connecticut and New Jersey, similar legislation has been proposed. In the case of California, the same bill plans to establish a minimum standard efficiency for lamps of about 60 lumens per watt (lm/ W). In 2007, federal legislation was introduced as a part of the 'Energy Independence and Security Act' which set maximum wattage requirements for all incandescent lamps producing 310 to 2600 lm of light. This effectively banned importing or manufacturing of most incandescent lamps. It was proposed to introduce another set of regulations, which would become effective in 2020 and require all general purpose lamps to produce at least 45 lm/ W.

Another solution to replace energy inefficient lighting is the advent of energy efficient light emitting diode (LED) lamps. The application of LED lamps for lighting is rather new. As late as 2010, LED lamps made up only 0.2% of residential lighting and 1.8% of lighting in commercial applications (source: statista). However, the development of semiconductor technology continues to change this statistic year after year. Since 2010, the efficiency of LED lamps has increased and their cost has reduced dramatically. Similar to Moore's law (1965), which predicted that the performance of microprocessors would double every two years, the performance of LED lights has been following the so called 'Haitz's law' [14, 15]. It states that the luminous output of individual LED devices is

increasing at a compund rate of 35% per year and that the cost per lumen is decreasing at 20% per year. Just to put the statistics into perspective, LED lamp manufacturers are already claiming efficiencies as high as $100 - 110\,\mathrm{lm/W}$ and lifetimes of $15 - 20$ years [16]. This high efficiency, long life and ever decreasing cost make LED lamps an attractive alternative to both incandescent lamps and CFLs. LED lamps are certainly becoming popular in domestic and commercial applications. In 2013, 19 million of the 140 million streetlights installed were LED lamps. The LED lamp market is projected to grow by more than twelve-fold over the next decade, from $2 billion in the beginning of 2014 to $25 billion in 2023, a compound annual growth rate (CAGR) of 25% [17].

Although LED lamps have a comparatively higher price (compared to CFLs and incandescent bulbs) at the given moment, the higher efficiency of these devices leads to savings in terms of energy consumption and studies have shown that the cost of operating a domestic lighting system with LED lamps is about a quarter of operating the same system with incandescent lamps and about two thirds of operating the system with CFLs [18].

1.3 Supraharmonics and LED lamps

Cases of interference with solid state lighting from supraharmonics have been reported in the United States and Europe. A recent study in the US done by Duke Energy demonstrates a case of LED lamp flicker observed by a medium sized commercial customer. Voltage and current data recorded at the customer end show the presence of high frequency distortion and notches in the input voltage. A sample of the voltage and current is shown in Figure 1.2. The voltage distortion shows frequencies between 5 and 10 kHz with peak amplitudes as high as 30 V. As can be seen by careful inspection of Figure 1.2, this distortion changes in frequency from cycle to cycle and sometimes even during the same cycle. Further, it was observed that the distortion was not entirely synchronized with the voltage waveform, and over a course of 5 s the distortion signal changes the point on which it appears on the fundamental wave.

The reported cases of interference and flicker with LED lamps, due to high frequency voltage distortion, motivate studies of the compatibility between these lamps and the grid. LED lamps use power electronic drivers, which can also cause voltage waveform distortion. This has been studied in a lot of papers, both for low-frequency and for high-frequency distortion [19, 20]. The impact of the voltage distortion on the performance of the lamps has however not been systematically studied.

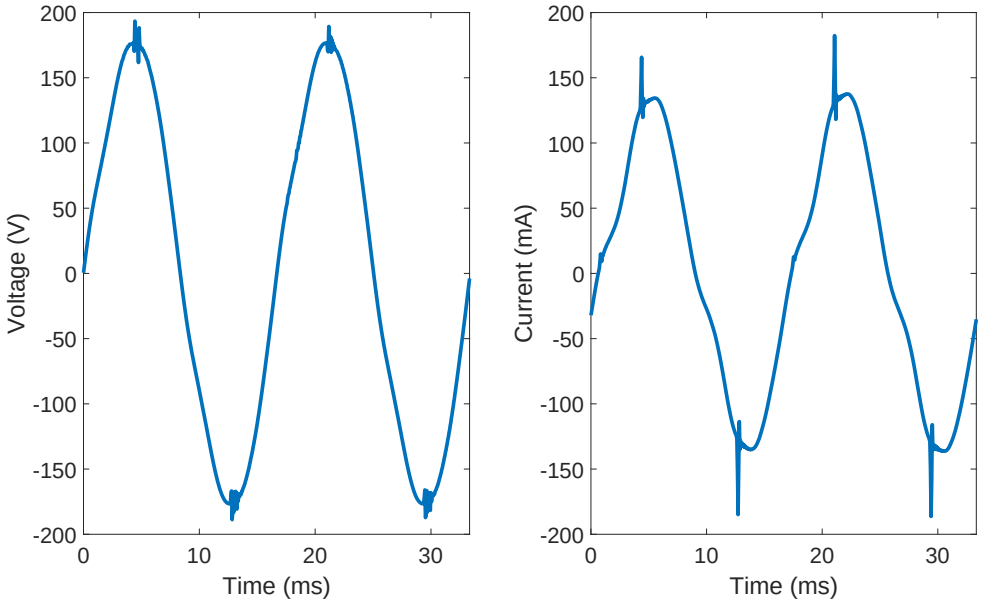

Figure 1.2: Input voltage (left) and input current (right) measured at the terminals of an LED lamp in the field. Data courtesy of Duke Energy

Further, there is a lack of immunity standards and limits regarding illumination equipment in the low harmonic frequency range (50 to 2000 Hz), as well as in the higher range above 2 kHz for conducted disturbances [21].

1.3.1 Scope of the thesis

This thesis focuses on the interference from conducted disturbances (from supraharmonics) with LED lamps and dimmers and in particular on the problem of LED flicker. This thesis is aimed at advancing knowledge of flicker, as is observed in the case of LED lamps. The change in lighting technology also changes the flicker paradigm and the current existing knowledge of interference mechanisms with light producing sources is unable to predict the effects of high frequency distortion (2 to 150 kHz) on LED lamps. This thesis contributes to the knowledge of this field in the following by:

- Subjecting LED lamps to realistic high frequency voltage disturbances found in the power system and showing the effects on light output.
- Reproducing the same results in simulation for a popular LED driver solution and performing

root cause analysis for the flicker mechanism.

Utilizing laboratory experiments, the conditions in the power system were reproduced. The factors that affect flicker from LED lamps were of particular interest. These have been discussed in detail later on in the thesis.

The simulation portion of the work focused on answering the 'how' and 'why' part of this work i.e., the mechanism by which high frequency distortion causes variations in light output was the subject of focus. Although the simulation focused on one particular LED driver type (flyback converter based LED drivers), experiments showed that the buck and buck-boost based drivers have very similar response. Degradation of components has been discussed, but in the absence of special facilities to test temperature changes, these could not be verified empirically. Further, the failure modes of the control system of the LED driver have been discussed but a detailed technical discussion of the improvements that can be made in this regard are considered beyond the scope of this work.

1.3.2 Contributions

The contributions of this thesis can be summarized as follows, where contribution 1 and 2 concern systematic demonstrations of light degradation and/or flicker from LED lamps. Contributions 3 and 4 are related to the factors that affect the light variations. These are intended to be used by standard makers and/or manufacturers to consider while designing standards for immunity testing of these lamps or similar equipment. Contribution 5 is aimed at demonstrating the shortcoming of one particular power electronic control scheme which can lead to flicker from these lamps. The results can be used as a design guideline for future research into LED drivers. Contribution 6 is more of an educational rather than research contribution.

1. The laboratory results show that in the presence of high frequency voltage distortion, LED lamps can produce visible flicker.

2. The empirical evidence shows a new type of interference mechanism. In electrical engineering, flicker typically refers to low frequency input voltage modulation that produces visible flicker, typically from an incandescent bulb. However, the fact that high frequency distortion can also produce the same effect (from an LED lamp) was a hitherto unknown phenomenon. In the case of an LED lamp, this implies that modulation of AC voltage at the input produces DC changes in the output (i.e. light), a completely unexpected result.

3. The results show that the flicker from LED lamps depends upon the point-on-wave of high frequency distortion. In some cases, light output from the LED lamp is sensitive to high frequency distortion appearing near the zero crossings of the fundamental frequency and in some other cases, it is more sensitive to high frequency distortion appearing near the peak of the fundamental frequency.

4. This work demonstrates that LED lamp response to conducted high frequency disturbances is independent of LED driver topology. Similar driver topologies can have completely different response to the same input disturbance. Further, topologies that employ transformers to provide galvanic isolation and use discontinuous conduction mode are not immune to these input voltage changes either.

5. Unlike the electrical engineering definition of flicker, in the domain of lighting the word 'photometric flicker' is used to refer to the 100/120 Hz modulation of light. This work demonstrates that high frequency distortion affects the photometric flicker from LED lamps. Further, the existing flicker metrics date back to the time when this was considered to be a problem associated with incandescent bulbs. This thesis shows that the existing time based methods of flicker quantification are in fact inferior to existing frequency domain methods used in analysis of power electronic circuits. Frequency domain methods give more information to designers for both types of flicker that we talk about. They give information about the spectrum of the electrical flicker and the spectrum of the photometric flicker. The information obtained can thus be translated back to power electronic design and/or control modifications as necessary.

1.3.3 Structure of the thesis

- In chapter 2 the existing immunity standards with regards to high frequency distortion are presented. The limitations of these standards are examined, using field measurements of voltage distortion. Alternative approaches presented in literature have been discussed and the approach used in this thesis has been described.

- In chapter 3 the experimental setup used in this work is described.

- Chapter 4 presents the effects on LED drivers and dimmers, from conducted disturbance due to supraharmonics.

- Chapter 5 discusses the various factors affecting the performance of LED lamps with voltage containing supraharmonics.
- Chapter 6 is devoted to the software simulation setup and results. Details of the converter control are presented, to aid with root cause analysis of the flicker mechanism.
- Chapter 7 is used to discuss the conclusions from the work along with suggestions for future research.

Chapter 2

Existing immunity standards

As consumer electronic devices employing power electronic switching become more popular, the nature of source voltage in distribution systems changes gradually because of the harmonic currents these devices generate. Under such circumstances, it becomes necessary to investigate the immunity of household equipment towards frequencies other than the fundamental. Until about 20 years ago, electrical equipment used to be designed with the basic assumption that the source voltage contains only the fundamental frequency. In recent years, because of the enforcement of harmonic emission standards and stricter regulation with regards to power factor, consumer electronic devices may also carry active power factor correction (APFC) circuits on their front end. However, this is not a universal development and in many countries such as the United States, legacy devices with no power conditioning at the front end continue to be sold [22, 23]. As a result, modern consumer electronic devices are now designed to be immune to lower order harmonic frequencies normally associated with rectifiers. However, the immunity of devices towards frequencies in the higher end of the spectrum 2 to 150 kHz is not normally checked in spite of the fact that there have been reported cases of interference with different types of lamps under different conditions, in the frequency range above 2 kHz [10, 13, 24].

2.1 IEC $61000-4-19$

The existing electrical standard that deals with the subject of device immunity with regards to frequencies in the range 2 to 150 kHz is IEC $61000-4-19$ [1]. This standard describes test

methods to analyze immunity of devices towards high frequency distortion in power supply. So far, almost no commercially available products utilize this standard, and more importantly, lighting equipment is not required to comply with this standard or any of the testing procedures or test levels that it prescribes. This standard provides methods for differential voltage and current tests to test the immunity of equipment. Differential voltage tests are applicable to all equipment while current tests are normally carried out for devices with a current A. C. port, such as an electricity meter. Various test levels are defined for this purpose. Two tests are described for the normal operation of equipment. These involve modulating the fundamental frequency wave with various test frequencies. In the first test, the fundamental wave is modulated with continuous wave (CW) pulses with pauses in between while the second test is carried out with blocks of rectangularly modulated pulses.

2.1.1 Voltage Test levels

The immunity tests do not prescribe a single magnitude for the test frequency to be utilized while testing. Rather, the test frequency magnitude is dictated by the type of equipment under test and the environment in which this equipment is operated. The standard makes the following distinction between the environments:

- Class 1: Well protected environment. This class of testing is normally used for equipment connected in an environment where the internal power network is isolated from the mains by isolation transformers or similar equipment. These installations are normally found in laboratories or well protected industrial environments.

- Class 2: Protected environment. Such installations are characterized by direct connection to the low voltage mains network. Electronic equipment is usually earthed and installed using dedicated filtering preventing interference to and from the network. Examples may include control rooms or terminal rooms in a dedicated building of industrial plants.

- Class 3: Typical residential, commercial and light industrial environment. Installations are characterized by direct connection to the low voltage or medium voltage mains network and electronic equipment connected to the earthing system of the installation (ground network).

- Class 4: Severe industrial environment. The installation is characterized by direct connection to the low voltage or medium voltage mains network and electronic equipment connected to the

earthing system of the installation (ground network) common to HV equipment and systems.

- Class X: Special situations. The voltage test levels can be adjusted to test equipment connected to installations that do not fall into any of the above defined classes.

For differential voltage testing, based upon the environment, the following test voltage levels are prescribed. The test levels in column 1 of Table 2.1, are the prescribed test levels for the corresponding environments defined above.

Table 2.1: Prescribed test voltage levels for differential mode testing

Test Level	Open circuit test voltage V (r.m.s)		
	2 kHz-9 kHz	9 kHz-95 kHz	95 kHz-150 kHz
1	0.5	0.5-0.1	0.1
2	3	3-0.6	0.6
3	12	12-2.4	2.4
4	20	20-10	10
X	special	special	special

Table 2.1 shows that the test voltage is not kept constant for differential mode testing. Rather, the test voltage level is constant upto 9 kHz and then decreases linearly with the logarithm of test frequency between 9 and 95 kHz. The test voltage is then kept constant for test frequencies above 150 kHz. This information is summarized in Figure 2.1

2.1.2 Test methods

Based on investigations, the following two methods of differential mode testing have been described in the standard:

2.1.2.1 Method 1

The first test is carried out with CW pulses in the frequency range from 2 to 150 kHz with pauses that can vary from 100 ms to 500 ms. The duration of the CW pulse is defined as T_{pulse} while the duration of the pause is defined to be T_{pause}. T_{pulse} is chosen to be such that its not less than the amount of time required for the equipment under test (EUT) to respond. Further, after every cycle of $T_{pulse} + T_{pause}$, the frequency of the CW pulses is stepped up to 102% of the previous frequency. Thus, starting at 2 kHz and ending at 150 kHz, the equipment is subjected to pulses of various frequencies that have been superimposed onto the fundamental. The test voltage waveforms are shown in Figure 2.2.

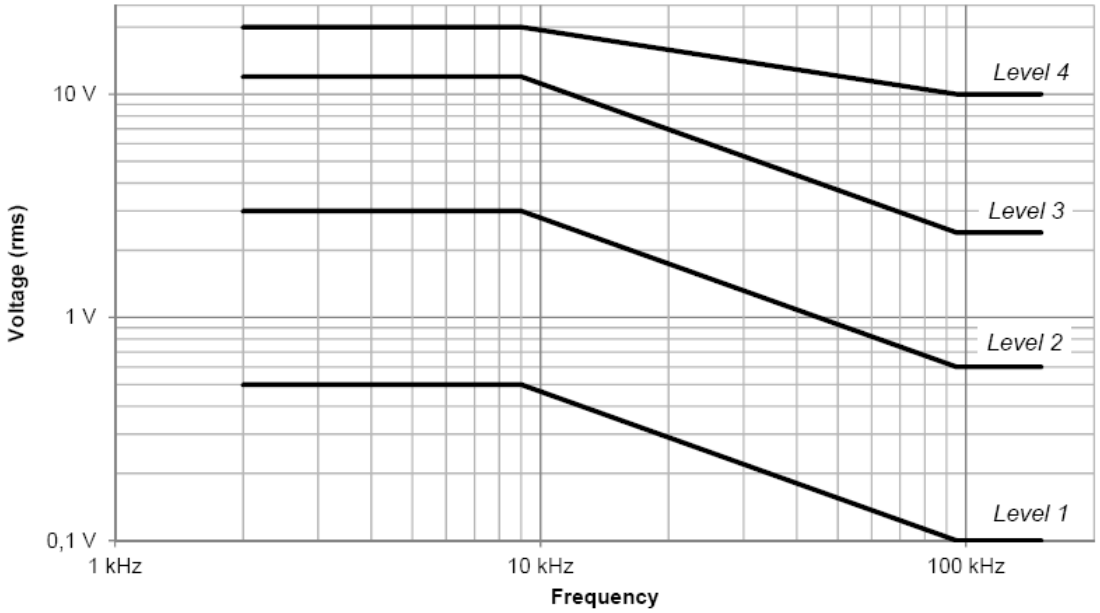

Figure 2.1: Voltage test levels prescribed by IEC $61000-4-19$ [1].

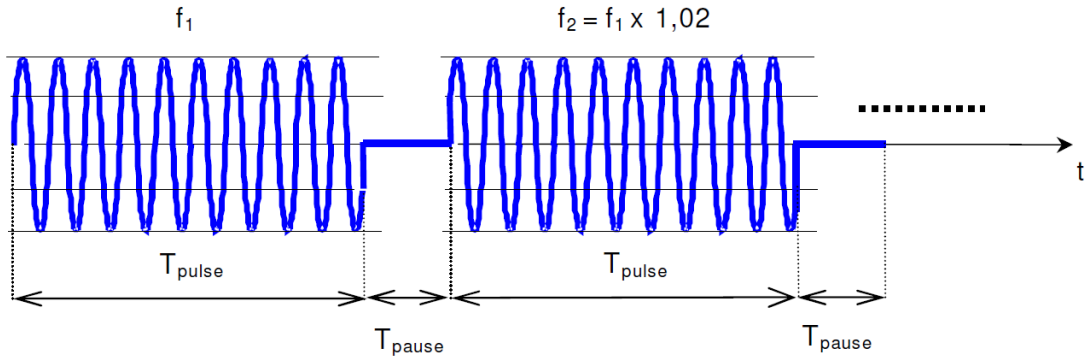

Figure 2.2: Test method 1.

2.1.2.2 Method 2

The second test is carried out by applying a pulse modulated test voltage with a duty cycle, so that the equipment is not subjected to just a single 'burst of frequency pulses, but is rather subjected to multiple 'blocks of frequency pulses, as would be the case in powerline communication. The test frequency is ramped up again in steps of 2% over the previous frequency and the frequency

is changed after every modulation cycle. Thus, the frequency is increased after every period of $4 \cdot T_{modulation}$ where $T_{modulation} = 3\,\text{s}$. For a power frequency of 50 Hz, the duty cycle is set to 50% and the four modulation frequencies that are used are 3 Hz, 100 Hz, 300 Hz and 600 Hz. For a fundamental frequency of 60 Hz, the modulation frequencies are scaled up by a factor of 1.2. The pulses of test voltage may not be synchronized with the zero crossings of the fundamental voltage wave. This process is shown in Figure 2.3.

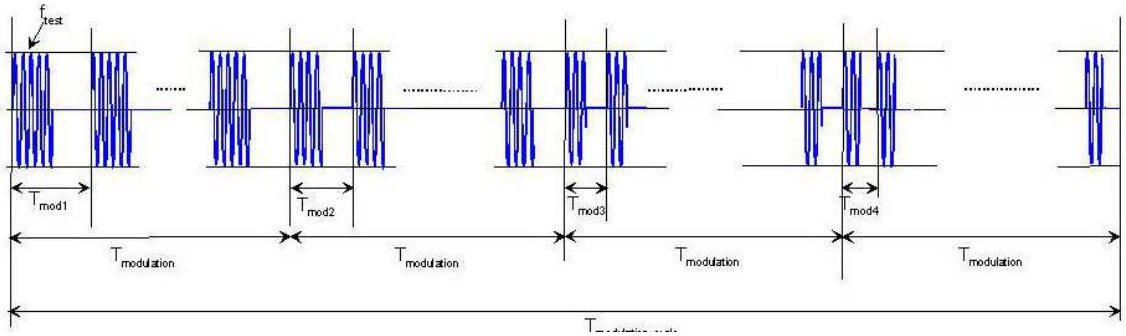

Figure 2.3: Test method 2.

2.1.3 Desired characteristics of Test Equipment

Since the frequency range 2 to 150 kHz is very different from the lower harmonic range, special arrangement has to be made for the test setup. The desirable characteristics of such a setup have also been described in this standard. Aside from the requirement on input-output isolation, the test equipment is required to have a waveform generator capable of covering this frequency band and providing the test pulses. Some other features of the voltage generator are:

- waveform: sinusoidal, total harmonic distortion (THD) less than 5% across the frequency range of interest (2 to 150 kHz).
- open circuit output voltage range (r.m.s): 0.1 V(-10%) to 20 V($+10\%$).
- impedance at terminals of equipment under test (EUT): 10 Ω($\pm 30\%$).
- frequency range: 2 to 150 kHz.

The coupling decoupling network (CDN) that was utilized in the experimentation was built in accordance with this standard. A schematic diagram of such an implementation has been shown

in Figure 2.4. The main departure in the method of testing from the standard was that the waveform generator shown in the figure was connected in series with an amplifier, to change the magnitude of the injected high frequency as required.

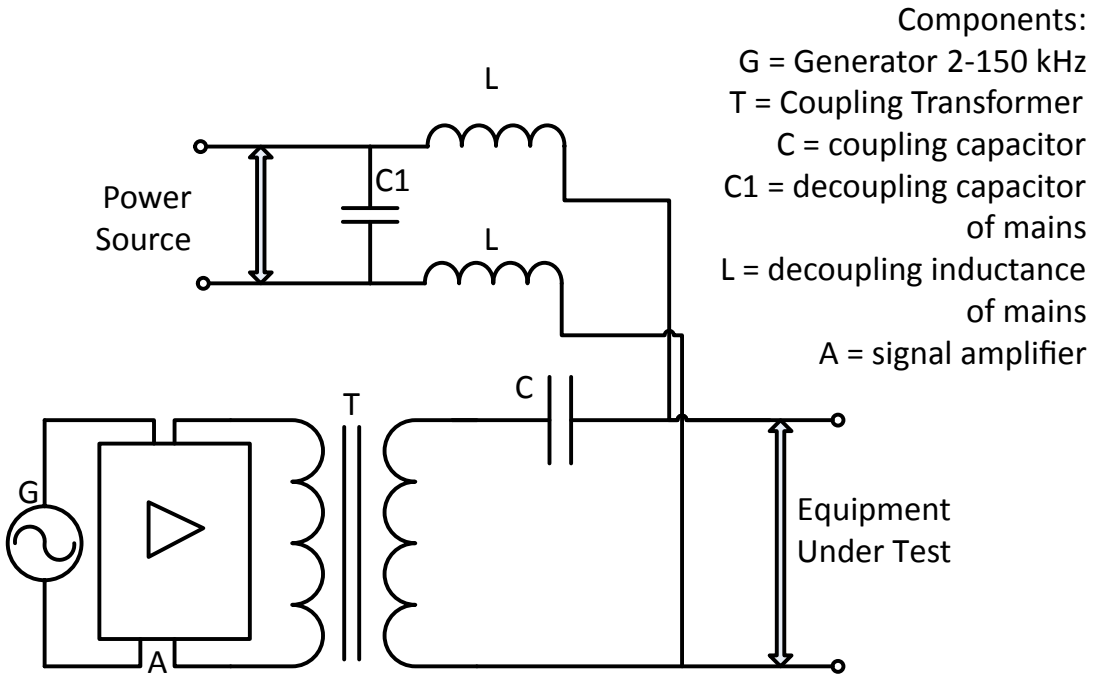

Figure 2.4: Schematic layout of the CDN.

The values of inductance and capacitance were chosen based on the requirements of the circuit.

2.2 Limitations of the standard

The IEC standard requires the modulation of the fundamental voltage wave with a single test frequency of fixed amplitude (depending upon the test level). This frequency is then varied in a fixed manner. The purpose of this method is to provide a clearly reproducible method for the testing of electrical equipment. However, there are some clear limitations with this method.

1. When the electrical equipment is tested using this methodology, it is subjected to high frequency distortion produced by a single frequency only. Field measurements described later on in this report show that this is seldom the case. More often than not, equipment operating in

the field is subjected to groups of frequencies in the higher end of the spectrum. Hence, it cannot be definitively said that any sort of malfunction that is produced in electrical equipment is due to a single frequency acting alone (which is inherently assumed in the tests).

2. The introduction of test levels requires that the equipment be tested at certain fixed amplitude of the test pulse. However, it has been seen from field observations that the magnitude of the frequency distortion changes continuously and it may not be present all the time. The components of this distortion can be classified into the following categories [5]:

   - Narrowband components.
   - Broadband components.
   - Narrowband distortion that shifts in frequency over time.
   - Recurrent oscillations.

   The standard fails to account for these various components of the supraharmonic frequency spectrum (and in particular the recurrent oscillations) and the impact that they may have on equipment.

3. The standard fails to take into account the variable point-on-wave conditions that are created by the lack of synchronization between CW pulses and the fundamental voltage wave. No method has been suggested to record the relationship of these point-on-wave conditions to the output quantity of interest or to calculate the relationship. This makes it harder to reproduce the experiment later on.

4. The methods presented in the standard are time consuming and relatively expensive to implement.

2.3 Other proposed immunity limits

Research done by Bollen et al. [25] has shown that the so-called 'supraharmonic' frequency range (2 to 150 kHz) is composed of various frequency components. The components can be grouped into three categories:

- Narrowband components: consist of single frequency components due to PLC.

- Broadband components: consist of multiple frequencies in the supraharmonic frequency range. As an example, broadband components are generated by end user equipment with power factor correction.

- Recurrent oscillations: Damped oscillations that occur around the zero crossing due to limitations of power electronic converters (remnants of commutation).

In order to get a better idea of the distortion in this frequency range that any connected equipment is likely to face, it has been argued that immunity tests for equipment should take into account the emission standards for the individual frequency components since the distortion found in the grid is unlikely to exceed these values [21, 25]. Standards for emission of narrowband and broadband signals already exist. However, standards for recurrent oscillations do not exist and the level of oscillations around the zero crossing in this frequency range is unknown and a subject of active investigation.

2.3.1 Narrowband components

The emission limits for narrowband components are, in practice, the limits for PLC. Maximum emission due to power-line communication is given in the form of voltage limits in EN $50065-1$ [26] and in IEC $61000-3-8$ [27]. Voltage characteristics are given in EN 50160 [28], where they are referred to as "voltage levels of signal frequencies". Note that the emission limits are expressed in terms of voltage. There is no reference impedance associated with this limit; the voltage after injection of the communication signal shall not exceed the indicated limit in the actual network. For frequencies up to 95 kHz the limits are the same for both standards. EN 50065 does not cover frequencies above 150 kHz. IEC $61000-3-8$ does give limits but these are an order of magnitude more restrictive than below 150 kHz. This is to prevent interference with commercial broadcasting (the long-wave band starts at 148.5 kHz). The existing narrowband signal limits are shown in Figure 2.5.

The limit according to EN 50065 and IEC $61000-3-8$ is at 134 dBμV (about 2% of 230 V) for frequencies between 3 and 9 kHz. The voltage characteristic according to EN 50160 is equal to 5% of the nominal voltage. The margin between the emission limit and the voltage characteristic is to allow for the presence of multiple devices and for amplification of voltage distortion due to resonances. At 100 kHz, the emission limit according to EN 50065 is at 120 dBμV (about 0.5%

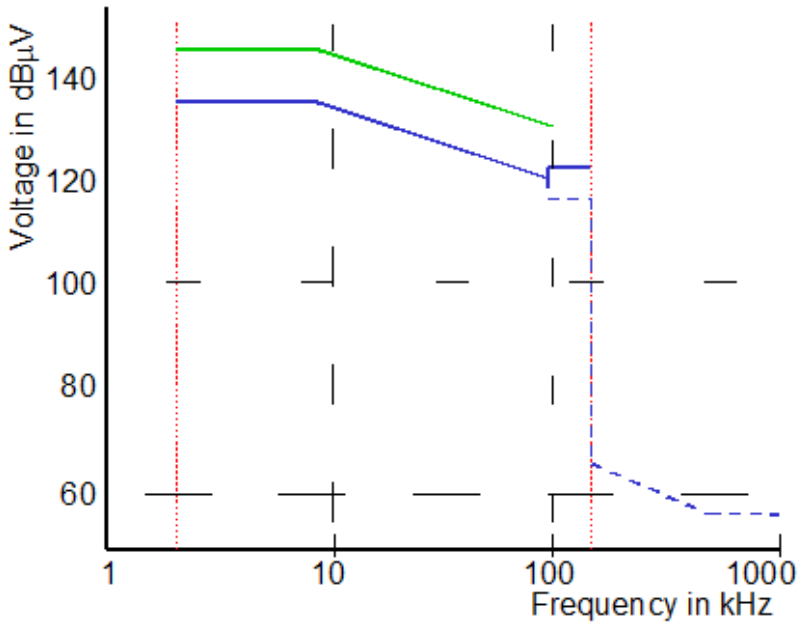

Figure 2.5: Voltage characteristics for narrow-band signals according to EN 50160 (green solid line) and emission limits for narrow-band signals according to EN 50065 (blue solid line) and IEC $61000-3-8$ (blue dashed line). Up to 95 kHz the limits are the same for these two standards.

of 230 V) whereas the voltage characteristic is slightly above 1%. It is proposed in [25] to set the compatibility levels for narrowband signals equal to the voltage characteristics in EN 50160. The immunity limits are proposed to be set 6 dB above the compatibility levels.

2.3.2 Broadband components

Emission limits for broadband signals by lighting equipment are given in CISPR 15 [29]. These limits are given as a voltage against a reference impedance. Limits for the emission by PLC equipment at frequencies not used for communication purposes are given in EN 50065. For frequencies above 150 kHz those emission limits are the same as those in CISPR 15. It is proposed to extend the CISPR 15 limits to lower frequencies (from 2 kHz) and to apply them to all equipment. It is further recommended to set a compatibility level about 6 dB above the emission limit and an immunity limit another 6 dB above the compatibility level, as shown in Figure 2.6.

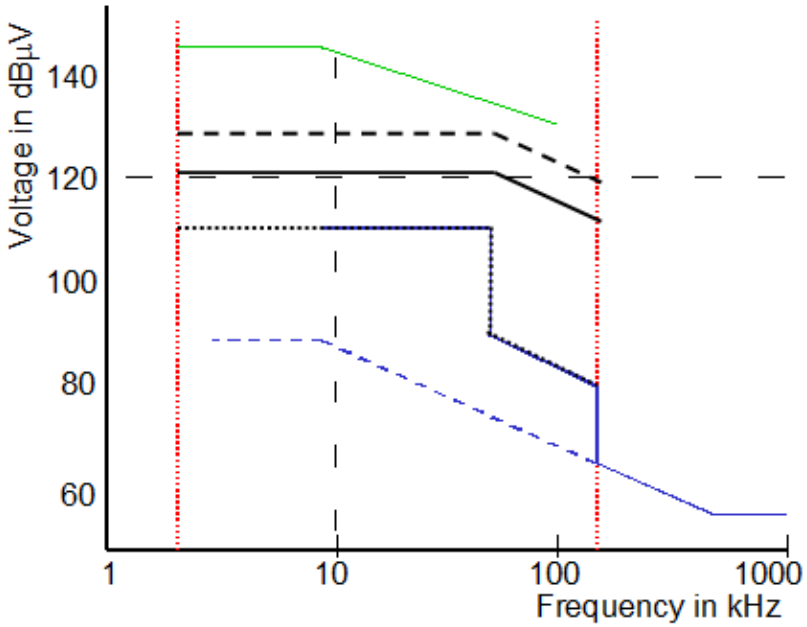

Figure 2.6: Emission limits for broadband signals according to CISPR 15 (blue solid line) and EN 50065 (dashed line). The voltage characteristics for narrowband signals according to EN 50160 (green solid line) are given as a reference.

2.4 Methodology used in the thesis

In the present thesis, an attempt has been made to follow the recommended immunity standard, IEC $61000-3-19$ as much as possible. The equipment guidelines described in the standard have been followed and the test signal generator has been built accordingly. However, to overcome the limitations of the standard, proposals made by Bollen et al. have been followed. Rather than utilizing a single frequency component superimposed onto the grid voltage (as proposed in IEC $61000-3-19$), realistic test signals were obtained from measurements taken in the distribution network in Sweden. Signal recorders were set up at various locations in the Swedish power grid and the source voltage was recorded at defined intervals of time. These voltage signals were then passed through a high pass filter so that all the content below 500 Hz was eliminated. The high frequency part of the signal was thus obtained. Instead of using a single test frequency, the fundamental voltage waveform was modulated using this high frequency test signal. Using this, most of the drawbacks associated with the IEC standard were taken care of. The equipment was not subject to a single frequency alone, but rather to a group of frequencies and more importantly, it was possible to get

an idea of equipment response to real conditions of voltage that are observed in the field. As a final note, it is also worth mentioning that this project utilized only narrowband frequency distortion for the purpose of testing. In one of the test signals that was used, the narrowband components shifted in frequency over time. The method of obtaining these signals, the signals themselves and the locations of recording these signals have been described in the next chapter.

The emission limits set by EN 50160 have been considered as the upper limit for the amplitude of the test voltage superimposed on to the fundamental voltage wave. In each case, the distortion signal was amplified to have a peak amplitude under 1.5% of the fundamental peak voltage amplitude for any individual frequency component. The incoming voltage from the grid and the high frequency distortion that was superimposed were not synchronized to each other. A positive side effect of this was that it allowed for observation of the impact of the 'point on wave' of high frequency distortion on equipment. In other words, the 'phase angle' at which the high frequency distortion was applied was floating along the fundamental frequency wave so as to understand whether the point where the distortion was applied, had any effect on the equipment that was being tested. The process of capturing the test signals, the experimental setup and the results of the experiments are explained in subsequent chapters.

Chapter 3

Field Measurements on LED lamps

The background voltage distortion is known to be different at different sites and it also varies over time. It is important when controlling the immunity of the lamps, to have a realistic background of what type of waveform distortion the lamps can be exposed to. Several long term measurements were conducted in the lab and at different locations and with different types of lamps (no LED lamps though) over the years to get an overview of the voltage waveform distortion at different locations, both in the harmonic range and in the frequency range between 2 and 150 kHz. The aim of the measurements presented in this chapter was to map the electromagnetic environment at industrial locations. To do this, both the voltage and current waveform at the connection point of the LED lamp were recorded at all sites.

3.1 Measurement Technique

The measurement methodology in the harmonic range is well described in IEC $61000-4-30$ [30]. The latest edition of this standard (from 2015) also includes a discussion in an informative annex "measurement instruments for measurements in the range 2 to 150 kHz", where 2 to 9 kHz is referred to IEC $61000-4-7$ [31]. The range between 9 and 150 kHz is still under consideration and three options are described.

- Use the CISPR $16-1-2$ standard. The method described in CISPR 16 emphasizes emission and immunity tests in a laboratory environment, and may not be appropriate for in-situ measurements.

- Use a method where 32 short windows (0.5 ms) within a 10/12 cycle (roughly 200 ms) window are captured. This method generates a frequency separation of 2 kHz when applying a DFT on each smaller window. This allows for a method where the frequency over time can be analyzed with a fairly low amount of data. One drawback is that there will be gaps within the approximately 200 ms window and the frequency separation is quite low.
- Use the method described in IEC $61000-4-7$, Annex B. This document recommends taking a 200 ms time-domain sampled window of the signal, which is later analyzed for frequency components and extend this from 9 kHz up to 150 kHz.

In this project it was decided to use time-domain sampling according to the last point even above 9 kHz for the following reasons:

- Provide the possibility to measure several channels simultaneously compared with the CISPR method.
- Standard frequency-domain methods only give a magnitude as a function of frequency. As there is no phase information available, it is not possible to reproduce the time-domain waveform.
- When the frequency content of the signal changes fast, the spectrum can be hard to interpret. A-priori assumptions have to be made, which could again be a barrier for research and new developments. There are no such limitations with time-domain data.
- From previous knowledge we know that many components in the kilohertz range vary in frequency, synchronized with the fundamental frequency. Using very short windows, as described in the second method above, will not represent this very well.
- Time domain information can easily be used together with frequency domain information to give a better presentation/explanation.
- A time domain instrument is cheaper for the frequency range of interest.
- Once the time-domain data is available, it is possible to obtain the output from a measurement receiver by modeling that receiver.
- This project includes both frequency ranges (DC to 150 kHz) and therefore the method described in the last was used. This has the benefit that the same collected data can be used both for the harmonic and the higher frequency range.

The salient points of the measurement method given by IEC $61000-4-7$ Annex B are:

1. A band pass filter that attenuates the fundamental frequency and components above 9 kHz. The attenuation of the fundamental should be at least 55 dB.

2. The sampling does not need to be synchronized to the fundamental period of the power-system frequency.

3. A rectangular window of 200 ms can be used (corresponding to approximately 10(12) fundamental periods of 50 Hz(60 Hz)).

4. The total uncertainty should not exceed $\pm 5\%$ when tested with a single-frequency emission in the frequency band considered.

5. The output DFT is grouped into bands of 200 Hz, as in (3.1), in order to harmonize with the 9 to 150 kHz bandwidth in CISPR $16-1$.

$$G_b = \sqrt{\sum_{f=b-90\,\mathrm{Hz}}^{b+100\,\mathrm{Hz}} C_f^2} \tag{3.1}$$

The voltage and current measured was recorded at different sites using a measurement recorder. The recorder has a total of 16 channels and a maximum sampling speed of 100 MS/ s but the sampling speed depends upon the settings and specifications of the measurement. In general the magnitude of the components in this frequency range decreases with the frequency and in the range from 2 to 150 kHz the amplitude is just a small fraction of the power system frequency. Therefore, IEC $61000-4-7$ prescribes the use an analog filter in the frequency range from 2 to 9 kHz for voltage measurements. To achieve the 150 kHz measurement range, a band-pass filter starting at 2 kHz and band stop set at 209 kHz, developed by Technical University of Dresden was used in most parts of this project [32].

All of the current measurements done in this frequency range were done with Pearson current probes model 411. This current probe has a transfer of 100 mV/ A, the lower 3 dB cut-off at 5 Hz and the high cut-off at 20 MHz. In the frequency range of interest the accuracy is $-0, +1\%$ dB. The phase error of the probe is less than 1 degree from 300 Hz to 33.3 kHz and increasing to 6 degrees at 2 MHz. For measurement in the higher frequency range there is no need to filter the current by an analog filter. The 12-bit resolution of the instrument is enough to analyze the data.

The instrument used was a Yokogawa DL850 oscilloscope and recorder, with a sampling frequency of 1 MS/ s. Voltage (100 kS/ s), current (1 MS/ s), and filtered voltage (1 MS/ s) were recorded. The input module had an anti-aliasing filter in the equipment and the current and filtered voltage had a band limit of 500 kHz. The unfiltered voltage had a bandwidth of 10 kHz.

3.2 Measurement Results

3.2.1 Lamps tested

The first LED lamp, lamp 'A', was made for industrial use and it has a matrix of 165 LEDs. Measurement in the lab showed an active power of 63 W, and 10% total harmonic current distortion (ITHD) (tested with 1.88% VTHD) and a displacement power factor (DPF) of 0.972.

The second LED lamp, lamp 'B', was a street lamp composed of a matrix of 16 LEDs. It had an active power of 56 W, and according to measurements, ITHD 11.3% and a DPF of 0.966.

The third LED lamp, lamp 'C', was also a street lamp which consists of a matrix of 30 LEDs. The measured active power was 42 W, ITHD 19% and a DPF of 0.96. In this case, the fundamental of the current was 192 mA, and the peak current absorbed was 0.26 A.

The fourth LED lamp tested, lamp 'D', was a dimmable 12 W lamp intended for domestic use. Measured active power was 12.6 W, ITHD 70%, DPF 0.972, the fundamental component of the current was 56 mA, and the peak current was 175 mA.

The current waveform differs between the different lamps. Figures 3.1, 3.2, 3.3 and 3.4 show the voltage and current waveform measured at the terminals of the four lamps in the laboratory, where the current is shown in green and voltage is shown in blue with corresponding color on the axis. The current drawn by lamp A is fairly sinusoidal except for some small deviations around the zero crossing of the current waveform and some small distortion at both positive and negative peak of the current. The distortion around the zero-crossing is also referred to as 'zero-crossing distortion' or 'cross-over distortion' and will be referred to as 'recurrent oscillation'. At the peaks there is a 'widening' of the waveform which indicates a higher frequency component. Lamp B, when connected at the same site, shows more waveform distortion. The zero-crossing distortion is also visible along with some lower-order distortion represented by some additional superimposed wave on the current waveform. The third lamp, shows another waveform of the current where it deviates even more from a purely sinusoidal waveform than the previous two lamps. In the current waveform

there is also a fairly large spike close to the zero-crossing of the voltage. The last lamp, shown in Figure 3.4, shows the most distorted waveform where current shows a large deviation from a pure sinusoidal waveform. The current also shows a large high-frequency component almost throughout the whole period.

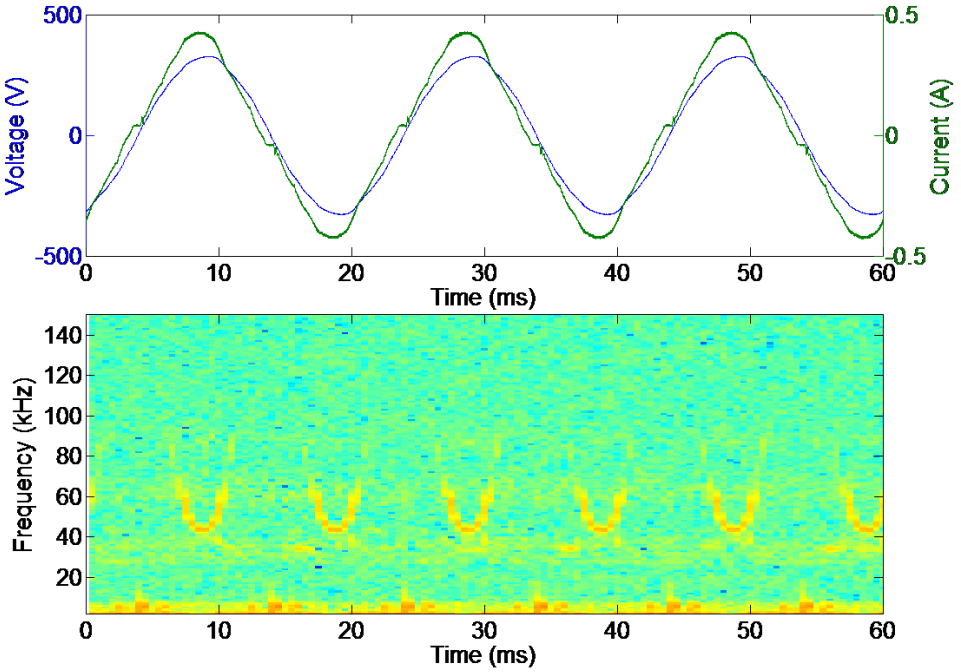

Figure 3.1: Voltage (blue) and current (green) waveforms drawn by lamp A (top). Frequency components of current are plotted as a function of time at the bottom.

When applying a Short Time Fourier Transform (STFT) [5] (bottom half of Figures 3.1, 3.2, 3.3 and 3.4) on the current waveform it is noticeable that the high frequency component starting at 40 kHz is actually a narrowband component that varies in frequency with time, repeating every 10 ms. The STFT gives a plot of the power spectral density. In these plots, the total power in the signal at a given point in time is divided into its frequency components. Red represents maximum power and blue represents the lowest power. The vertical scale gives frequency while the horizontal scale gives time. Thus, the plots show the amount of power at every frequency at any moment in time. The same pattern appears for lamp C and D while lamp B has a constant narrowband component slightly above 20 kHz. The recurrent oscillations show up as vertical bands at a low frequency. Note that a short damped oscillation is not well represented by a Discrete Fourier Transform (DFT). The wide spread HF distortion in lamp D current shows up as a broadband frequency component between 2

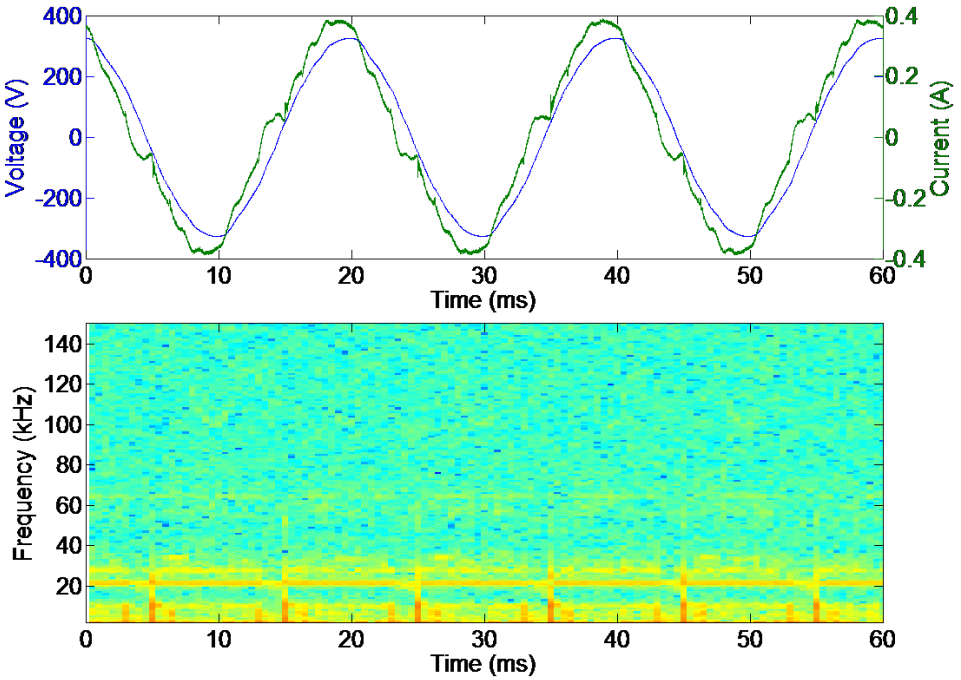

Figure 3.2: Voltage (blue) and current (green) waveforms drawn by lamp B (top). Frequency components of current are plotted as a function of time at the bottom.

and about 50 kHz in the spectrogram.

By applying a digital band-pass filter, 2 to 150 kHz, to the measured current, it is easier to observe the distortion content of the current drawn by the different types of lamps in time domain (Figures 3.5, 3.6, 3.7 and 3.8). From the filtered current, the first three lamps show different levels of recurrent oscillations close to the voltage zero-crossing. The recurrent oscillations reach about 20 mA for lamp A (Figure 3.5), 40 mA (Figure 3.6) for lamp B and 100 mA for lamp C (Figure 3.7) in peak amplitude. Lamp D (Figure 3.8) does not show the same oscillations. Lamp D is below 25 W and also based upon the shape of the current waveform it is most likely not equipped with an active power factor correction front-end. Also, by observing the filtered current it is notable that there is a high frequency component in the current and relatively high levels of a wide spread high-frequency distortion.

Throughout the rest of this chapter a number of spectra, both harmonic and supraharmonic range, will be shown. All of these will show the absolute value of the component at each harmonic frequency. Figure 3.9 shows the spectra up to 9 kHz not including the fundamental. Each lamp has the highest level of current at harmonic 3 which is 25 to 30 mA.

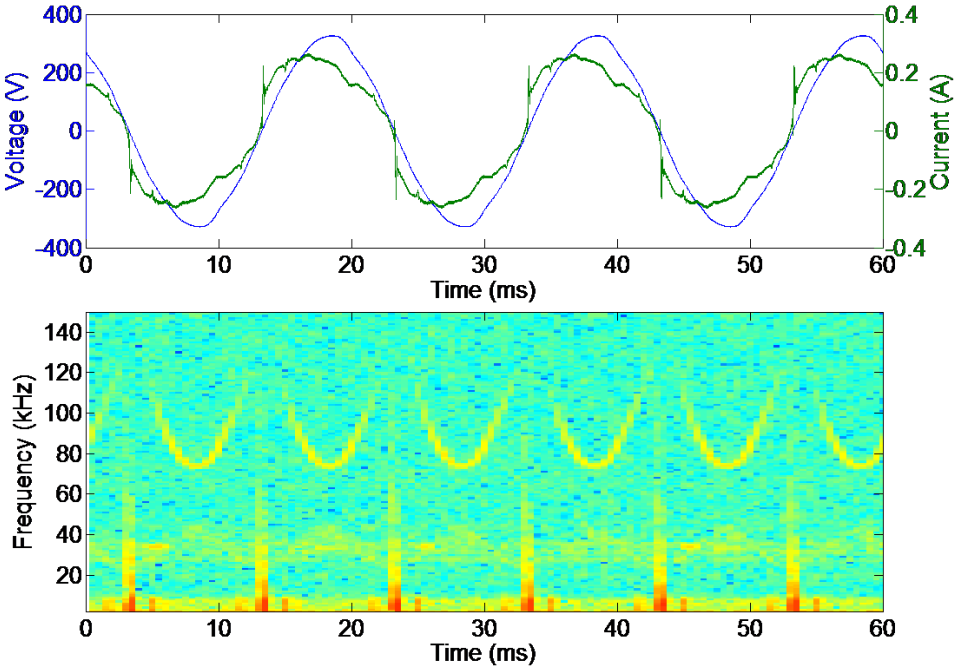

Figure 3.3: Voltage (blue) and current (green) waveforms drawn by lamp C (top). Frequency components of current are plotted as a function of time at the bottom.

In the higher frequency spectra, shown in Figure 3.10 it is notable that the emission from the lamps is different. Lamp D has the highest individual component of 0.7 mA at 45 kHz and also almost the rest of the frequency components are higher than the other lamps. Lamp A has the highest magnitude slightly above 40 kHz and lamp B has also a relatively high magnitude but at a frequency between 10 to 15 kHz. Lamp C has its highest magnitude between 10 and 15 kHz.

Clearly the current drawn by each of the lamps contains emission caused by the lamp itself. If other nearby loads also emit in this frequency range, the lamp can take some of this emission since most of this equipment contains a capacitor on the input side. So when performing current and voltage measurements at different sites the measurements will contain both emission coming from the equipment under measurement and other emission at the site. The emission coming from the equipment and going towards the grid is refered to as 'primary emission' and the emission coming from other nearby equipment towards the lamp is referred to as 'secondary emission'. Note that it is impossible to distinguish between primary and secondary emission just from one measurement at the lamp terminals.

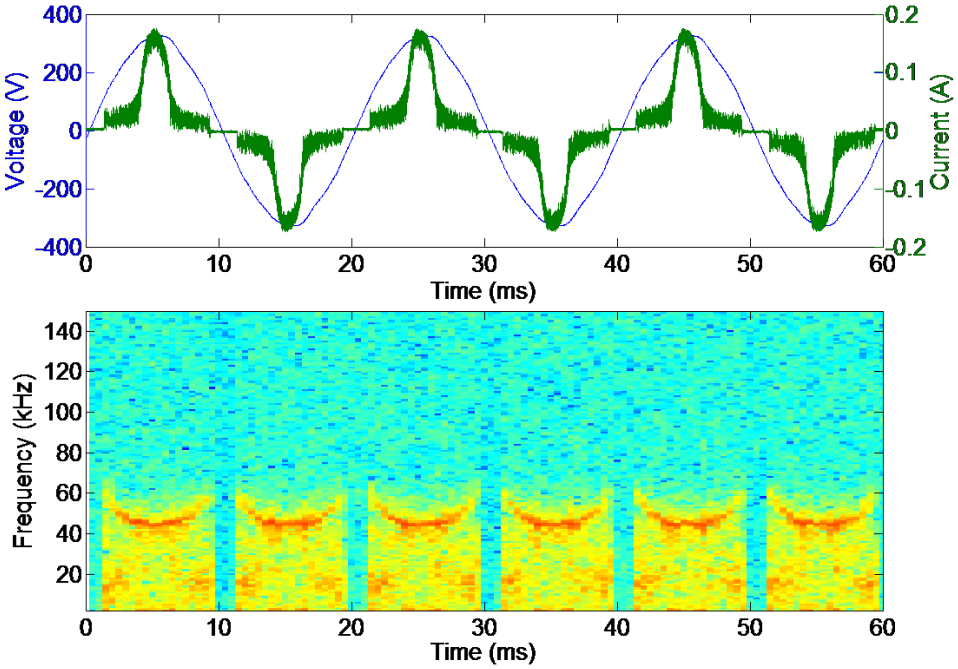

Figure 3.4: Voltage (blue) and current (green) waveforms drawn by lamp D (top). Frequency components of current are plotted as a function of time at the bottom.

3.3 Measurement Sites

3.3.1 Description of the sites

Previous measurements with similar aims were carried out at offices, domestic homes, hospitals, shopping centers etc. Within this project, more industrial sites were included and they are presented here and some results are presented in [33]. Note that, later on when immunity test are performed other voltage signals are also used.

Site 1 was the laboratory in Sweden where the measurements shown in the section above were taken. This site was included as reference since the electrical environment is well known and the level of distortion is generally low. Note however, that the electrical environment in the laboratory is not controlled in any way. It is fed via a separate cable from the distribution transformer. This means that a small amount of secondary emission coming from other parts of the laboratory building will show up in the measurements in the lab in the same way as in field measurements. However, most of the sources of emission in the laboratory were known and the electrical environment can be more or less regarded as an office or residential building since most of the equipment connected is

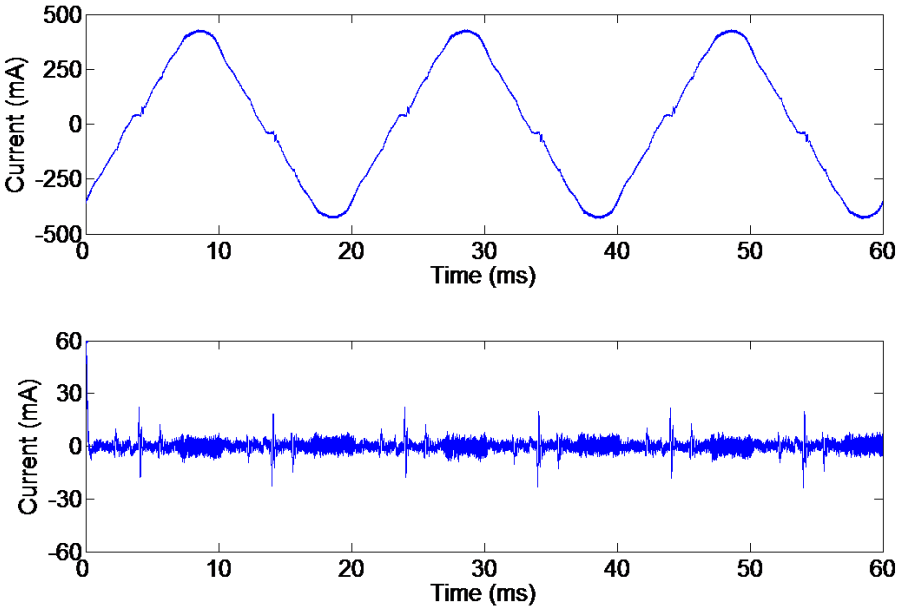

Figure 3.5: Current waveform (upper) and 2 to 150 kHz band pass filtered current waveform (lower) for lamp A.

common in these cases.

Site 2, was a workshop where the main activities were maintaining and repairing machines. The machines that can be found there are: a welding machine, hydraulic press, lathe, drill and milling machines. The lighting at the workshop consisted of 48 (8 rows with 6 lamps in each row) fluorescent lamps ($2 * 80$ W- T5 tubes). The lamps were fed by a three-phase system and in this case, measurements were done with the different lamps connected to the same cables that the existing lights were connected to.

Site 3 was a hydraulic component manufacturer where measurements were done at an outlet in the workshop. This workshop, similar to site 2, contained metal processing machines such as welder, grinder, lathe, mill, hydraulic presses etc. The lighting system at the workshop was also a three-phase system, but in this case, the lamps were individually connected to one of the phases (phase C) of a 3-phase power outlet available at the industry. The measurement interval was 1 s. The variables recorded were 3 voltages (100 kS/ s), 3 analog filtered voltages (10 MS/ s) and 1 current (1 MS/ s).

Site 4 was a smelter and the measurement was performed at a workshop 'electrically' and

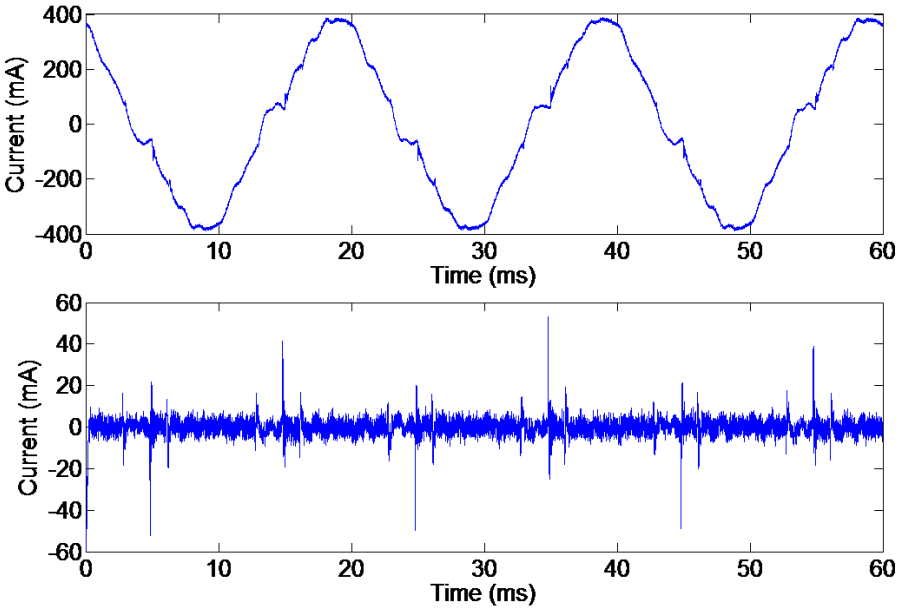

Figure 3.6: Current waveform (upper) and 2 to 150 kHz band pass filtered current waveform (lower) for lamp B.

physically close to an electrolysis process with large rectifiers. In this case the measurement interval was 1 min. Again, it was also a three-phase system, and the lamps were individually connected to one of the phases (phase A) of a 3-phase power outlet available at the industry. The variables recorded were 3 voltages (100 kS/ s), 3 analog filtered voltages (1 MS/ s) and 1 current (1 MS/ s).

Site 5 was a combined workshop and garage at an airport. Compared with sites 2 and 3, machining activity was much less. The airport garage was partly rebuilt in 2013 when LED lights were installed in a section of the garage. The aim of this activity was to evaluate the use of LED lighting at the airport. Also, the feeder of this part of the installations was redone, which resulted in a separate feeder from the LV busbar at the transformer to the light installation. At the same time the old feeder was kept which made it possible to measure with both feeders.

Site 6 was a fairly new built office, with a disturbance at a light installation in a 7000 square meter office building. Since the opening of the office in 2009 the control functions of the office lights (dimming, corridor and attendance control) were not always working properly. Specifically, the lamps remained in low dimming mode and light intensity could be increased.

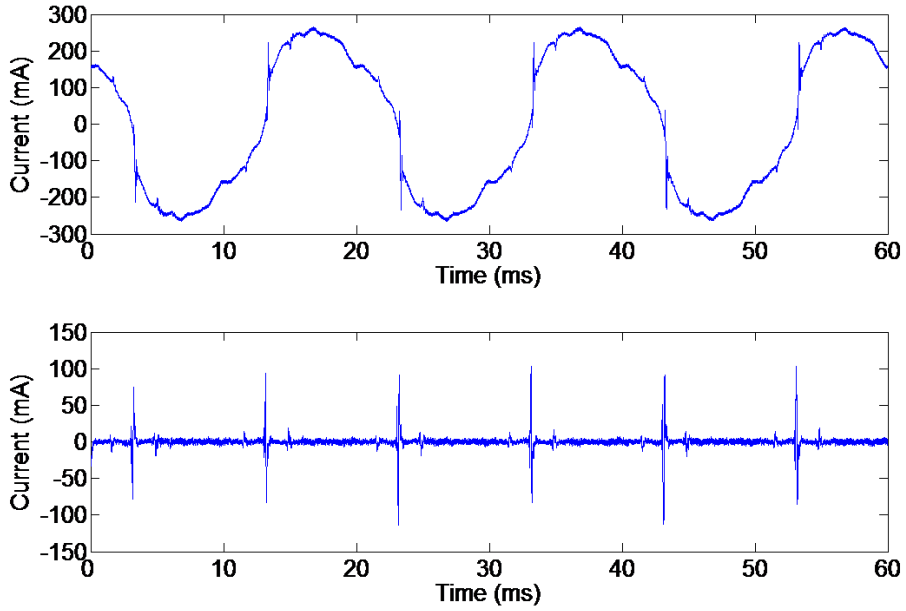

Figure 3.7: Current waveform (upper) and 2 to 150 kHz band pass filtered current waveform (lower) for lamp C.

3.3.2 Result of snapshots with Lamp A at different sites (sites 1 to 5)

Figure 3.11 shows the result from time domain measurement of a window, taken with lamp A connected at the five different sites. The voltage waveform is represented in blue and the current waveform is represented in green with corresponding axes on left and right. As can be seen from site 1 (laboratory), the current drawn by the lamp is fairly sinusoidal except for some small deviations, especially around the zero crossing of the current waveform. When the same lamp is connected at sites 2 and 3, the voltage is still fairly sinusoidal but the measurement shows a difference in the current drawn by the lamp. The current waveform is 'wider' which indicates a higher high frequency component superimposed upon the current drawn by the lamp. This probably relates to secondary emission coming from other loads connected at these sites. At site 4 there is a fairly high distortion visible in the voltage and it is reflected in the current drawn by the lamp. This has a lower frequency, which is in the harmonic range. Note that these harmonic components are also due to secondary emission at this site. At site 5, where little activity was going on, the waveform is pretty sinusoidal again and it resembles the result from the laboratory.

When applying a band-pass filter, 2 to 150 kHz, to the measured current at the different

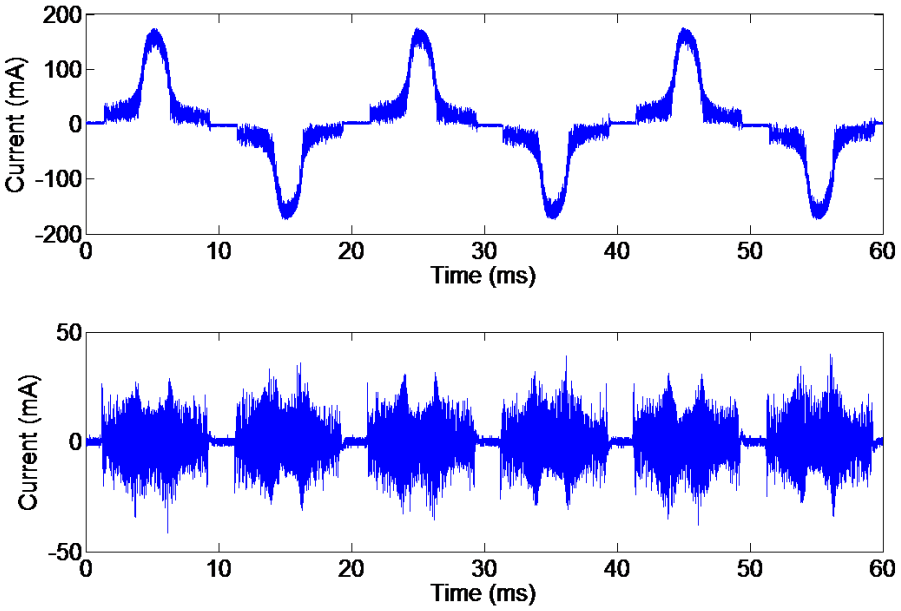

Figure 3.8: Current waveform (upper) and 2 to 150 kHz band pass filtered current waveform (lower) for lamp D.

locations (1 through 5), shown in Figure 3.12, it is noticeable that these components are different at the different locations. Both workshops, sites 2 and 3, show a high frequency component in the filtered current. Sites 3 and 4 show less high frequency distortion while site 1 shows the lowest levels. However, all sites show recurrent oscillations occurring every 10 kHz, close to the zero-crossing of the voltage, but with different amplitudes for the different locations.

Figure 3.13 shows the spectrogram for each site where the first spectrogram, site 1, is compared with the waveform at the same site. From site 1 we observe that the high frequency component visible at the peak of the current, shows up as a narrowband component that shifts in frequency with the fundamental power system frequency. Its lowest frequency is about 40 kHz. This is a primary emission from the lamp. The recurrent oscillations close to the zero-crossing of the voltage show up as a vertical band with a low frequency, mostly below 10 kHz. Note that this is also a primary emission from the lamp. Both frequency components are most likely remains from the active power factor correction in the lamp [5]. When placing the same lamp at site 2 several frequency shifting narrowband components show up in the spectrogram. Note that the lamp was connected together with the 'ordinary' light in the workshop in this case. From the time difference

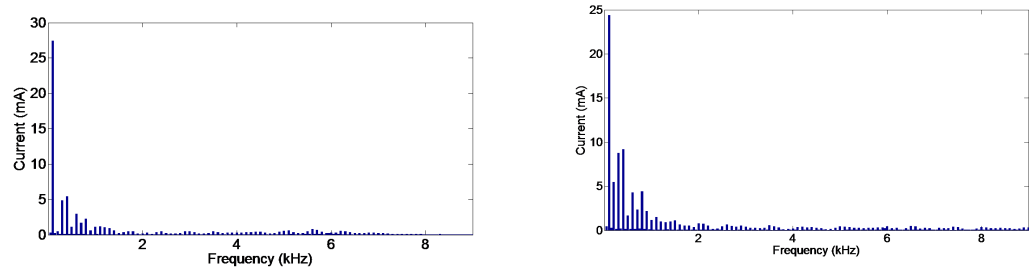

(a) Lamp A

(b) Lamp B

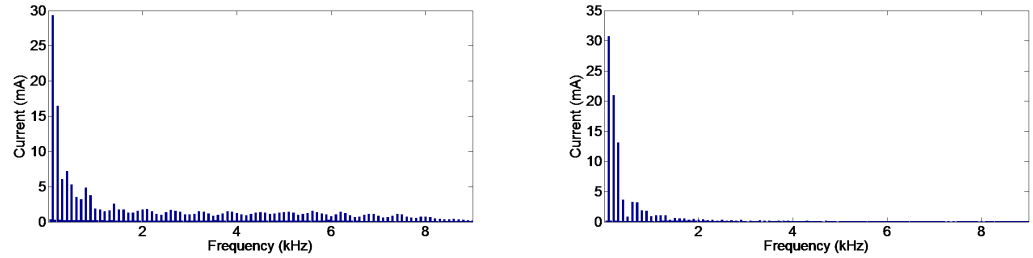

(c) Lamp C

(d) Lamp D

Figure 3.9: Harmonic spectra of the current waveform of each lamp up to 9 kHz.

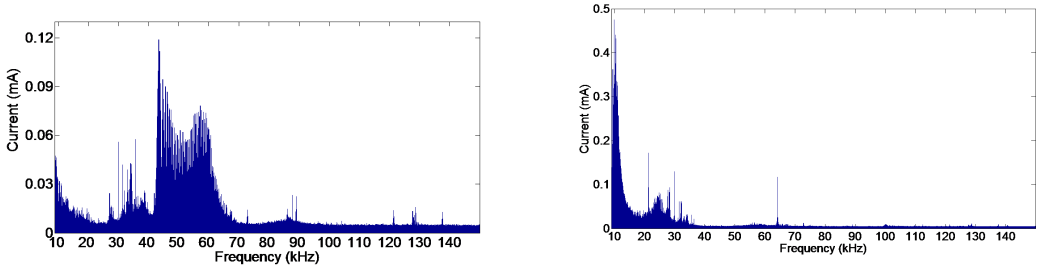

(a) Lamp A

(b) Lamp B

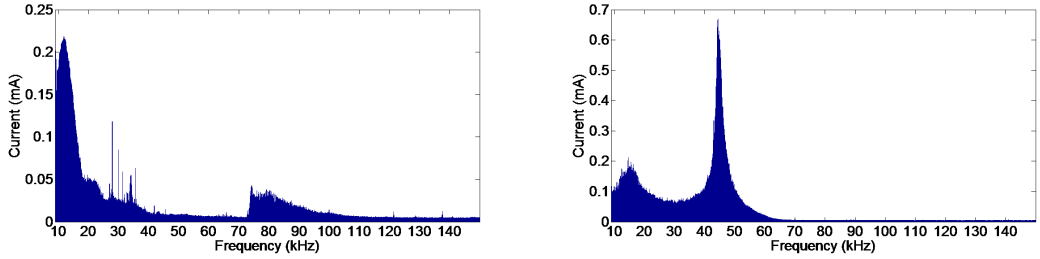

(c) Lamp C

(d) Lamp D

Figure 3.10: Resulting spectra of the current waveform between 9 kHz and 150 kHz for each lamp.

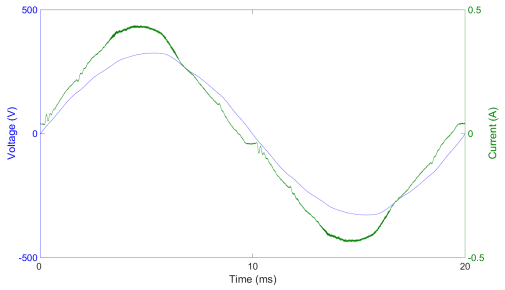

(a) site 1

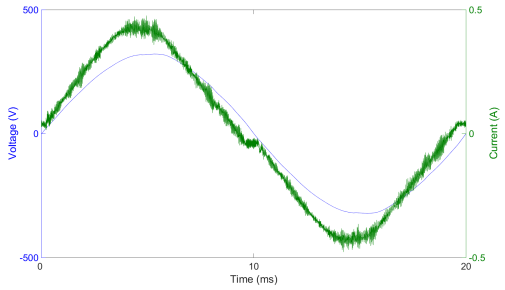

(b) site 2

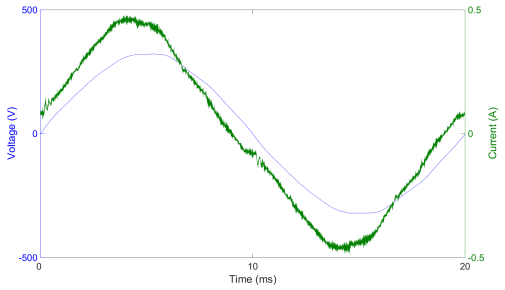

(c) site 3

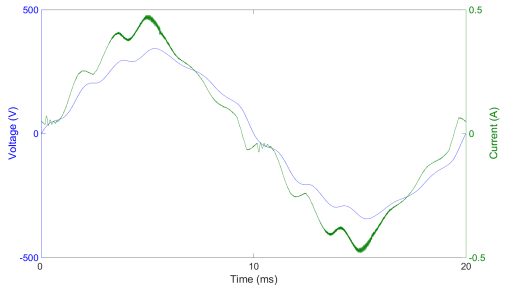

(d) site 4

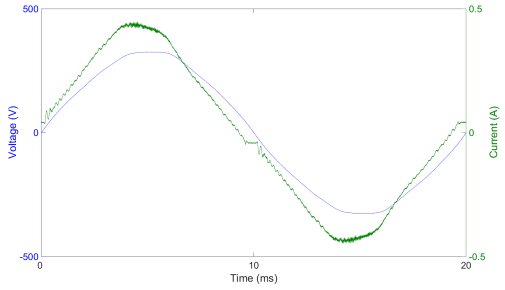

(e) site 5

Figure 3.11: Voltage and current waveforms from lamp 1 at site 1, site 2, site 3, site 4 and site 5.

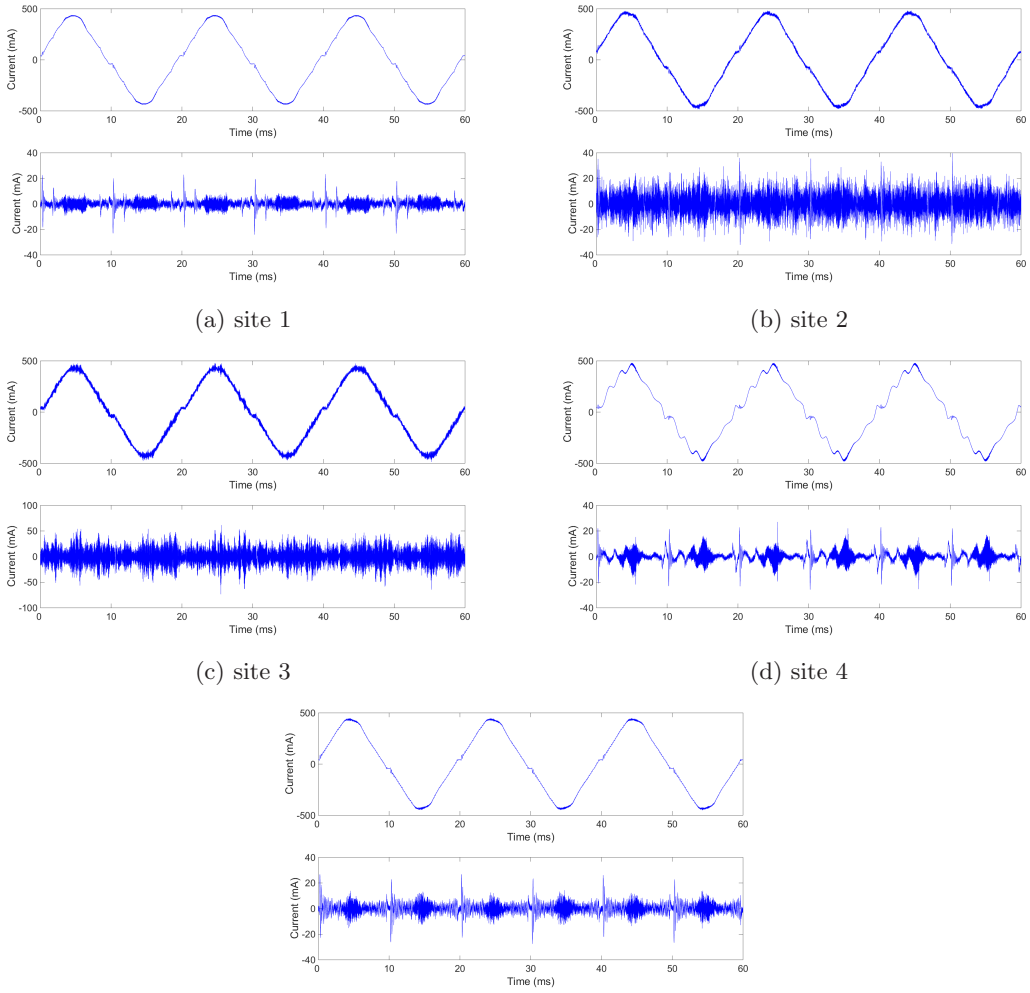

(a) site 1

(b) site 2

(c) site 3

(d) site 4

(e) site 5

Figure 3.12: Current waveform and 2 to 150 kHz band pass filtered current waveform from each site with Lamp A. Note the difference in vertical scale for site 3.

of approximately 3 ms it can be deduced that this originates from the rest of the light installation at the site, consisting of a 3 phase-connected fluorescent lamp with electronic ballast equipped with APFC. In this case the lowest frequency of this component is about 30 kHz, i.e., this is secondary emission from the rest of the light installation and the primary emission from the lamp A is partly visible as a frequency shifting component with its lowest frequency above 40 kHz. There is also a narrowband component visible around 20 kHz that is shifting amplitude with the power system frequency (every 10 ms). This is also most likely a secondary emission coming from nearby equipment at the workshop. Recurrent oscillations also show up at this site.

For the remainder of this chapter, only measurements from the different sites outside the lab are shown since the first part of this chapter shows most of the results from the lab.

3.3.3 Variation in background voltage distortion with time

Measurements of the background voltage were made at all sites before the lamps were connected at each site. The background distortion was measured for periods ranging from a couple of hours to more than 48 hours, depending upon the site. The variation of the background voltage distortion is different between sites. Note that this is not the result from a STFT. Rather, it is the plot of all spectra from each window taken in Figure 3.14. At site 2 (Figure 3.14a) the distortion is pretty much the same during the whole measurement while sites 3 (Figure 3.14b) and 5 (Figure 3.14d) show fairly large variations and site 4 (Figure 3.14c) some variations.

Site 2 shows two narrow band emissions: slightly below 20 kHz and slightly below 140 kHz, which are continuous through the whole measurement. It also shows a broadband component starting at 30 kHz and decreasing with frequency up to about 80 kHz. As mentioned above, this is due to the installed light in the workshop and this shows up as secondary emission at the lamp terminal when the lamps are connected as shown in Figure 3.13. Sites 3, 4 and 5 show mostly narrowband components recurring intermittently during the measured time period at each site. Normal working hours at site 2, 3 and 5 are 07:00 to 16:00 while site 4 is in continuous operation.

To compare the background voltage emission between the sites, both the 99 and 95 percent spectra over time were calculated. The rms value of the 99% background voltage spectra at the four different sites compared, varies from 0.1 mV up to slightly above 1 V in the range from 2 to 150 kHz (Figure 3.15). Site 2 shows, in general the highest background voltage and the other three sites have rather similar amplitudes.

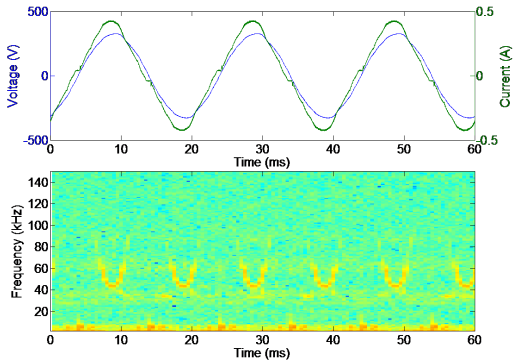

(a) site 1

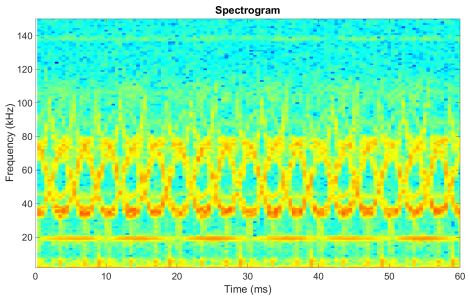

(b) site 2

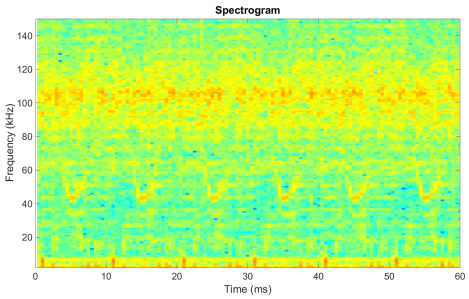

(c) site 3

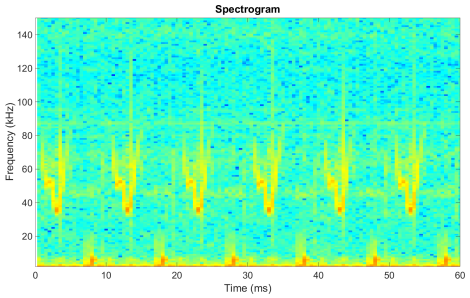

(d) site 4

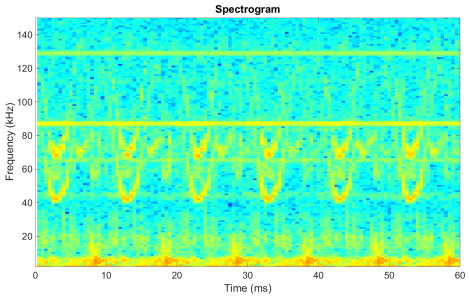

(e) site 5

Figure 3.13: Spectrogram of the current drawn by Lamp A at the different sites.

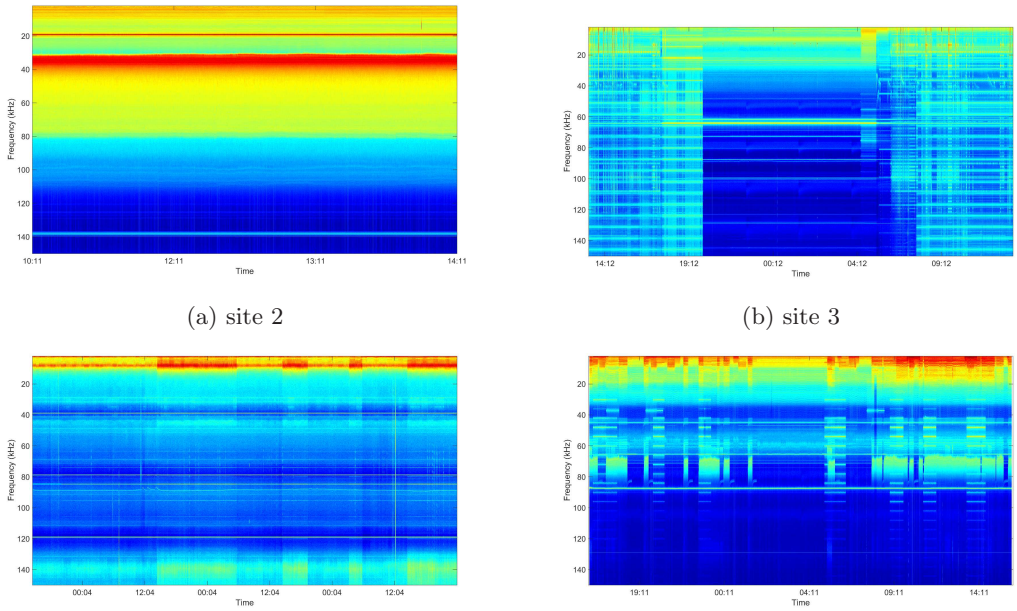

(a) site 2

(b) site 3

(c) site 4

(d) site 5

Figure 3.14: Voltage spectra variation over time from 2 to 150 kHz. Note the difference in horizontal scale between the plots.

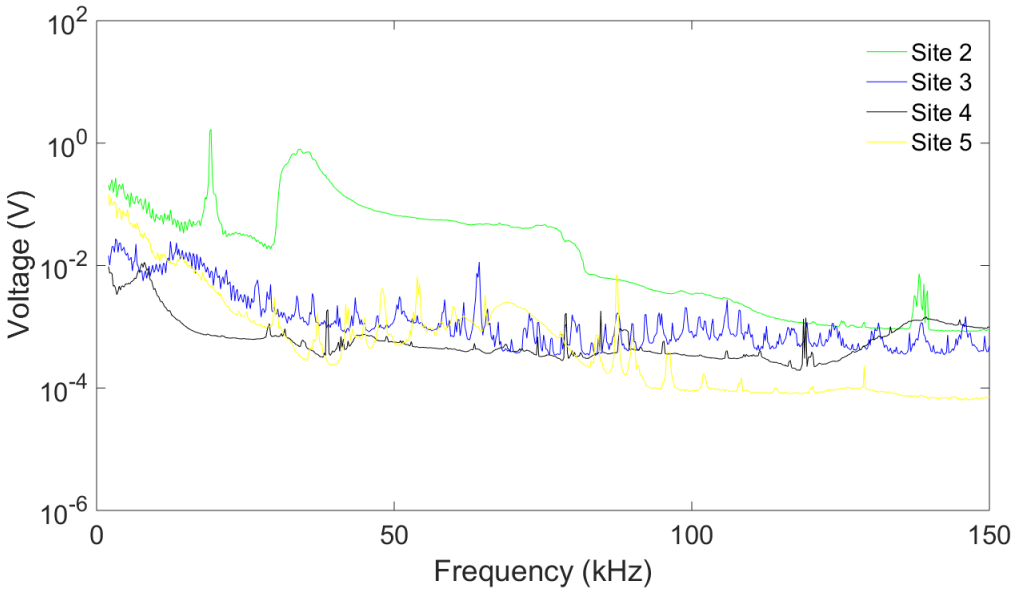

Figure 3.15: 99% value of the background distortion at the four different sites

Figure 3.16, shows the average value of the spectra at each site and the difference is not large compared with the 99 percent value. Still, the rms value varies from slightly below 0.1 V to

1 V and site 2 shows the highest average value.

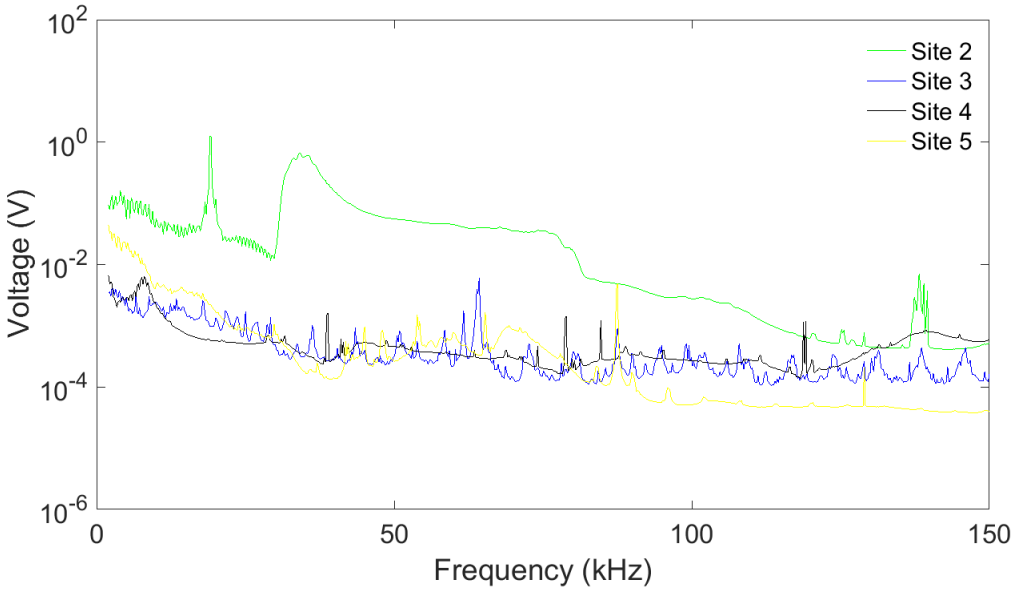

Figure 3.16: Average value of the background distortion at the four different sites

3.3.4 Variations of voltage and current distortion for the lamps

It is known that the distortion of both, the current and voltage waveforms varies with time. Figure 3.17 shows a 31-hour period of the VTHD and ITHD (up to 2 kHz) at site 4. The average VTHD is about 6% percent and varies about ±0.5%. The ITHD, while Lamp A was connected, was about 14% but varies slightly more than ±0.5%.

The individual harmonics are shown in Figure 3.18, where the variation of the harmonics is shown for each harmonic with 10th and 90th percentile. It can be seen that there is a larger variation for harmonics 11 and 13 compared with the rest. In the voltage, these harmonics have the highest magnitude but for the current, the third harmonic is the highest and has a low variation. The most probable cause for this is that the production at the smelter causes 11th and 13th harmonic (secondary emission) and that these have a very high variation. The 3rd harmonic caused by lamp A (primary emission) is constant and the reason is that the light is on during the whole period.

In the higher frequency range, above 2 kHz in Figure 3.19, the variations in voltage are relatively lower e.g. the 40 kHz component in the voltage spectra changes about 2.5 times between

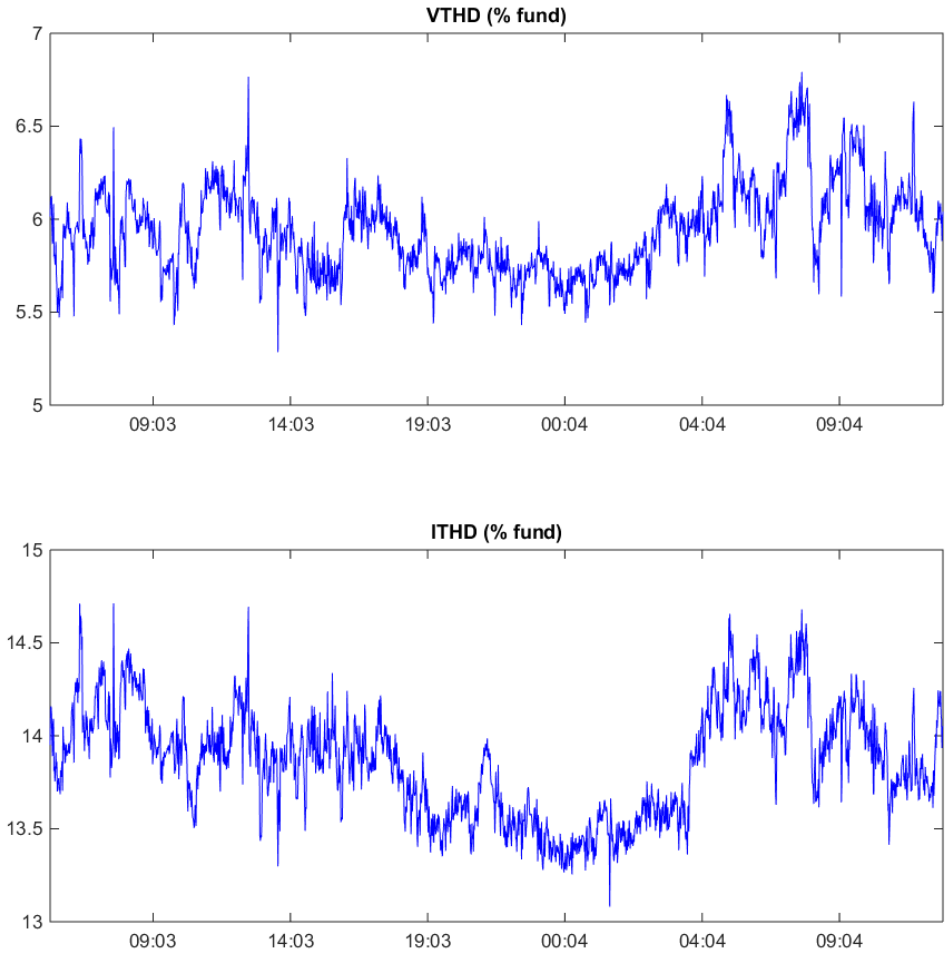

Figure 3.17: Variation in VTHD (upper) and ITHD (lower), up to 2 kHz, over the 30 hour period when Lamp A was connected at site 4.

the 10th and 90th percentile which is higher than in the harmonic range. At this site, both the primary emission at 40 to 60 kHz and secondary emission below 20 kHz are visible. Note that this is mainly primary emission coming from the lamp in the higher frequency range but still the variations are fairly large.

All the spectra were plotted in a spectrogram and the results are shown in Figure 3.20. What can be seen is that the dominant frequency in the primary emission of the lamps shifts over time. The lowest switching frequency changes between 35 and 40 kHz. The variation, not shown

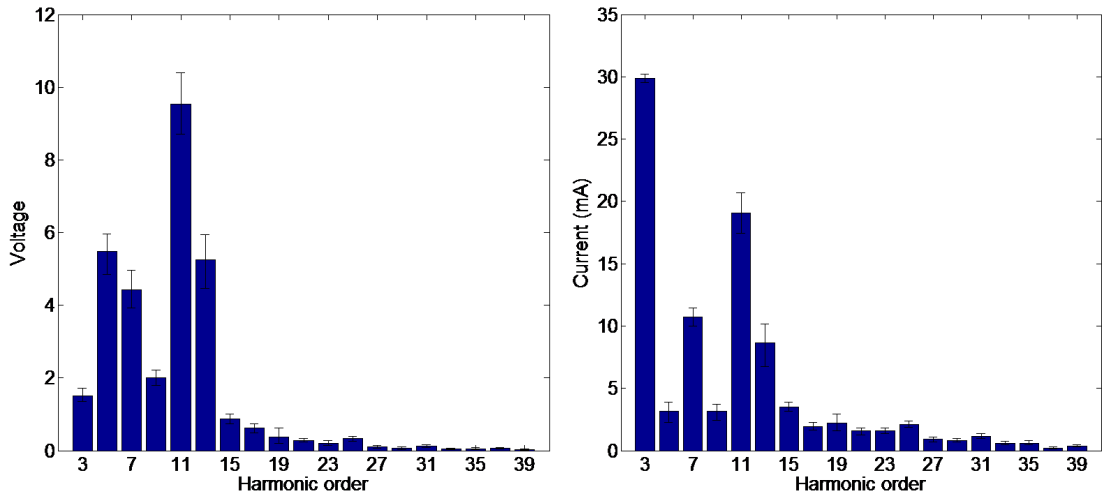

(a) Voltage spectrum

(b) Current spectrum

Figure 3.18: Harmonic spectra of the voltage (left) and current (right) waveforms with the 10th and 90th percentile over a 30 hour period. The 10th to 90th percentile is shown as a vertical whisker on each bar.

here, appears to be strongly correlated with the variation of RMS voltage over time. The frequency spectra are grouped into 200 Hz bands according to equation (3.1) which means that the highest magnitudes will move between frequency bands and cause the variation to look larger in Figure 3.19. The distortion in voltage, around 10 kHz, also increases between 16:00 and 06:00. This change is not that visible in the current. From previous studies it was concluded that it is caused by the fact that the rest of the lights in the workshop are turned off. Since the ordinary lamps at the workshop will act as a filter for some frequency components, this filtering effect will disappear when the ordinary light turns off and the distortion levels in the voltage will increase [34]. The vertical lines visible in both the voltage and current are not yet accounted for.

3.4 Measurement at site 6 with light immunity problem

This measurement was performed at a 7000 m^2 office building, where interference at a light installation was reported. Since the opening of this office in 2009, the lights have not worked properly. The problem with the lighting is that control functions (dimming, corridor and attendance control) don't always work properly. The lamps remain in low dimming mode and the light intensity cannot be increased. Measurements at the office building were carried out at different times, different places

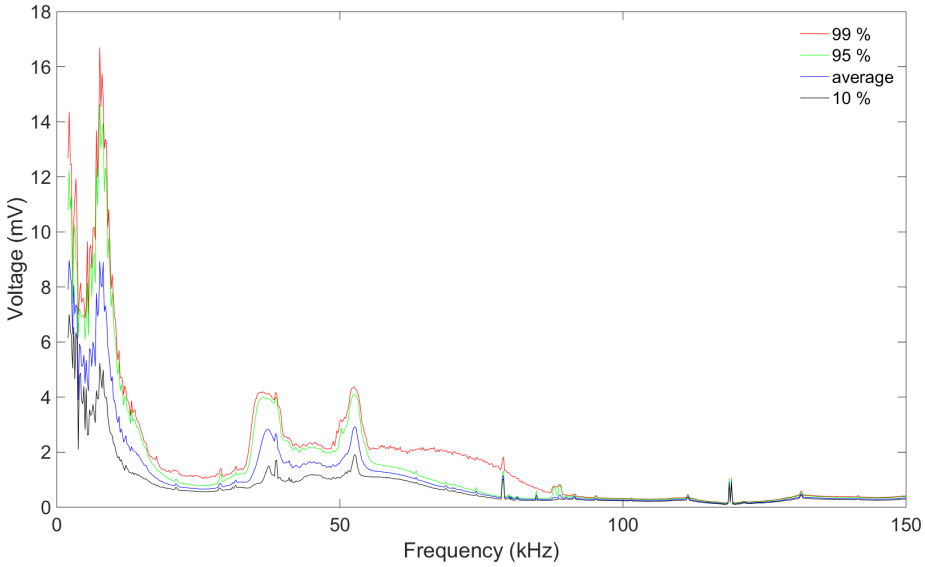

(a) Voltage spectra

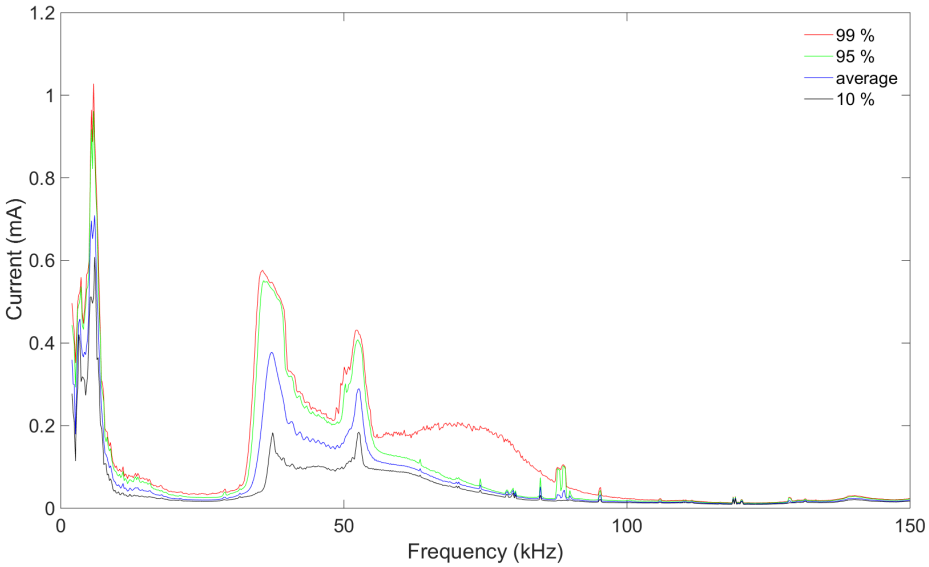

(b) Current spectra

Figure 3.19: Voltage (upper) and current (lower) spectra over time with the 10th percentile (black) average (blue), 95th (green) and 99th (green) percentile shown.

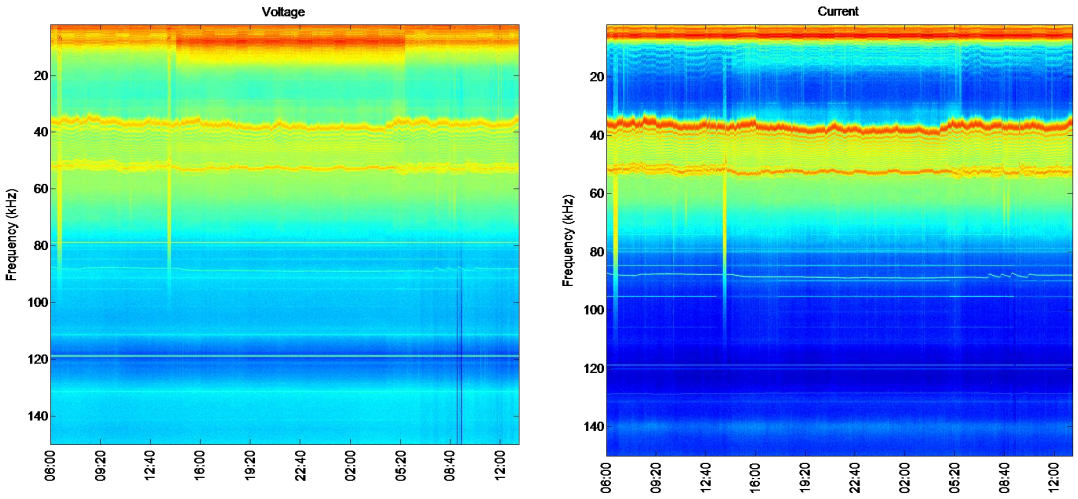

(a) Voltage spectra

(b) Current spectra

Figure 3.20: Voltage (left) and current (right) spectra (2 to 150 kHz) over time, from 6 am to 1 pm the next day (31 hours)

and with different loads connected.

Figure 3.21 below shows a simplified scheme of the electrical installation at the office. The building has two busbars, B1 and R1. Busbar B1 serves general loads in the building, such as computers, light etc. Busbar R1 is used for preferential loads such as sprinklers, ventilation, elevators etc. which are backed up by a reserve generator (G). Additionally, there is also a server hall connected to this busbar, via two online UPS.

The upper left waveform in Figure 3.22 shows the voltage at the connection point of the fluorescent light during normal operation in one office. As can be seen, the voltage waveform is heavily distorted, at least for this type of load (office-building). The waveform contains several notches over a one-cycle period. A trial was preformed where the backup generator was started and busbar R1 was disconnected from B1. The result from a measurement of the voltage waveform at the same office, during this trial, is shown in the upper right waveform in Figure 3.22. The waveform shown in the bottom half of Figure 3.22 is the difference in voltage waveform before and after disconnection of R1. The result shows that the lamp is exposed to recurrent voltage peaks of about 40 V.

Some parameters obtained from the voltage waveform are shown in Table 3.1. In the harmonic range, both VTHD and the highest individual harmonic (H7) drop more than 3 times after

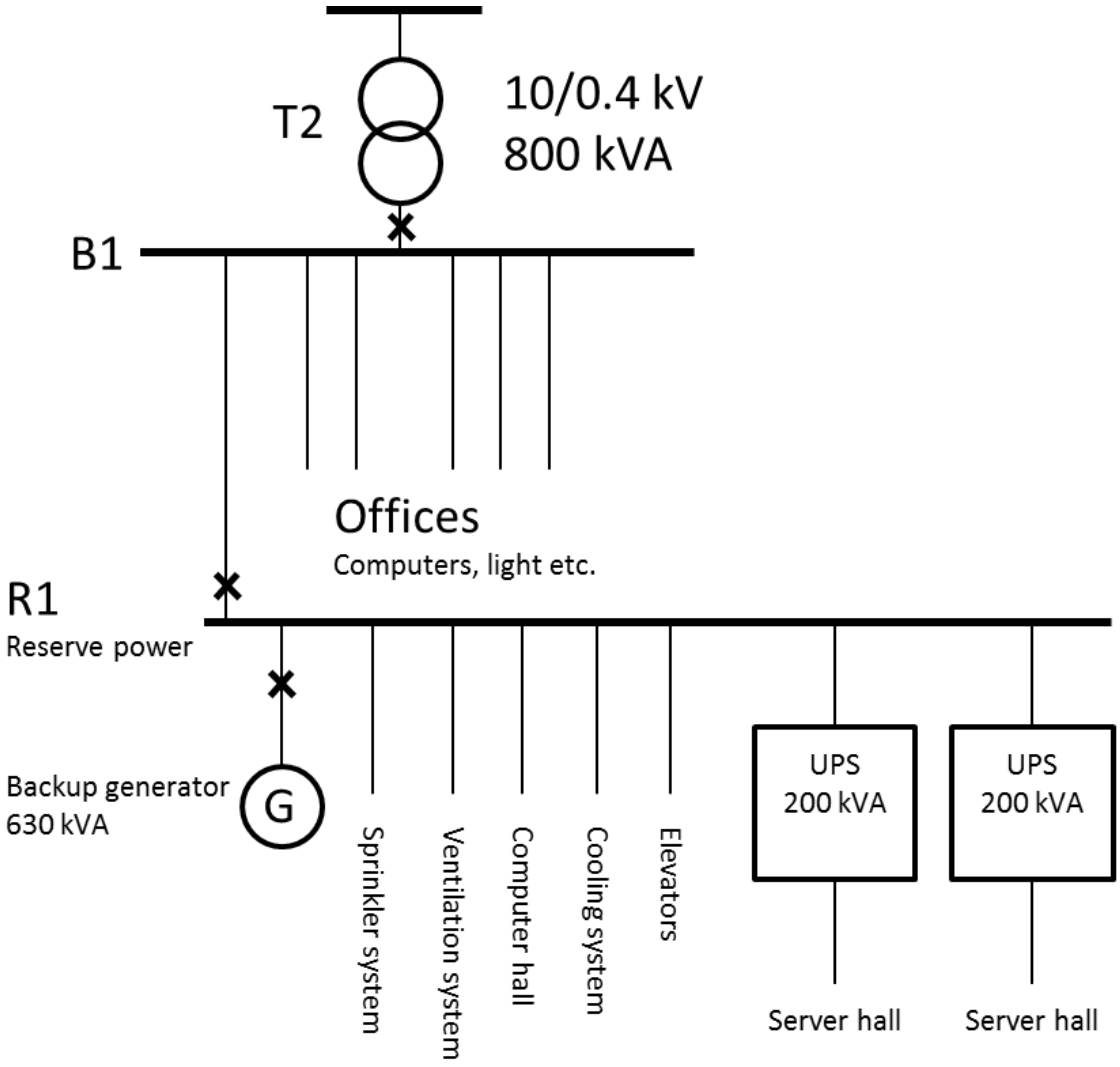

Figure 3.21: Schematic layout of the electrical system in the office building.

disconnecting busbar R1. While busbar R1 was disconnected all lamps at the office worked perfectly.

In the frequency range between 2 and 9 kHz, VTHD drops around 7 times and between 9 and 150 kHz, VTHD drops more than 2 times while the UPS is supplied from the generator. This indicates that the largest change in distortion takes place between 2 and 9 kHz. The left graph of Figure 3.23 shows the resulting harmonic spectra, before (blue) and after (red) disconnecting R1. From the harmonic spectra we notice that the characteristic harmonics are $h = n \bullet 6 \pm 1$, which is indicative of a 6-pulse rectifier creating the voltage distortion. The largest change among the characteristic harmonics is H19 which reduces about 10 times between the two measurements.

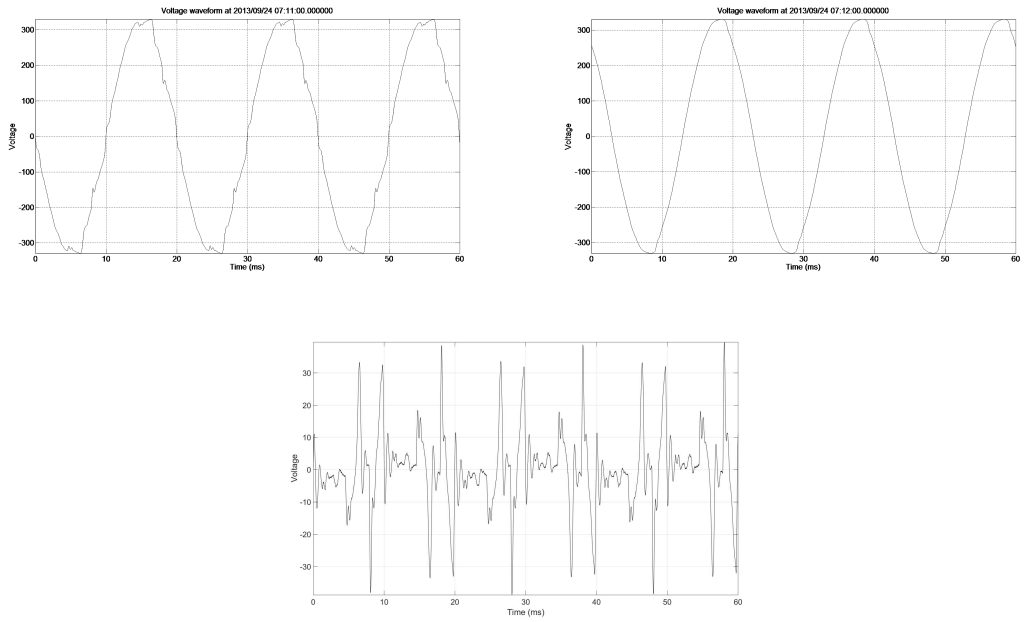

Figure 3.22: Voltage waveform at the connection point of a fluorescent lamp in one of the offices before disconnecting the UPSs (upper left) and after (upper right). Resulting waveform (bottom) when subtracting the waveform before disconnection from the waveform after

Table 3.1: Parameters from voltage waveform

% of fund.	VTHD	H7	VTHD($2-9\,\mathrm{kHz}$)	VTHD($9-150\,\mathrm{kHz}$)
Before	5.1	3.1	0.84	0.18
After	1.6	0.93	0.12	0.085

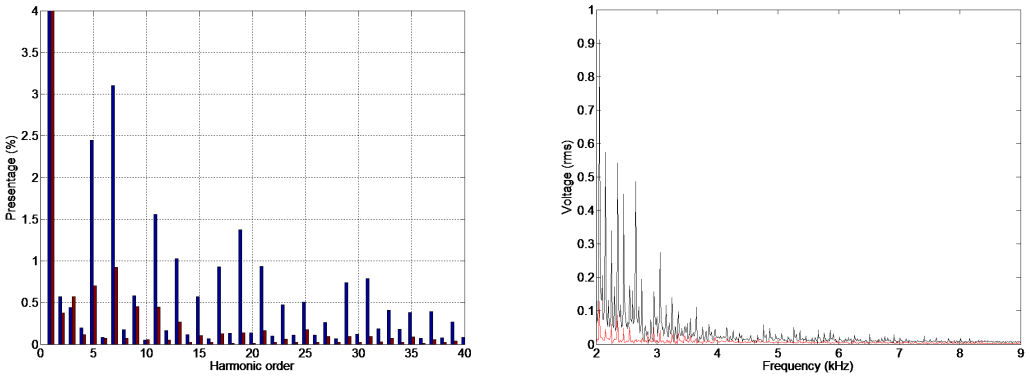

Figure 3.23: Harmonic spectra before (blue) and after (red) busbar R1 was disconnected (left) and spectra between 2 and 9 kHz before (black) and after (red) busbar R1 was disconnected (right)

When comparing the measured harmonic spectra of the voltage waveform with immunity test levels given by IEC $61000-4-13$, the individual harmonics at the lamp terminals are all below class 1 test levels. These test levels are intended for immunity test of very sensitive equipment. The voltage measurement shown in the top half of Figure 3.22 above was performed with a sampling speed of 200 kS/ s. The resulting DFT of the measured windows, before (black) and after (red), is shown below in Figure 3.23. In the lower part of the higher frequency range, between 2 and 9 kHz, there is clearly also a drop in emission between the measurements

The reason why there is a large variation between harmonics 15 and 21 is not yet fully understood but since more loads, other than the UPS were disconnected at the same moment, it might have been related to some of those loads.

The spectra of the two measurements, between 9 and 150 kHz, are not shown here since this part of the spectra does not reveal any large differences, as indicated by VTHD ($9-150$ kHz) in Table 3.1. When comparing the spectra between 2 to 9 kHz with the lowest immunity test levels given by IEC $61000-4-19$ the only component that is higher, is at 2055 Hz. Note that both above-mentioned immunity test standards do not apply to lighting equipment.

During the test, when busbar R1 was disconnected from B1 and instead fed from the backup generator, a measurement of the voltage and current feeding one of the 200 kVA UPS's was carried out. The voltage and current drawn by the UPS are shown in Figure 3.24. The result shows that the UPS system is most likely the cause of the voltage distortion in the office. Note that the waveform distortion is much larger due to higher (mostly inductive) source impedance. The current shows a

typical pattern for a six pulse diode or thyristor rectifier with a voltage stiff DC link. The differences in magnitude of the current pulses are most likely due to an unbalanced voltage supply.

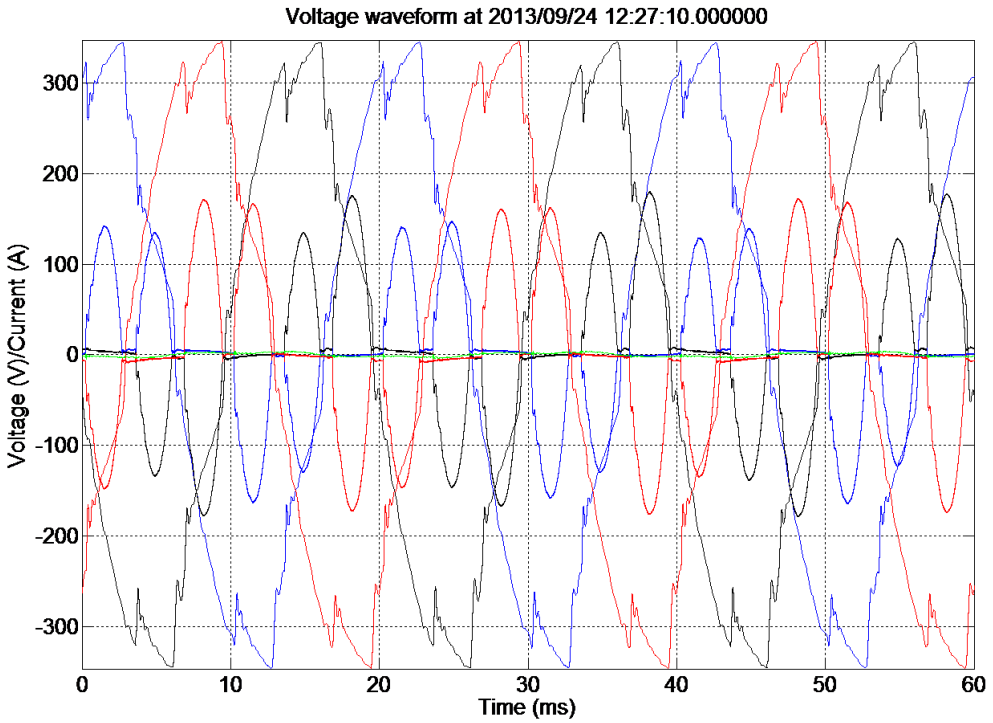

Figure 3.24: Voltage and current waveform at bus-bar R1 when running on backup generator (G). Note that the voltage and current are indicative of the six pulse rectifier from the two online UPS's indicated in Figure 3.21.

During the test of disconnection of busbar R1, for a couple of hours it was reported that the light dimming was functioning properly in the office rooms. To handle the problem, it was decided in this case to reconfigure the feeders at the office to minimize the disturbances from the UPS's. Note that when busbar R1 is disconnected, the distortion for the islanded load is very high and another study is most likely needed to find out if this can endanger reliability during island operation. After the measurement at the office, one of the lamps from the office was installed in the lab. From the voltage measurement at the office the distortion was filtered out and applied in the same manner as described in chapter 4. The result was that the lamp started to show the same immunity issue. More information about these results can be found in [33].

3.5 Conclusions from measurements

From the measurements performed with the different lamps shown above, it is clear the lamps produce different types of emission (primary emission), especially in the higher frequency range. The current waveform also shows a different appearance. In the harmonic range, the waveform distortion is similar for the different types of lamps and the levels seem at least, to be about the same for all of these, independent of the power rating.

When placing a lamp at different sites it is clear that the electrical environment has an effect. This is because the background voltage distortion or secondary emission affects the current drawn by the lamp. In the harmonic range and in the high frequency range the current waveform will be affected. There is also a variation of this secondary emission over time which is explained by equipment in the same low-voltage installation being turned 'ON' and 'OFF' which affects both the background voltage distortion and the grid impedance.

A case where an immunity problem was reported was also described. It was found out that it was a UPS system that was causing the problem. The current drawn by the UPS system caused notches or recurrent oscillations in the voltage which resulted in malfunction of the dimmer function for fluorescent lights in an office complex. The malfunctioning lamps where brought to the laboratory where they were tested with a similar voltage causing the same problem in the test set up.

Chapter 4

Interference with LED lamps

Chapter 3 showed the results from field measurements in the power system in Sweden. The existing background distortion present in the grid was characterized along with the current harmonic emission from LED lamps. A case study where background distortion interfered with the working of LED lamps was also presented. In this chapter, the interference observed from high frequencies with LED lamps and dimmers is presented and characterized through a series of laboratory experiments. The voltage waveforms recorded in the grid (explained in the previous chapter) were applied to commercially available LED lamps and the light output was measured in each case. Changes in light output that resulted have been shown. For the benefit of the reader, the components of light output and their impact on the end user have been explained in the appropriate sections.

4.1 High frequency distortion

In order to understand the effects of high frequency distortion (2 kHz to 150 kHz) on LED lamps, various voltage and current waveforms were captured at different locations in the Swedish power grid. Out of these, two representative signals were chosen and the low frequency components in the voltage were removed using a digital high pass filter with a cut off frequency of 500 Hz [5]. These waveforms were reproduced in a laboratory environment, amplified to match the limits for PLC in this frequency range, and superimposed onto the grid voltage. The resulting voltage signals were applied to commercially available LED lamps; voltage, current and illumination were measured with high time resolution. The high frequency components of the signals used to test equipment

response to high frequency distortion are described next.

4.1.1 Test signal 1

The time domain signal (plotted up to 40 ms, but periodic in time and measured for 200 ms), its spectrum and a plot of frequency components versus time (spectrogram) for the first signal (referred to as 'test signal 1' throughout this thesis) are shown in Figure 4.1.The spectrogram is a short time fourier transform (STFT) that is implemented using Matlab. DFT of the signals was calculated by using 10000 points, corresponding to 1 ms. The signal was sectioned to perform windowing and a 5000 point overlap was used between the various sections. An estimate of the short term, time-localized frequency content of the signal is returned by this operation. The spectrogram uses different colors for different magnitude, with yellow representing the highest and blue the lowest magnitude (see color scale in figure). The spectrogram of the signal shows that the dominant high frequency components of this signal are found between 2 and 50 kHz.

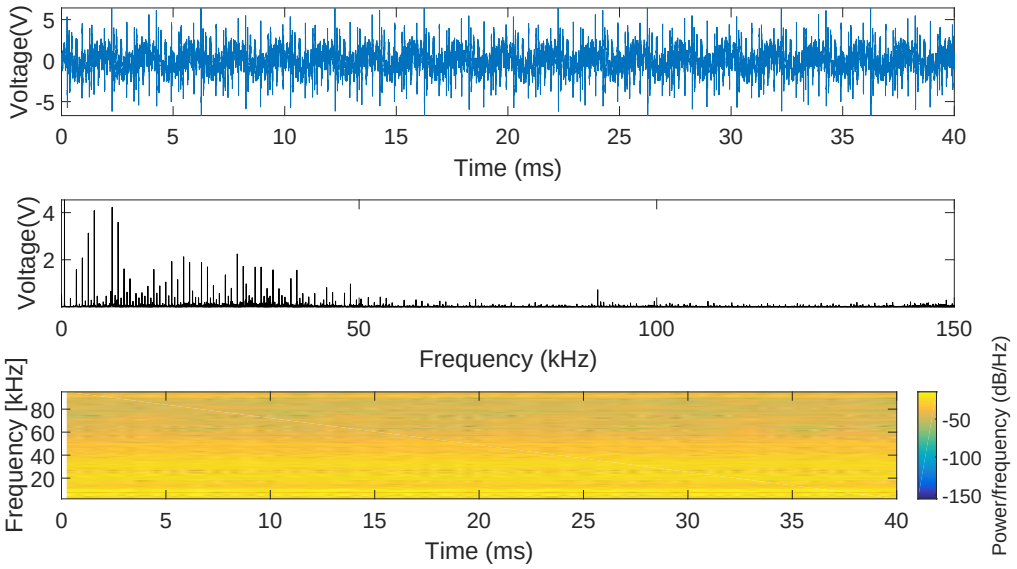

Figure 4.1: High frequency distortion test signal 1 (top), spectrum of test signal 1 (middle) and spectrogram of test signal 1 (bottom).

More importantly, this disturbance, when superimposed on to the supply voltage wave, appears as uniformly distributed noise in the time domain. In the frequency domain, the signal

appears as a broadband component between 2 kHz and 50 kHz.

4.1.2 Test signal 2

The second signal superimposed onto the background voltage contains dominant frequency components between 40 and 80 kHz. The signal was recorded at a commercial establishment and is shown in Figure 4.2. This signal is referred to as 'test signal 2' throughout the rest of this thesis.

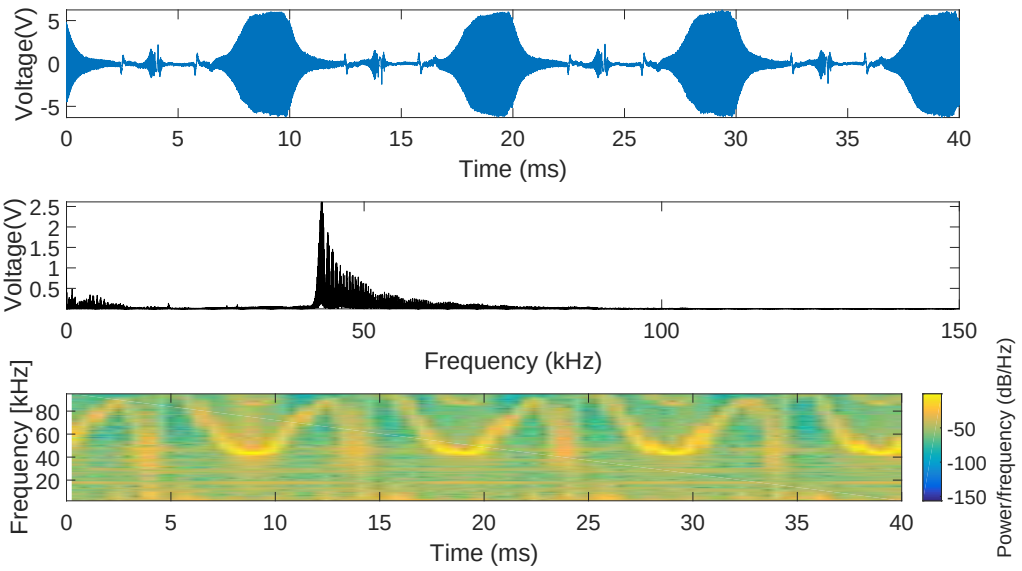

Figure 4.2: High frequency distortion test signal 2 (top), spectrum of test signal 2 (middle) and spectrogram of test signal 2 (bottom).

The spectrogram of test signal 2 shows that the dominant frequency components do not hold steady with time. Rather, these components shift frequency with time. The envelope of oscillating frequencies lies between 40 and 90 kHz. The signal, in time domain, appears as a disturbance that is clustered in one part of the fundamental supply voltage wave and therefore has point-on-wave characteristics.

4.1.3 Signal conditioning

The measured voltage waveform obtained from the field measurements was reproduced in the laboratory, amplified and superimposed onto the grid voltage via a Coupling and Decoupling

Network (CDN) as specified in IEC standard $61000-4-19$ [1]. Before being placed on the input terminals of the CDN, the high frequency distortion was adjusted in amplitude (peak) to match the peak limits for PLC in this frequency range. The incoming voltage from the grid and the high frequency distortion that was superimposed were not synchronized to each other. The 'point on wave' at which the high frequency distortion was applied was floating along the fundamental frequency wave. This was done so as to understand whether the point on the fundamental waveform where the distortion was applied, had any effect on the equipment under test (i.e., LED lamps).

The voltage at the terminals (the 'lamp voltage') is obtained as the sum of the grid voltage and the injected signal. All voltage and currents shown in the remainder of this thesis are measured at the lamp terminals, unless specified otherwise. The light output from the LED lamp was then measured in three different operating conditions: (*i*) voltage containing only background distortion from the incoming voltage; (*ii*) test signal 1 superimposed onto the background voltage and (*iii*) test signal 2 superimposed onto the background voltage. Recall that all the tests were conducted in the laboratory, whose background distortion characteristics have been explained in considerable detail in the previous chapter.

In order to decide how much peak distortion voltage could be added, the existing emission standards for the high frequency range were used as suggested by Bollen et al. in [21]. In particular, the European voltage characteristics standard EN 50160 was used for this purpose. Based upon this standard, the distortion signal was amplified to have a peak amplitude under 1.5% of the fundamental peak voltage (for any individual frequency component), obtained over a 200 ms without grouping.

4.2 Experimental setup and measurement apparatus

4.2.1 Experimental setup

The experimental setup used for this project was designed in accordance with IEC $61000-4-19$ as described earlier. The quantities measured were input voltage and current, input distortion signal from the signal generator and the light output from the LED lamp. A simplified layout is shown in Figure 4.3. Note that in this case 'EUT' refers to Equipment Under Test, which is the LED lamp under test.

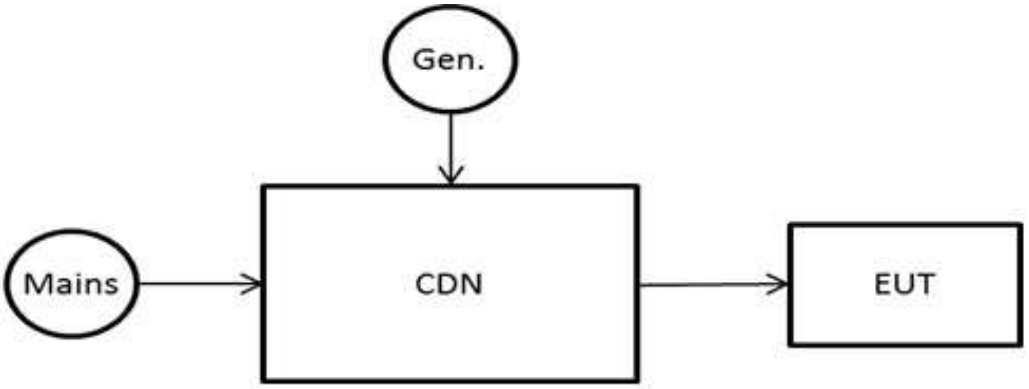

Figure 4.3: Laboratory setup for testing light equipment for immunity against high frequency distortion.

4.2.2 Measurement apparatus

The measurement apparatus used in these tests has been described previously. In addition to the measurement probes, another crucial component of the test setup was the light meter used to measure light output from the LED lamps. The light meter used for measurements was a Hagner S2 universal photometer. The maximum measurement range of the instrument is 200 lux (abbreviated 'lx' from here forward). The basic light sensitive components of the photometer are two silicon diodes, filtered to give a spectral response close to that of the human eye, as defined in CIE standards. One (internal) detector is built into the optical system for measuring luminance within a 1° circular field (viewing field approx 11° circular). The other (external) detector, which is cosine corrected and connected to the instrument by a flexible lead, is used for measuring illuminance. The internal detector on the instrument has been used in this set of experiments since its meant for scanning for luminance variations. More details about the instrument can be accessed at [35].

As before ,the instrument used for recording voltage and current waveforms was a Yokogawa DL 850 and a maximum sampling frequency of 10 MS/ s was used for these measurements.

Two types of measurements were performed:

1. 200 ms measurement window to record the spectrum of input voltage, current and light inten-

sity.

2. 30 s window for analyzing long term light intensity variations.

While measuring the 30 s window, the instrument automatically reduced the sampling speed to 50 kS/ s. In the case of these tests, only magnitude variations in light output were considered because of this limitation in sampling speed.

4.2.3 Lamps tested

For the purpose of this study, LED lamps of various representative sizes were purchased from 3 different commercial establishments in Sweden. The lamps represented 5 manufacturers and have been listed in Appendix A. For the purpose of reference throughout this thesis, each lamp has been addressed by its serial number as mentioned in the Appendix. The power range of the lamps tested was 0.9 W to 12 W and 32 lamps were tested. These lamps had a mix of dimmable and non-dimmable lamps and the majority of lamps produced white light, with 2 non-white lamps (red and blue respectively) also tested.

4.3 Illuminance measurements

The amount of radiation emitted by a lamp is referred to as the 'radiant flux' and this covers all wavelengths. As our eyes are not sensitive to all the frequencies in the same way, the radiation is weighted with the sensitivity of our eyes for different wavelengths and therefore the term 'luminous flux' is used instead. The luminous flux is measured in 'lumen' and the lumen rating of all the lamps used in this project has been indicated in Appendix A. Illuminance (or light intensity) is the amount of light that falls onto a given area. Illuminance is measured in lux (lx) [14]. The relationship between lux (lx) and lumen (lm) is given by:

$$E_v(\,\mathrm{lx}) = \frac{\varphi_v(\,\mathrm{lm})}{A(\,\mathrm{m}^2)} \tag{4.1}$$

Where E_v is illuminance in lx and φ_v is the luminous flux in lm and A is the surface area in square meters (m^2). For a spherical surface area, we can write:

$$E_v(\,\mathrm{lx}) = \frac{\varphi_v(\,\mathrm{lm})}{4\pi r^2(\,\mathrm{m}^2)} \tag{4.2}$$

Where r is the radius of the spherical area, measured in meters (m). For the purposes of this document, all light outputs have been indicated in lux (lx). Our interest was primarily in the variation of light with time as opposed to its absolute value. This variation was measured against the average value of light under voltage conditions where no distortion is present in the source voltage. This has been indicated in the appropriate sections which deal with light intensity variation.

4.4 Results of light measurement

4.4.1 Light output with background distortion only

In the domain of lighting, it is generally accepted that the light output from electrical sources consists of two parts: average light output and a modulation in the light output, at twice the line frequency of 50/60 Hz. In the past decades, light flicker has been a subject of considerable research. However, with the advent of LED lamps, the nature of problems in lighting is likely to shift. Poplawski and Miller [36, 37] have shown that the modulation component of light can be drastically different in solid state lighting. Their research work shows that the wave shape and the amount of modulation being produced by LED lamps can be much higher in comparison to incandescent bulbs. This can be observed in Figures 4.4-4.7. Figure 4.4 shows the input voltage, current and light output of a 100 W incandescent light bulb. In all cases, the voltages and currents are the ones measured at the terminals of the LED lamp, unless indicated otherwise. No dimmer was used in any case, unless specifically indicated. The light output signatures and waveshapes observed with LED lamps of different manufacturers are shown next. For brevity, lamps 8, 24 and 27 have been shown here. These three lamps have the same input power rating but are made by three different manufacturers. Lamp 27 has a manufacturer claimed input power factor (p.f) of 0.95 and it can be seen in Figure 4.7 that the current and voltage of the lamp have a very small phase difference between them. Three other lamps from the same manufacturer have these same characteristics also (refer to Appendix A). It is seen that in comparison with an incandescent lamp, the modulation produced by an LED lamp is less sinusoidal. The modulation produced by an incandescent bulb is

almost purely sinusoidal whereas the modulation produced by LED lamps has a completely different shape.

LED lamps utilize DC-DC converters as their drivers. The light output of a light emitting diode is proportional to the forward current through it. Therefore, the modulation in light output from an LED is indicative of the current ripple in the output stage of the converter feeding the LED array. It is observed from Figures 4.4-4.7 that this ripple has different shapes. The input current waveforms of these three LED lamps are also different. Therefore, it can be concluded that the light output is a byproduct of the LED driver circuit configuration. It is possible to design these converters such that the light output contains only a DC component. This was the case in 8 lamps out of the 32 lamps tested. However, in the other 24 lamps (75%), a ripple between a few percent and 60% was observed in light. It was observed that the light output wave was identical in shape for various lamps produced by the same manufacturer.

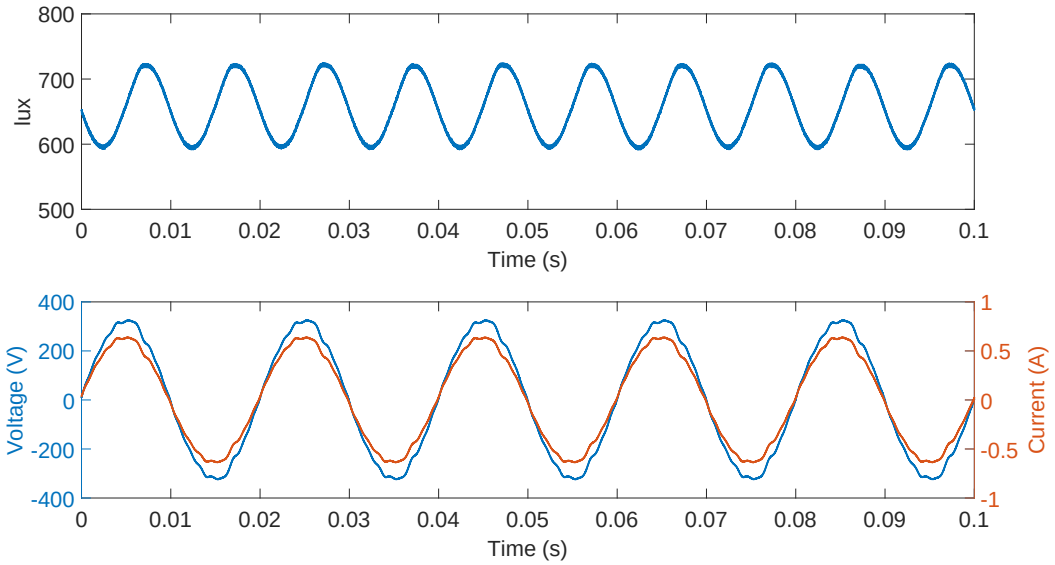

Figure 4.4: Illuminance plotted against time for 100 W incandescent lamp (top) along with input voltage and current (bottom).

A better metric for comparing these waveshapes is the spectrum of the light output which is shown in Figure 4.8. The incandescent lamp light output contains a DC component (the average light output) as the dominant element and a 100 Hz modulation (twice the power system frequency) as an additional component. In comparison, the light output from an LED lamp contains all these

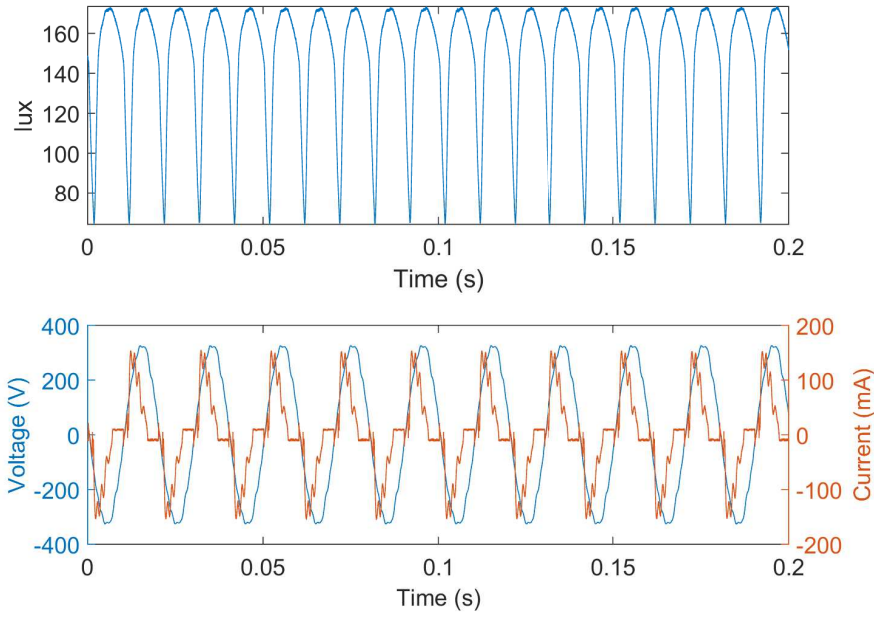

Figure 4.5: Illuminance plotted against time for lamp 8 (top) along with input voltage and current (bottom).

components and it also contains frequency components at integer multiples of 100 Hz. This results from a non-sinusoidal ripple in the output stage of the LED driver. For these reasons, while analyzing the impact of high frequency distortion on the light output from these lamps, in the remainder of this thesis the modulation component is analyzed separately from the average light output. Later on in this chapter, various methods to characterize the light output modulation have been presented along with a discussion of the impacts on health from this modulation.

4.4.2 Effects of high frequency distortion - short term variations

Utilizing the CDN described in the previous sections, a voltage containing high frequency distortion was applied at the terminals of the LED lamps. The light output from the LED lamps was then compared for three cases:

- Background distortion.
- Test signal 1.
- Test signal 2.

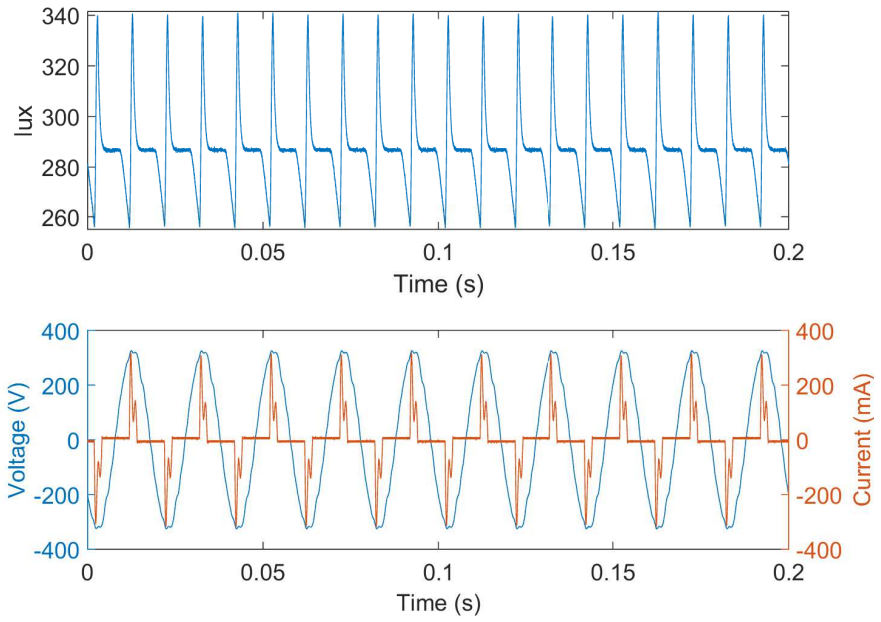

Figure 4.6: Illuminance plotted against time for lamp 24 (top) along with input voltage and current (bottom).

This comparison is shown for the three lamps mentioned previously. The impact of high frequency distortion on the average light output and modulation of light output is analyzed separately for each lamp.

For lamp 8, the spectrum of light output in the three cases is shown in Figure 4.9. It can be seen from Figure 4.9, that the presence of high frequency distortion in the supply voltage causes the light output to drop in magnitude for this lamp. This drop is noticed in both the average light output (this is the DC quantity in the spectrum) as well as the modulation of light.

When normalized against the light output with background distortion, it was observed that the reduction in the average light output was about 1.25% with Test signal 1 and about 9.5% with test signal 2. This data is summarized in Table 4.1 for the average light output for the three lamps. Figures 4.10 and 4.11 show the impact on light output from lamps 24 and 27 respectively. For lamp 24 it is seen that the high frequency distortion causes the average light output to drop as before and the modulation of light output to get almost completely attenuated (Notice that frequency components apart from DC have almost zero magnitude with test signals 1 and 2). It was noticed that lamp 27 showed minimum impact of high frequency interference with the average light output

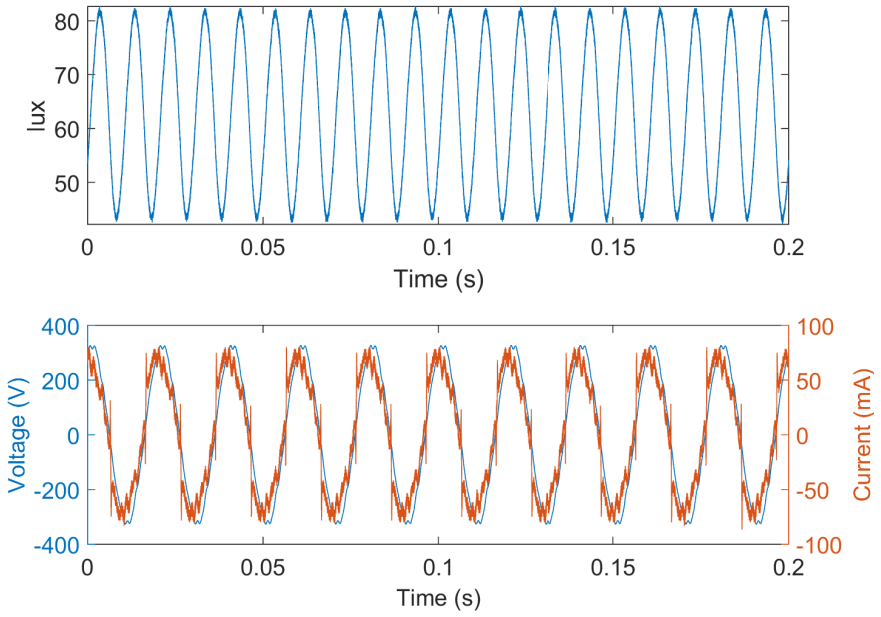

Figure 4.7: Illuminance plotted against time for lamp 27 (top) along with input voltage and current (bottom).

Table 4.1: Average light output from lamp 8 in the three operating conditions

Lamp Number	Background distortion (lx)	Test Signal 1 (as % of original)	Test Signal 2 (as % of original)
8	208	98.7	90.5
24	406	98.3	95
27	89	99.5	99.7

(both average light output and modulation). This can be seen from both, Table 4.1 and Figure 4.11. The spectrum of light output from lamp 27 shows minimum change in the average light output and the modulation components.

As a final important note, the impact of high frequency distortion on the modulation envelope of light is presented in Table 4.2. It is noted that in the case of lamp 8, the reduction in modulation is about 15% due to test signal 1 and about 20% due to test signal 2. On the other hand, the reduction in the modulation is fairly large in the case of lamp 24, as the ripple component gets attenuated by more than 90% in each case. Conversely, lamp 27 shows hardly any change in the ripple output in the three cases.

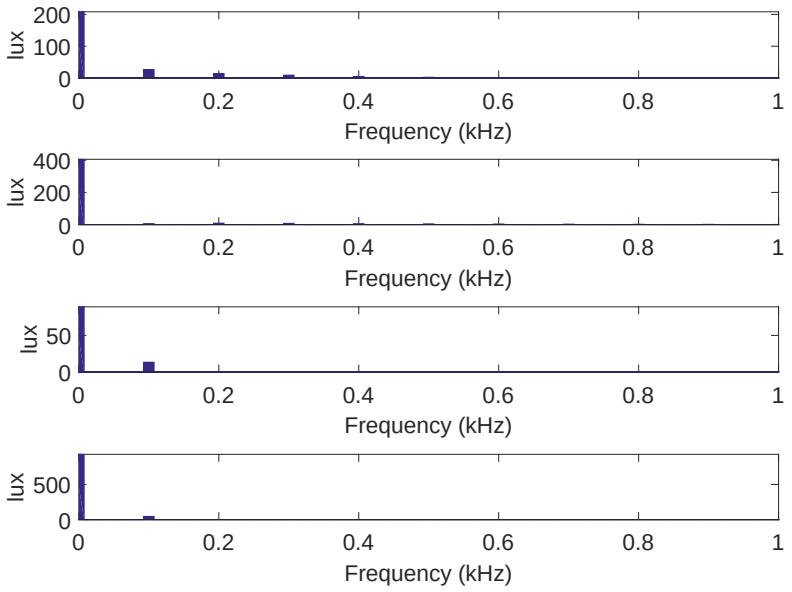

Figure 4.8: Spectrum of light output for lamp 8 (top), lamp 24 (second from top), lamp 27 (third from top) and a 100 W incandescent lamp (bottom)

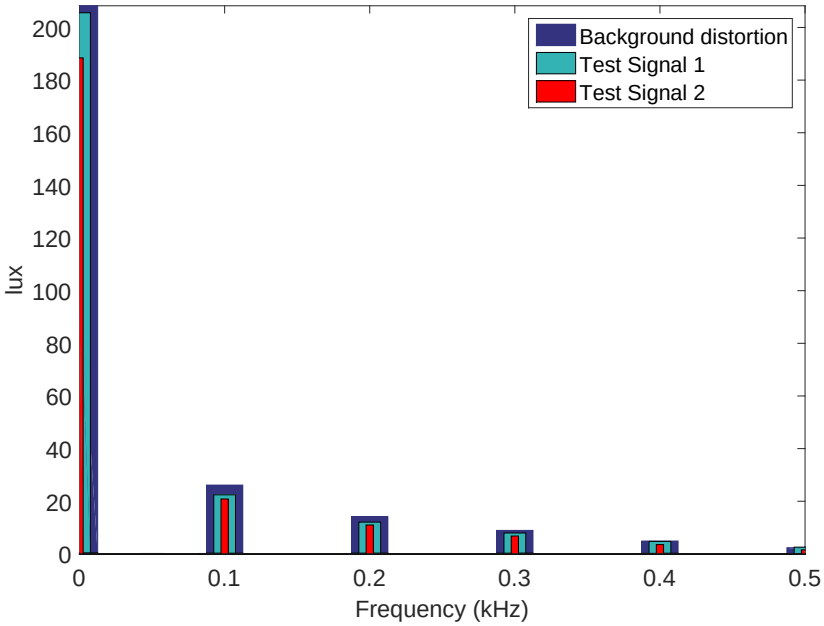

Figure 4.9: Spectrum of light output from lamp 8 in three cases.

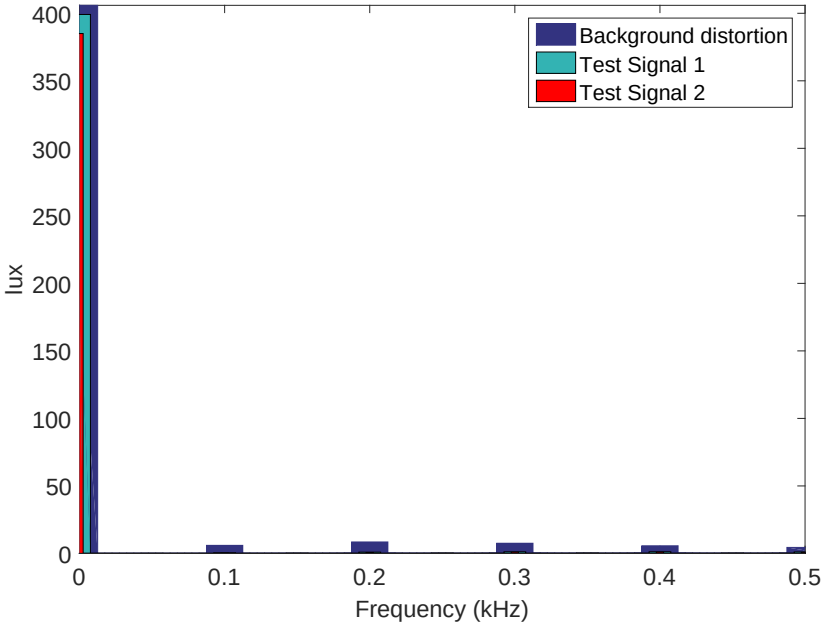

Figure 4.10: Spectrum of light output from lamp 24 in three cases.

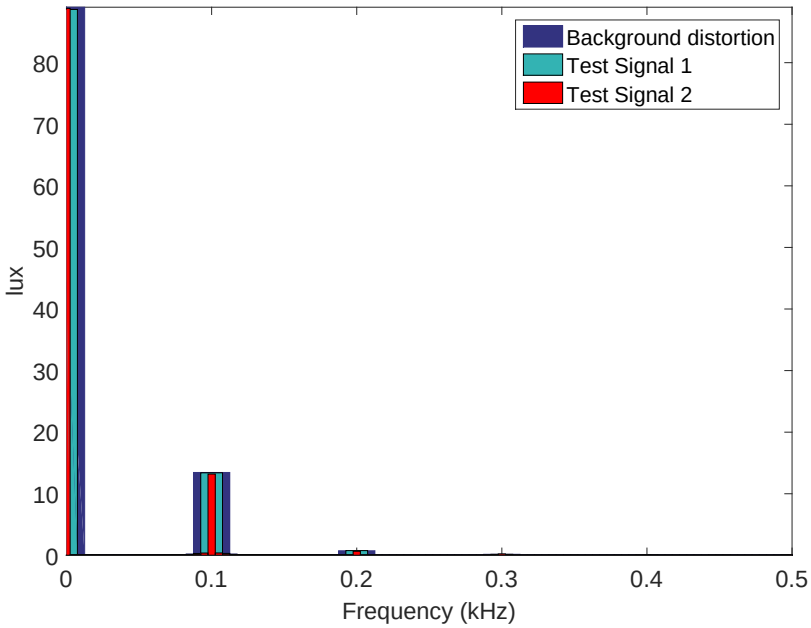

Figure 4.11: Spectrum of light output from lamp 27 in three cases.

Table 4.2: Modulation of light output in the three operating conditions

Lamp Number	Background distortion (lx)	Test Signal 1 (as % of original)	Test Signal 2 (as % of original)
8	26.1376	86	80
24	6	7.5	5.3
27	13.4	99.5	98.1

4.4.3 Effects of high frequency distortion - Long term variations

A look at the envelope of light observed over 30 s shows that the light output also contains slow moving components. The 30 s envelope of light observed with and without the two test signals superimposed on to the background voltage have been shown in Figure 4.12 for lamp 8. This plot of light output shows that the light output has fast variations when the two test signals are superimposed onto the test voltage. There are also slow variations in light output with time. These slow variations can be better understood on the basis of the average light output. The average light output, taken over each single cycle (20 ms) for 1500 cycles is shown in Figure 4.13. Figure 4.13 shows that the average light output gets reduced with the introduction of high frequency distortion in the source voltage. However, this reduction is not uniform either. It is seen that test signal 2 causes the light output to vary slowly between 0 and 10 s and then again between 20 and 30 s. The factors that cause this slow variation and their quantification are explained in subsequent chapters.

Similar plots have been shown for lamp 24 in Figures 4.14 and 4.15.

In the case of lamp 24, two bursts of light are observed in Figure 4.14 with test signal 2, similar to Figure 4.13. Unlike lamp 8 however, these bursts do not show up in the plots of average light output, shown in Figure 4.15. This is because, in the case of lamp 24, the slow variation is observed in the case of the modulation. The average light output gets reduced in magnitude as before. However, the ripple component not only gets attenuated but also shows variation in this attenuation (Recall that in the case of lamp 8, similar variation was observed in average light output). These 'bursts' in modulation have been analyzed subsequently.

Finally, the variation in light output with lamp 27 is presented in Figures 4.16 and 4.17.

In the case of lamp 27, it is observed that the lamp shows very low sensitivity to high frequency distortion in the supply voltage. The average light output remains steady in all three cases at a near-identical value. This characteristic was observed in about 20% of the lamps that were tested. The data indicating change in the average light output, in the case of all 32 lamps is

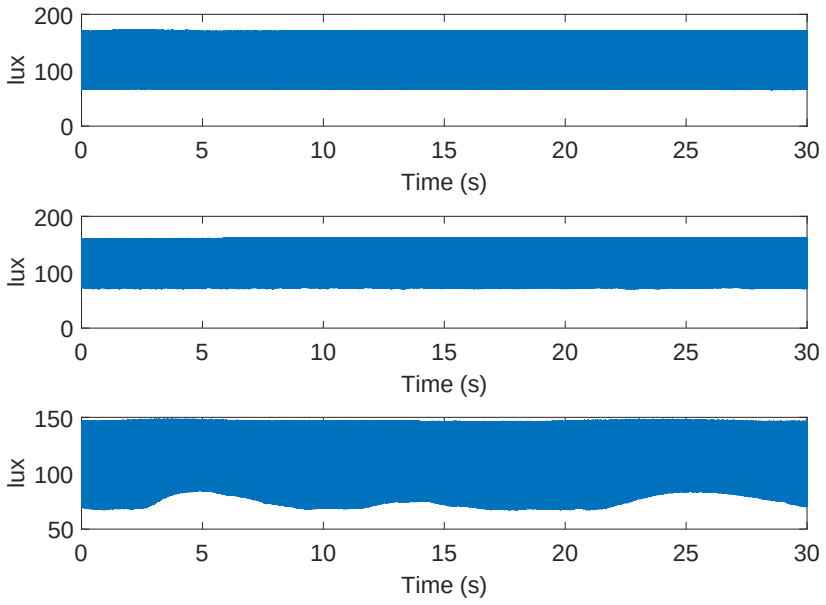

Figure 4.12: Light output recorded over 30 s for lamp 8 for three cases: background voltage (top), test signal 1 (middle) and test signal 2 (bottom)

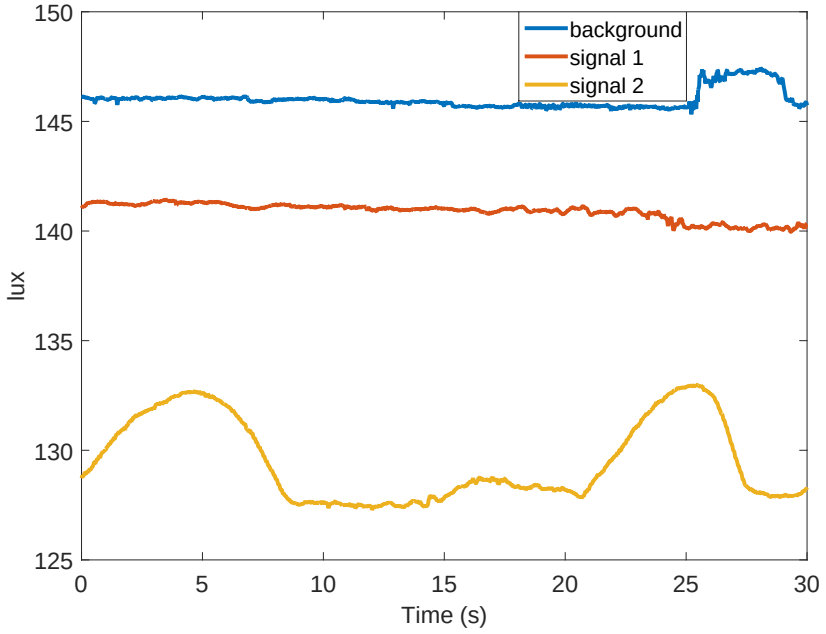

Figure 4.13: Average light output recorded over 30 s for lamp 8 for the three cases.

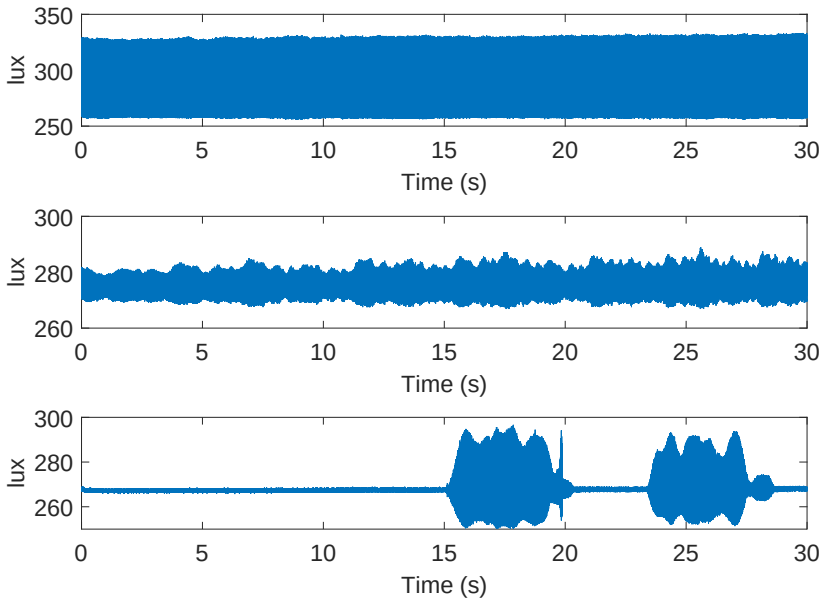

Figure 4.14: Light output recorded over 30 s for lamp 24 for three cases: background voltage (top), test signal 1 (middle) and test signal 2 (bottom)

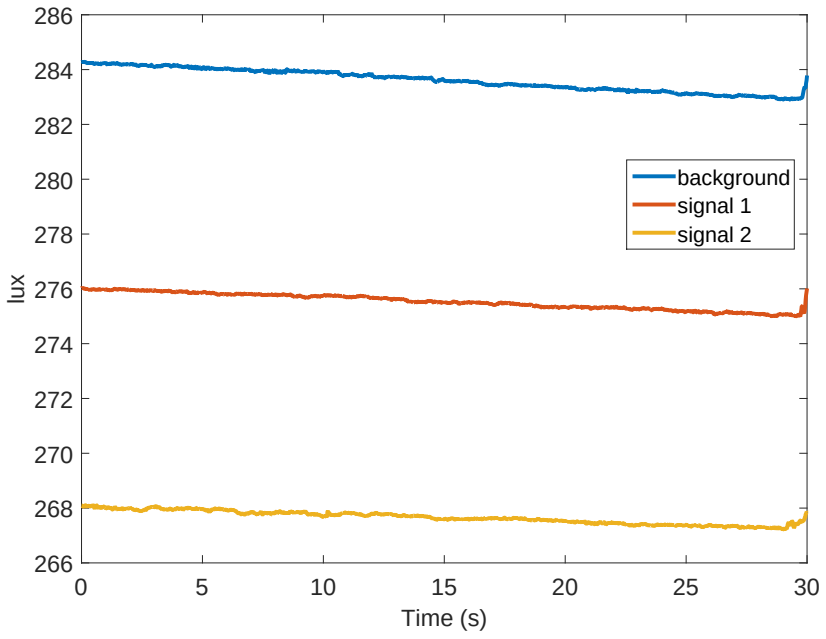

Figure 4.15: Average light output recorded over 30 s for lamp 24 for the three cases.

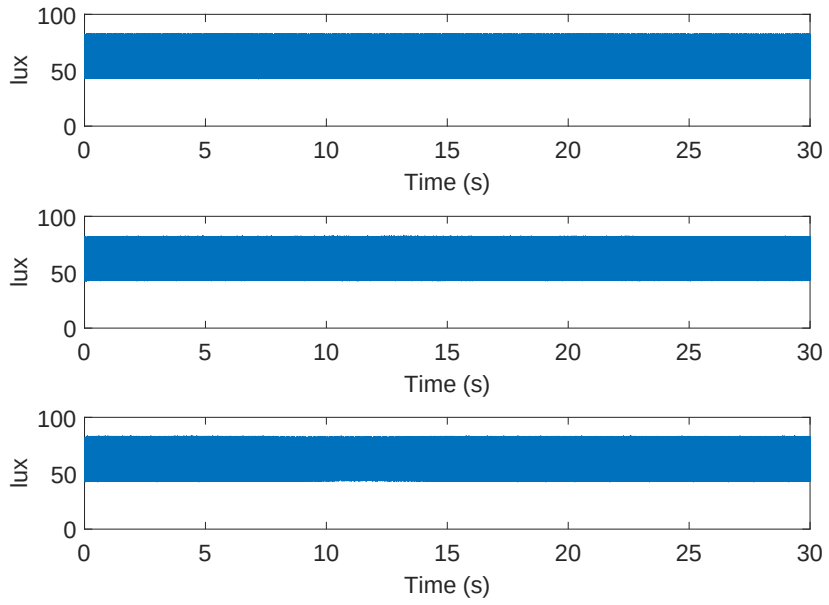

Figure 4.16: Light output recorded over 30 s for lamp 27 for three cases: background voltage (top), test signal 1 (middle) and test signal 2 (bottom)

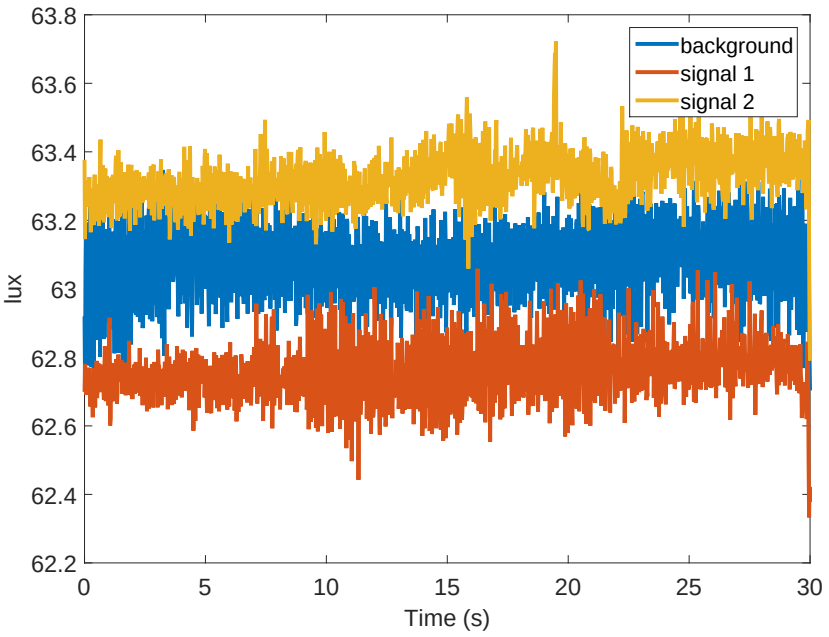

Figure 4.17: Average light output recorded over 30 s for lamp 27 for the three cases.

summarized in Table 4.3.

Column 1 of the table shows the value of average light output with background distortion only, while columns 2 and 3 show the value with distortion present, normalized against the light output with background distortion. This table indicates that in about 80% of the cases, the average light output gets suppressed due to the introduction of high frequency distortion in supply. This reduction can be as large as 50%, but in most cases is generally around $9 - 10\%$. This, coupled with the suppression of the 100 Hz component, which is the dominant frequency component in the modulation, then leads to a reduction in the light output from the lamp. In the remaining 20% cases, the light output was observed to increase, either with test signal 1, test signal 2 or both.

4.5 Effects on LED lamp input current

The light output of an LED lamp depends on the amount of forward current through the LED. In order to hold the light output constant, LED driver circuits employ DC-DC converters [16] to hold the current through the LED at a constant value. It is important to note that the input current drawn by the lamp is very different from the current going into the LED itself, since this current goes through various stages of the circuit before reaching the LED. However, a drop in the average value of light output would indicate a change in the duty cycle of the DC-DC converter itself. This would indicate interference with converter operation and a reduction in the average current pulse it produces at its output stage. Since the output stage of the LED driver circuit could not be monitored at this stage of experimental work, the change in the input current of the LED lamp was monitored and has been presented here. The input current THD of LED lamps has been discussed in detail in chapter 3. In this section though, the effect of high frequency distortion on current input THD from the lamps has been discussed.

The input current waveforms for lamp 24 are shown in Figure 4.18. The LED driver circuit draws current from the power supply via a rectifier. The current drawn by the LED under normal operation is the typical input current waveform of a rectifier. In the case when high frequency distortion appears in the source voltage of an LED lamp, the frequency of the input current pulse increases and instead of drawing current at the fundamental supply frequency, the LED draws current at the dominant frequency present in the high frequency distortion. However, it is also seen in Figure 4.18 (middle and bottom) that this input current pulse also has a higher peak value. This

Table 4.3: Effect of high frequency distortion on the average light output

Background only (in lux)	**Test Signal 1 (As % of original)**	**Test Signal 2 (As % of original)**
3.4	94.12	97.06
31.1	60.13	18.01
105.7	88.93	82.02
87.9	91.92	85.44
172.1	64.03	70.37
320.9	93.27	74.04
238.0	93.45	90.63
208.2	98.75	90.49
20.5	45.37	85.37
111.0	98.83	96.94
74.3	95.96	94.35
4.0	30.00	135.00
235.2	105.91	96.77
838.8	96.80	96.59
310.0	0.00	115.32
159.8	105.38	93.05
88.1	95.57	95.23
400.0	89.70	94.28
662.4	97.57	94.14
23.6	80.51	114.41
37.9	108.97	115.83
121.0	100.33	103.88
23.7	0.00	154.01
405.9	98.32	94.85
99.7	97.99	95.69
267.0	98.58	96.78
89.0	99.55	99.78
364.9	106.85	126.45
341.2	100.26	92.56
82.1	96.83	93.42
63.2	98.89	94.94
63.5	119.69	115.59

higher input current peak indicates that the LED lamp draws more peak energy from the power supply, when the input voltage contains high frequency distortion. However, it has been seen that the light output does not increase with the introduction of high frequency distortion (in the case of this lamp). Thus, this extra energy clearly does not appear as light output. This has been discussed in subsequent chapters.

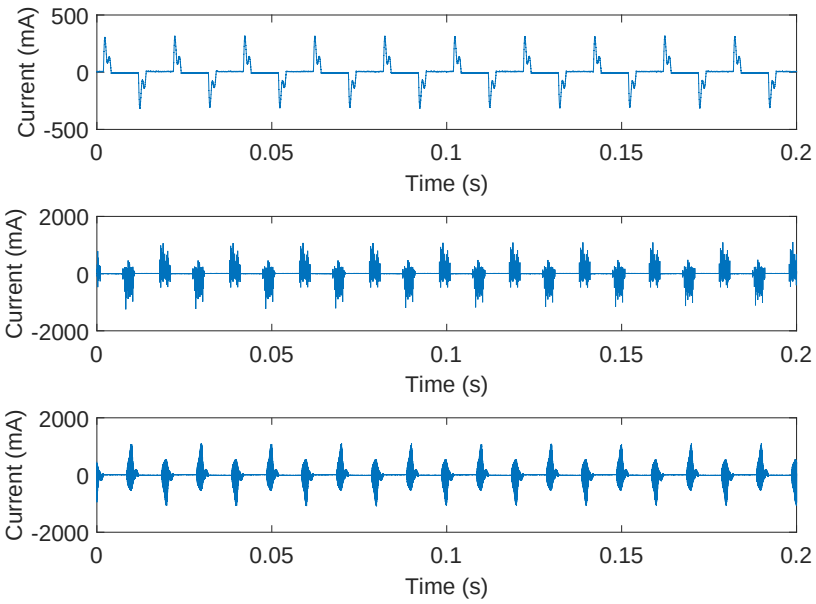

Figure 4.18: Input current plotted as a function of time for LED lamp 24, when input voltage contains no high frequency distortion (top), test signal 1 (middle) and test signal 2 (bottom).

4.6 LED lamps and Photometric flicker

The results shown in the previous section are indicative of a new type of problem that is emerging with the advent of solid state lighting. It was seen that in the case of the other LED lamps, the effects of high frequency distortion on light output were varied in nature. The effects can be summarized as follows:

- Change in average light output.
- Change in modulation of light output.

- Change in both average light output and modulation.
- Slow variations in both average light output and its modulation.

In the lighting industry, the modulation of light output is referred to as 'photometric flicker'. This is different from the definition of flicker used in power quality (typically defined for incandescent bulbs), which generally refers to modulation of the AC line voltage amplitude that directly manifests itself into variations of light output of the bulb (i.e., voltage fluctuations cause lamp flicker). The high frequency supraharmonics discussed in this paper would have essentially no impact on the light output of an incandescent bulb since the time constant of these devices was too large to follow rapid modulations of input voltage.

With the advent of LED lamps, however, this paradigm is changing. The light producing mechanism in LED lamps is entirely different and the LED driver control is certainly fast enough to respond to rapid voltage variations such as the ones shown previously. Hence, unlike incandescent bulbs, where low frequency modulation of input voltage would produce flicker, the mechanism of flicker production in LED lamps is entirely different. Any sort of disturbance in the input voltage must propagate through the power electronic circuit, to affect the light output. This mechanism has been discussed in detail in subsequent chapters.

4.6.1 Flicker - why it is important

Previous research work [36, 37] has shown that for LED lamps, this percent flicker can be much higher than for incandescent lamps. Photometric flicker can induce epileptic seizures in a certain sensitive portion of the population [38] and can also lead to headaches and eyestrain [39]. The stroboscopic effect of flickering light sources can be hazardous with moving machinery [40]. Additionally, flicker can lead to reduced productivity in individuals performing visual tasks [41] and it can cause disruptive behaviors in children with autism [42]. The health effects of LED lamp flicker is a subject of research within the IEEE also and IEEE standards committee 1789 is actively working on this topic, trying to quantify the photometric flicker and regulate it [43].

In this work, it has been shown that input voltage distortion in the frequency range 2 to 150 kHz can not only cause this 'photometric flicker' (and hence percent flicker) to change in magnitude but also cause the average light output to drop, leading to a reduction in the efficiency of the LED driver. Given the above mentioned concerns, it was necessary to quantify this change in

photometric flicker. There are existing methods to quantify this change. These are presented next, along with a new method from the domain of power electronics, which has been used to establish an input-output relationship between output light modulation and LED lamp input current THD.

4.6.2 Quantifying photometric flicker

In lighting technology, two metrics are defined to quantify photometric flicker:

- Percent Flicker: The 'percent flicker' is a parameter that is a measure of the peak to peak value of the light modulation. With reference to Figure 4.19, the percent flicker can be defined as:

$$\text{Percent Flicker} = \frac{\text{Max} - \text{Min}}{\text{Max} + \text{Min}} * 100\% = \frac{(A - B)}{(A + B)} * 100\% \tag{4.3}$$

- Flicker Index: The 'Flicker Index' is a little more mathematically involved than the percent flicker. Based upon Figure 4.19 again, the Flicker Index can be defined as:

$$\text{Flicker Index} = \frac{\text{Area above mean}}{\text{Total Area}} = \frac{\text{Area 1}}{\text{Area 1} + \text{Area 2}} \tag{4.4}$$

  Generally, the flicker index is considered a better metric than the percent flicker. The reasons for this reasoning are that the flicker index is able to account for changes in the duty cycle and wave shape. However, the utilization of the integral operator necessitates that accurate sampling of the waveshape is required and further complicates calculations.

The flicker index and the percent flicker lend themselves to cycle by cycle analysis of the light output since these are time domain techniques. These indices are normally not used this way. Generally, the information is obtained as one single number (as an average) over the period of measurement. As a result, information about the time variation in light is lost by the conventional approach. Applied to lamps analyzed previously, the cycle by cycle analysis reinforces our observations. These have been shown for lamp 8 and lamp 24 here. The variation of the modulation of light can be seen in both figures with test signal 2. For lamp 8, test signal 2 causes jumps in

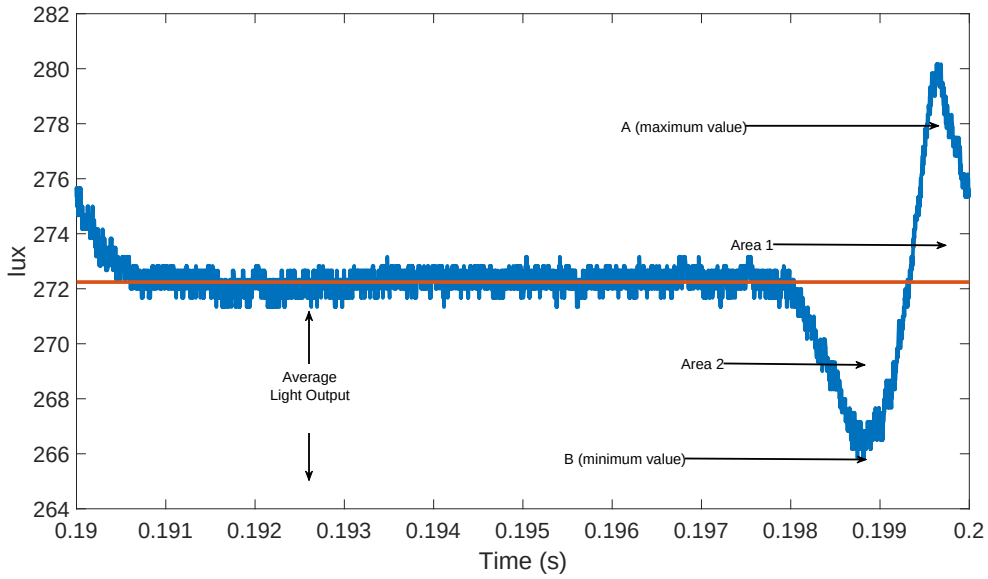

Figure 4.19: Single cycle of light output from lamp 24, with appropriate reference markers for traditional flicker metrics.

flicker percent between 28% to 38% (Figure 4.20). For lamp 24, the flicker percent varies between 0.5% and 8% over a 30 s period (Figure 4.21). The 'bursts' that were observed previously in Figures 4.13-4.15 are thus, accounted for by the percent flicker and flicker index (notice the bursts appear on the figures also, indicating a sudden change in modulation). The flicker percent shows the peak to peak magnitude of light output and the changes in it. Further, the flicker index shows the variation in waveshape of light with time. However, these indices do not give any idea as to the relationship between the current drawn by the lamp and the light output. This relationship can be understood on the basis of the indices defined in the next section. In this particular section, it can be seen on the basis of the flicker percent and flicker index that the photometric flicker from LED lamps can suddenly change due to the presence of high frequency distortion. The factors that cause this sudden change are analyzed in the next chapter. One interesting aspect of both the flicker index and percent flicker is that they do not give any information about the spectrum of light output and changes in it. Analysis of the response of the human eye to light is normally done in the frequency domain i.e., the frequency response of the eye is normally talked about. Hence, frequency domain information might actually be better in this case.

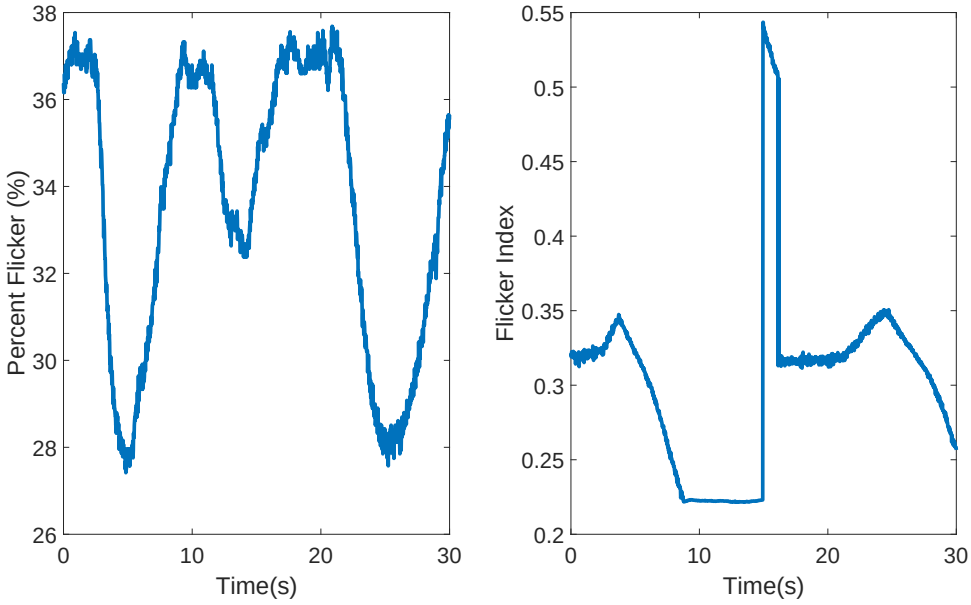

Figure 4.20: Percent flicker and flicker index for the light output from lamp 8 with test signal 2.

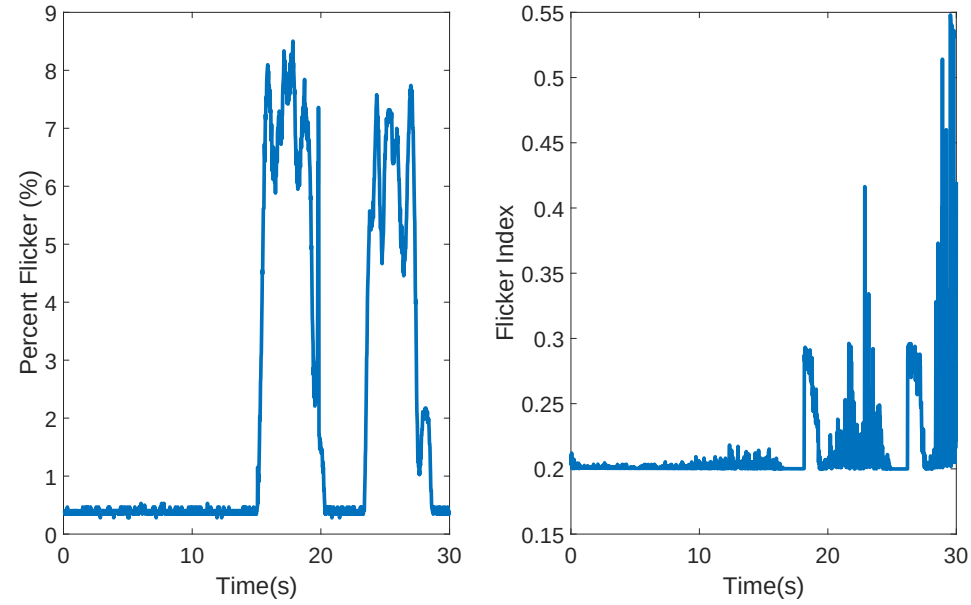

Figure 4.21: Percent flicker and flicker index for the light output from lamp 24 with test signal 2.

4.6.3 Quantifying photometric flicker from LED lamps

In the previous section, the percent flicker and the flicker index were defined as metrics to quantify the photometric flicker. The main problem with these indices is that they do not take into account the peculiarities of the newer generation of lighting. Unlike incandescent lamps, the amount of modulation being produced by an LED lamp is a controllable quantity to a large extent. The modulation is produced due to the ripple in the output current of the LED driver. In the domain of power electronics, there are pre-existing methods to quantify the ripple being produced by a converter. Unlike the flicker index and percent flicker, these methods are frequency domain methods. This essentially resolves the need to integrate the light waveform and/or do any other complex sampling of the light waveform (the frequencies of interest produced by the LED lamp are all below 1 kHz as seen previously). In essence, the utilization of frequency domain techniques makes much more sense for LED lamps. The output light spectrum can be related to the spectrum of forward current through the LED (this is the current outputted by the DC-DC converter). Any changes in the wave shape of modulation show up as changes in the frequency spectrum, either as the appearance of a new frequency or simply change in magnitude of an existing frequency component. This change in frequency can then be used to change the control and/or hardware settings on the converter to change the properties of output current ripple. Output light spectrum can thus be of more use to light manufacturers and engineers. The THD and the 'ripple factor' are two quantities that make use of the frequency domain techniques and have been used here to establish an input-output relationship for the LED lamps tested.

When high frequency distortion appears in the supply voltage waveform, the input current drawn by the LED lamp changes accordingly, as seen previously. In order to quantify this change in current, the Total Harmonic distortion (THD) of the input current has been compared in the three cases for the LED lamps. The THD of a signal is a measurement of the harmonic distortion present and is defined as the ratio of the sum of the powers of all harmonic components to the power of the fundamental frequency. THD is used to characterize the linearity of audio systems and the power quality of electric power systems. THD, in effect, characterizes the harmonic production of a system as a percentage of the fundamental frequency. This is especially suitable for a case where the input voltage contains distortion due to frequencies other than the fundamental. The formula for THD is:

$$THD_F = \frac{\sqrt{(V_2)^2 + (V_3)^2 + (V_4)^2 \dots}}{V_1} \tag{4.5}$$

where V_n is the r.m.s value of the nth harmonic and $n = 1$ is the fundamental frequency of the power supply.

In the previous sections, it was observed that under normal operation, LED lamps produce light with a large modulation along with the average light component. It was also observed that the envelope of light gets reduced when high frequency distortion is present in the source voltage, indicating a reduction in the modulation of light output. In order to understand how the various components in light get affected by the high frequency distortion present in voltage, the 'Ripple Factor (RF)' in light was compared against Total Harmonic Distortion (THD) in current. Ripple factor is a measure of ripple content in a signal and is defined in [44] as:

$$RF = \frac{V_{ac}}{V_{dc}} = \frac{\sqrt{(V_1)^2 + (V_2)^2 + (V_3)^2 \dots}}{V_{dc}} \tag{4.6}$$

where V_{dc} is the DC component in light and V_n is the r.m.s value of the nth harmonic of the 100 Hz frequency. When the THD of the input current and RF of the output light are defined thus, a plot of the input and output quantities can be obtained from the measurement data. For all 32 lamps, the data has been plotted for a case when no distortion is intentionally added into the source voltage (i.e., background distortion only).

Figure 4.22 shows that the lamps basically fall into three main groups (using typical values of THD = 70% and RF = 6.6%): lamps with low input THD and low RF (5 lamps), lamps with low THD and high RF (17 such lamps) and lamps with low RF and high THD. (10 such lamps) The number of lamps in the first group is limited and the majority (27 out of 32 or about 85%) of the lamps fall into either of the remaining two groups. Thus, majority of the lamps compromise on

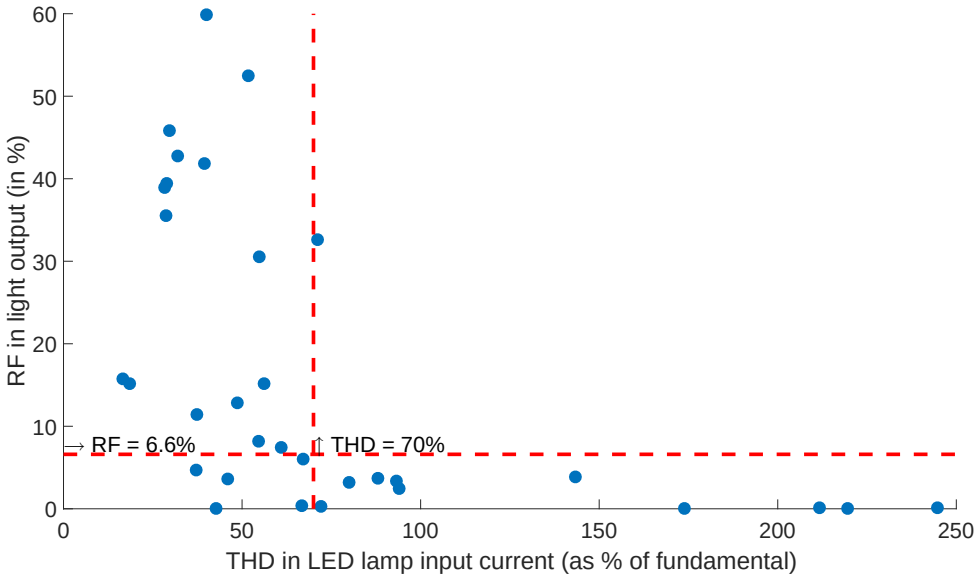

Figure 4.22: LED lamp output light RF plotted as a function of LED lamp input current THD for the cases when the lamp input voltage contains no distortion. Horizontal line indicates RF = 6.6% and vertical line indicates THD = 70% boundary.

either THD or RF for steady state operation.

The input current THD to output light RF relationship is a rather interesting one. In DC-DC converters, output ripple is a function of four quantities:

- Input DC voltage.
- Switching frequency.
- Value of inductance used.
- Duty cycle of the converter.

Out of all the factors listed above, current ripple (and hence light ripple or light modulation) is directly proportional to the input DC voltage and the duty cycle of the converter. Current ripple is inversely proportional to the switching frequency and the value of the inductance. The input DC voltage to the converter is further dependent on the value of the DC link capacitor which then impacts input current THD. Empirical data presented here suggests that input current THD and RF have an inverse relationship with each other. Literature reveals that the current direction of research, does not really stress on keeping the RF to a minimal value [15,16]. Hence, LED designers

sacrifice higher capacitance values at the output stage (hence lower ripple) to keep the BoM low. The argument that is used in favor of such an arrangement is that the human eye cannot perceive such ripple frequencies anyway.

The effect of high frequency distortion on the modulation in light output can be understood on the basis of the plots that follow. These plots show the ripple factor of the light output from lamps 2, 3 and 4 plotted against the input current THD. For lamp 2, it can be observed that the introduction of test signal 1 in the input voltage, leads to an increase in input current THD. At the same time, this increase is accompanied by a reduction in the ripple factor. Thus, test signal 1 causes the input current drawn by the lamp to be more distorted. At the same time, this is accompanied by a reduction in the modulation of light produced by the lamp. Test signal 2 also shows the same result. In this case, the reduction in modulation is even larger. However, at the same time, the input current THD does not increase as much as it did for test signal 1. This is shown in Figure 4.23.

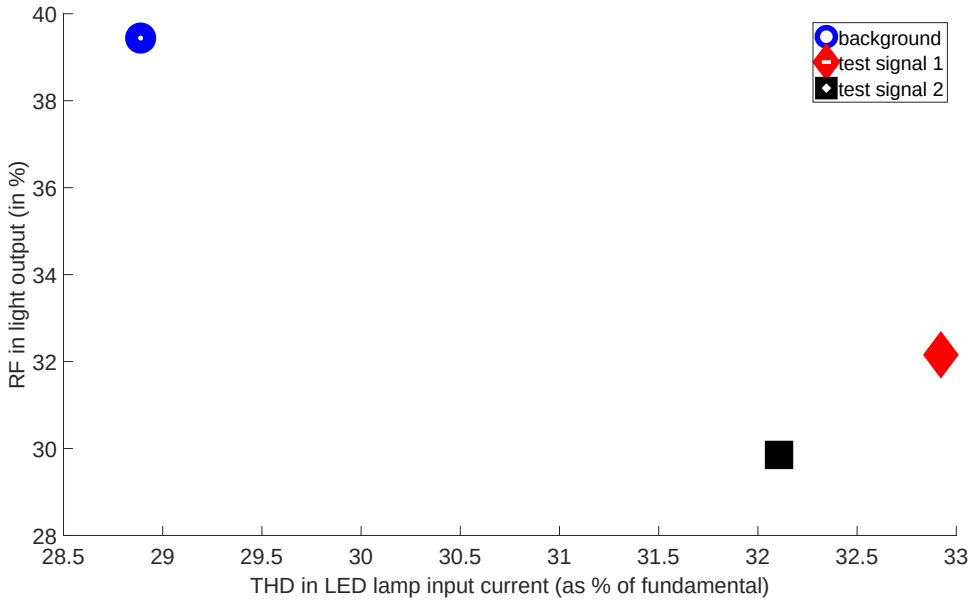

Figure 4.23: LED lamp 2 output light RF plotted as a function of LED lamp input current THD for the cases when the lamp input voltage contains no distortion and then test signals 1 and 2.

For LED lamp 3 (Figure 4.24), the behavior is quite different from the one observed above. Lamp 3, with background distortion, produces light with very low ripple factor. However, the input

current THD was observed to be quite high. With test signal 1, this input current THD reduces by about 90%. At the same time, the ripple factor decreases (the lamp produces less modulation in light output). With test signal 2, the input current THD reduces by 30%. However, it was observed that the ripple factor increases due to the introduction of test signal 2 into input voltage. i.e., the lamp produces more modulation in light output. Note that this behavior is quite the opposite of that observed with lamp 2.

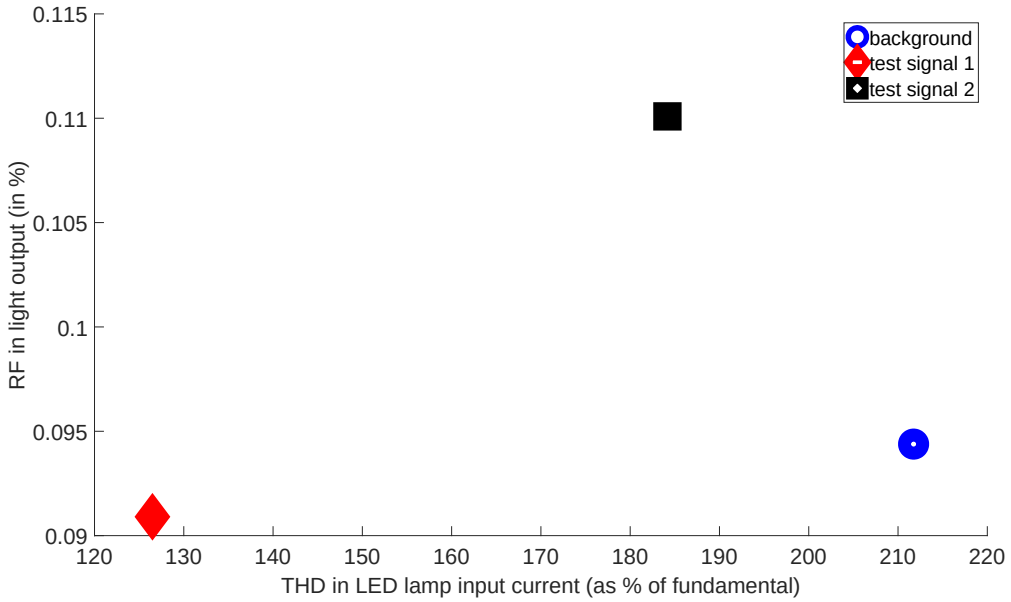

Figure 4.24: LED lamp 3 output light RF plotted as a function of LED lamp input current THD for the cases when the lamp input voltage contains no distortion and then test signals 1 and 2.

Finally, the results for lamp 4 have been shown in Figure 4.25. LED lamp 4 has a ripple factor of 2.5% at about 94% THD (high THD and low RF by the criteria given previously). With the introduction of test signal 1, this THD reduces to about 88% and the RF reduces to about 2.23%. With test signal 2, the THD is about 90.5% while the RF is about 2.15%. Thus, in this case also, the high frequency distortion causes the modulation of light output produced by the lamp to reduce in both cases. This is accompanied by a decrease in input current THD as well. Apart from a few exceptions, this reduction in RF was observed in the majority of the 32 lamps tested.

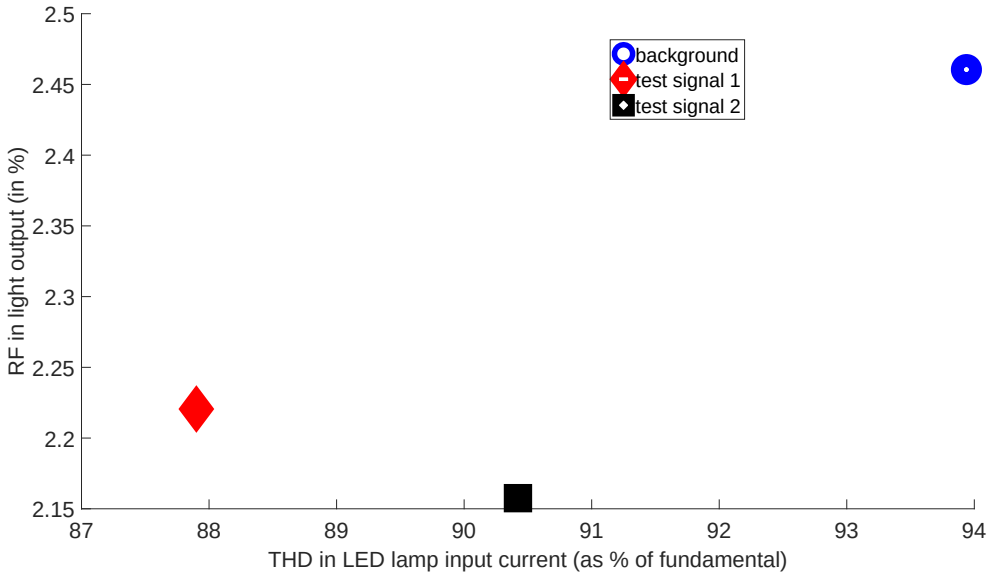

Figure 4.25: LED lamp 4 output light RF plotted as a function of LED lamp input current THD for the cases when the lamp input voltage contains no distortion and then test signals 1 and 2.

4.7 Interference with dimmers

In most household applications, LED lamps are used in conjunction with commercially available dimmers. The dimmers are connected in series with LED lamps and utilize a variac, a diac and a triac to achieve the dimming function. Figure 4.26 shows the schematic layout of such a dimmer.

In Figure 4.26, R1 and R2 create a voltage divider network across the supply and control the forward voltage of the diac. This ultimately controls the firing angle of the triac, since the diac is connected to the gate terminal of the triac. Controlling the firing angle allows for the control of the current conduction cycle in both the positive and negative half cycles. This changes the RMS value of the current through the lamp and hence the brightness. Because of the low forward voltage drops of the solid state switches, losses are low. More importantly, dimming is almost instantaneous. Some of the heat that is generated in these switches causes radio interference and hence inductors are used as EMI filters at the front end of such dimmers.

When an LED lamp is connected to a source voltage containing high frequency distortion, the distortion affects the functioning of the dimmer circuit also. Because the high frequency components change at a much faster rate and go through multiple cycles before the fundamental voltage

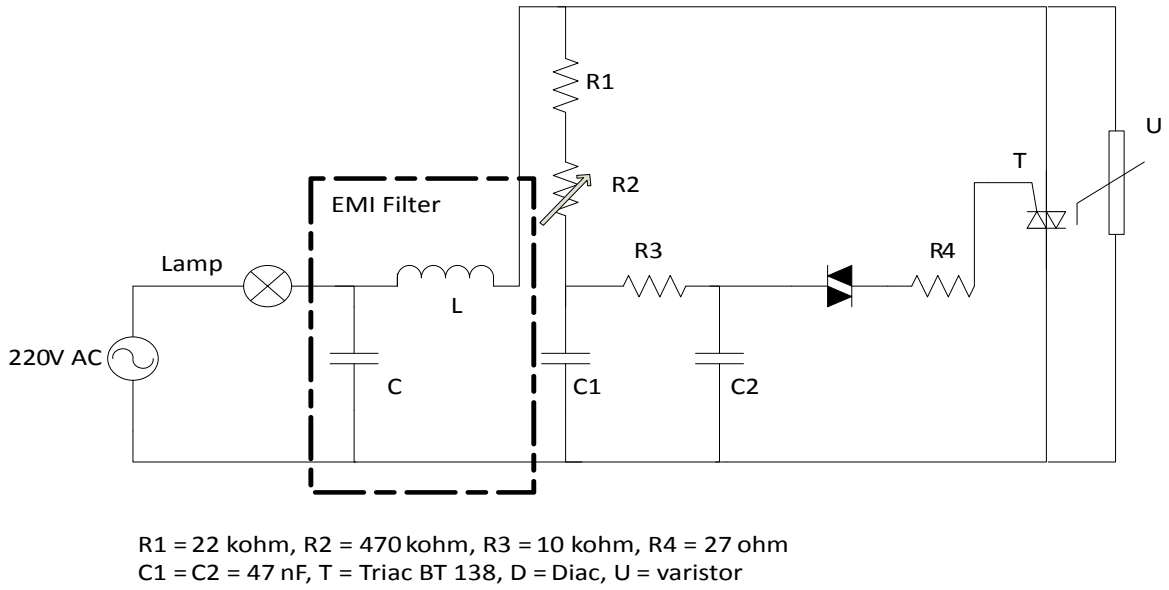

Figure 4.26: Schematic layout of a typical triac dimmer.

finishes one full cycle of its own, they interfere with the working of the solid state switches. When the distortion reaches a value at or near the reverse voltage of the switches, it causes the switches to turn off momentarily. As a result, the lamp gets turned off during one half cycle. It does not matter what sort of lamp is connected in the circuit as the high frequency distortion interferes with the dimmer itself. This has been shown in Figure 4.27.

Figure 4.27 shows that when a dimmer is connected in the circuit with an LED lamp, the solid state switches can fail to fire in a half cycle. This problem gets even more exaggerated when the lamp is dimmed. During the dimming of the lamp, as the duty cycle of the input voltage is reduced even further (by increasing firing angle of the triac), the high frequency distortion present in the supply causes the bulb to start blinking. This can be predicted from Figure 4.27. As the transition from a broader voltage wave to a narrower wave happens, the RMS value of the voltage reduces even further and the current through the LED does not hold steady. Further, as the amount of high frequency distortion is increased, the ratio of distortion voltage to fundamental voltage increases. Thus, the switches commutate prematurely and cause the lamp to blink and eventually the lamp turns off.

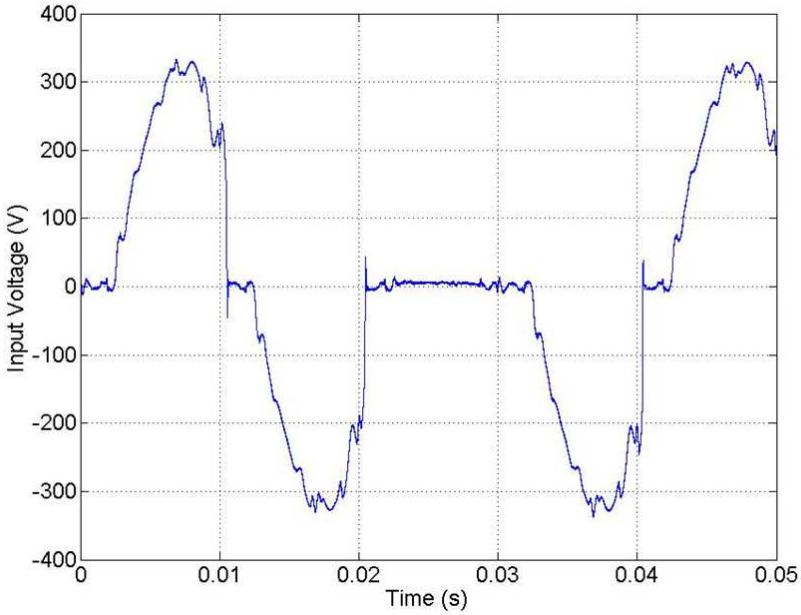

Figure 4.27: LED input voltage with dimmer present in the circuit and high frequency distortion signal 2 present in supply voltage.

Chapter 5

Factors that affect interference

In the previous chapter, the effects of interference from high frequency distortion in supply voltage, on the LED lamp light output were shown. It was shown that the LED lamp light output changes in the presence of high frequency distortion. It was observed further that this reduction was not always constant but rather varied slowly over time in a lot of cases. In this chapter, the factors that affect this reduction in light output are analyzed. First, the concept of 'point-on-wave of high frequency distortion' is introduced to explain the slow variation of light output with distortion. Next, the mathematical technique of cross-correlation is used to quantify the relationship between 'point-on-wave' and light output. Observations show that more than the magnitude and the frequency of the supraharmonics in voltage, it is actually the point-on-wave nature of supraharmonics, that the LED lamp is more sensitive to. Finally, further hardware testing is shown, which tries to understand the role that the LED driver plays on the response of the LED lamp to supraharmonics. It is shown through experimental evidence, that the response of the LED lamp (to supraharmonics) may not be so much related to LED driver topology, as it is to the control mechanism utilized by the circuit.

5.1 Point-on-wave of high frequency distortion

5.1.1 The concept of point-on-wave in the traditional sense

In power engineering, the concept of 'point-on-wave' was first prominently used as a way to characterize voltage sags. Normally, the terminology used in this context is 'point-on-wave of

initiation/termination'. This is used as a way to indicate the point at which a sag begins and ends. The 'point-on-wave of initiation/termination' in the context of a voltage sag is defined as the phase angle of the fundamental voltage where the instantaneous voltage starts and ends to experience a reduction in its magnitude. In other words, it is defined as the phase angle on the fundamental voltage at which the RMS value of the voltage goes below a predefined threshold. Point on wave of initiation corresponds to phase angle of the pre-sag voltage, measured from the last positive-going zero crossing of the pre-sag voltage, at which transition from the pre-sag to during-sag voltage is initiated. Similarly, point on wave of ending corresponds to phase angle of the post-sag voltage, measured with respect to the positive-going zero crossing of the post-sag voltage, at which transition from during-sag to post-sag voltage happens. [45–48]. This work is not intended to provide a detailed treatment of voltage sags. The interested reader may refer to [49] for a detailed treatment of the subject. In this work, the established definition of point-on-wave, first used in the context of voltage sags, is modified to understand how the movement of high frequency distortion signals, relative to the fundamental voltage affects the light output. The point-on-wave is thus meant to mean 'the phase angle of the fundamental wave at which a fixed point of the high frequency distortion (usually the maximum value) appears'. This definition and the context in which it is introduced, are examined next.

5.1.2 Power Line Communication

In Figure 1.2 and Figure 4.2 (test signal 2), it was observed that the supraharmonic distortion can have point-on-wave character. Further, since LED lamp flicker has been observed with such voltage, it was attempted to recreate the conditions in the field as accurately as possible. One of the prominent sources of high frequency distortion is Power Line Communication (PLC) and it has been observed that this disturbance also has point-on wave character. The voltage disturbance due to PLC appears in the form of packets of information at a higher frequency (9 kHz to 95 kHz in Europe), superimposed onto the fundamental voltage wave. An example of such a signal is shown in Figure 5.1. Figure 5.1 shows the voltage and current recorded at the terminals of a 'smart' energy meter. The energy meter communicates information with the network operator using a frequency of 43 kHz. Note that Figure 5.1 shows a singular example of PLC. The ways and methods in which PLC is implemented differs a lot between applications and manufacturers.

The point on the fundamental frequency wave at which the PLC may appear may not always

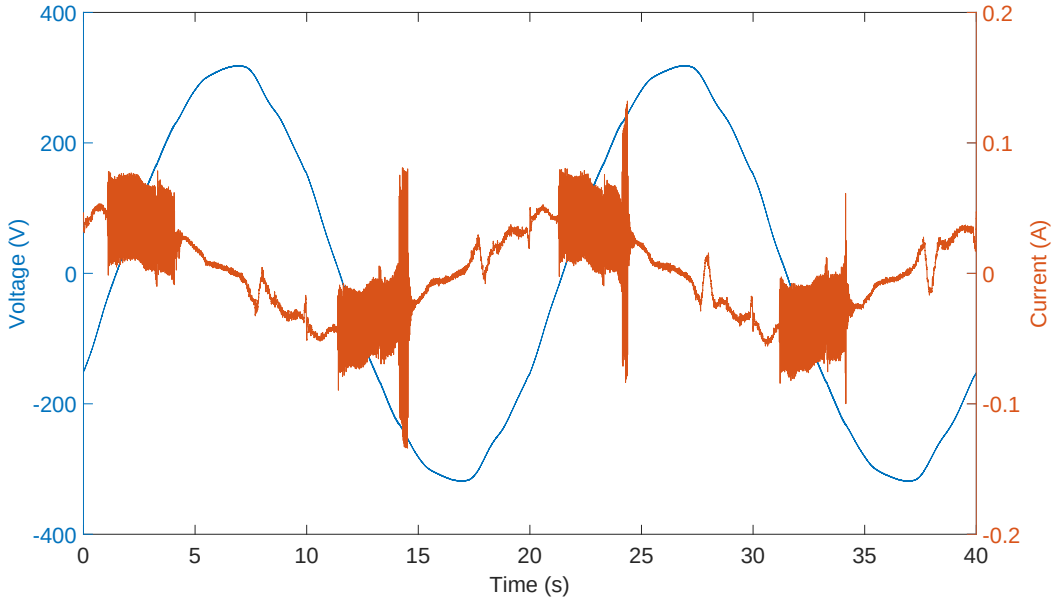

Figure 5.1: Voltage and current signal recorded at the terminals of a smart energy meter, communicating data using a frequency of 43 kHz. Note the point-on-wave character of the PLC signal in the current waveform.

be fixed. Power electronic switches often use the sinusoidal variation of the fundamental voltage for their operation. For example, the firing angle of SCRs or the line commutation of diodes depend upon the magnitude and phase of the fundamental frequency voltage. Thus, a clumped disturbance and the position of such a clumped disturbance on the fundamental frequency wave can have an impact on the operation of power electronics based devices such as LED lamps. This is explored further in the next chapter. For now, the analysis focuses on the recreation of this point-on-wave character and more importantly, quantifying it.

5.1.3 Testing for the impact of clustered disturbances

During the experimental work performed, the incoming voltage from the grid and the high frequency distortion that was superimposed were not synchronized to each other, as the frequency during measurement and during the experiment were not the same (recall that grid frequency fluctuates constantly in a small bound). The point on the fundamental voltage wave, at which the high frequency distortion was applied was kept floating. This was done so as to understand whether the point on the fundamental waveform where the distortion was applied, had any effect on the equip-

ment that was being tested. In this case, the output quantity of interest was the LED lamp light output. For the purposes of experimental work, test signal 2 was chosen since it shows the biggest variation in high frequency distortion during the fundamental frequency cycle and very closely mimics a PLC signal. However, in the absence of a formal method to define this variation in the point of application of the test signal, it would be difficult to reproduce the experimental work. This problem was overcome by formally defining the concept of 'point-on-wave of high frequency distortion'.

5.1.4 Definition

To quantify the point-on-wave of high frequency distortion, the fundamental voltage waveform is used as reference. The positive going zero crossing of this waveform is considered to be the zero degree point. Further, in order to quantify the voltage distortion signal, the peak amplitude of the frequency distortion signal is taken to be the second reference point. The 'point-on-wave of high frequency distortion' is defined as the phase angle, where the maximum value of the distortion signal appears, compared to the positive going zero crossing of the fundamental frequency voltage wave. With this definition, the analysis of the influence of point on wave then reduces to the analysis of two scalar quantities i.e., the point-on-wave in degrees versus the light output in lux. This is shown in Figure 5.2.

When defined in this manner, the point-on-wave measures a continuous shift between two signals at different frequencies. It differs from the traditional definition of point-on-wave in this way. Traditionally, point-on-wave has been used to mean a static point on the fundamental wave where a sag initiates or ends. However, in this case, it represents a dynamically shifting point on the fundamental wave where the maximum peak of the high frequency distortion signal appears.

5.1.5 Mathematical Quantification

In order to understand how much the distortion signal shifts relative to the fundamental frequency, it was necessary to find a mathematical tool that can fit the definition of point-on-wave defined above. The method of cross-correlation was chosen for this purpose. This follows from the mathematical definition of cross correlation. In the domain of signal processing, the cross-correlation between two data series is a measure of similarity of these data series, expressed as a function of the

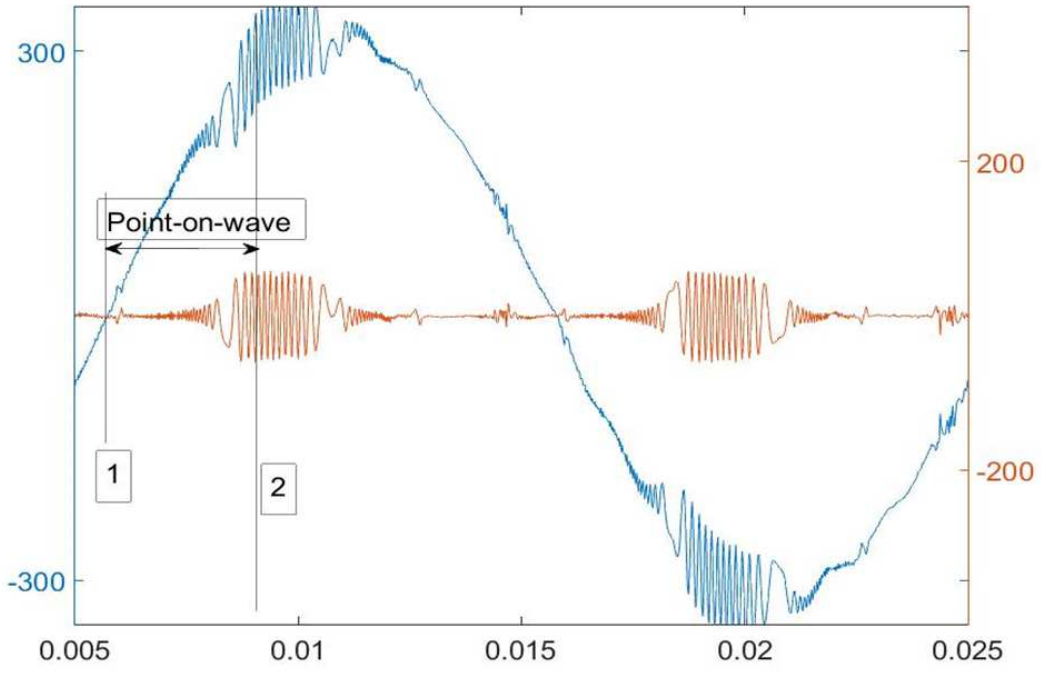

Figure 5.2: Quantification of point-on-wave of high frequency distortion. Source voltage (blue) and distortion signal (red). Point 1-zero crossing of fundamental wave, Point 2-Maximum amplitude of distortion.

time shift between the two. For two discrete functions f and g, the cross-correlation is defined as:

$$(f \star g)[n] = \sum_{m=-\infty}^{\infty} f^*[m]g[m+n] \tag{5.1}$$

where f^* denotes the complex conjugate of f, and n denotes the lag between the two signals. Assuming that $n = 0, 1, 2 \ldots, N-1$, the cross-correlation r at a delay d is given by [50]:

$$r = \frac{\sum_{n=0}^{N-1}(f[n] - mf) * (g[n-d] - mg)}{\sqrt{\sum_{n=0}^{N-1}(f[n] - mf)^2}\sqrt{\sum_{n=0}^{N-1}(g[n-d] - mg)^2}} \tag{5.2}$$

where mf and mg are the means of the respective functions. If the equation is computed for all possible delays, it results in a cross correlation series of twice the length as the original series. After calculating the cross-correlation between the two signals, the maximum (minimum in the case where the two signals are negatively correlated) value of the cross-correlation series indicates the point in time when the two signals are best aligned. Thus, the time delay between the two signals

is determined by the argument of the maximum of the cross-correlation as:

$$\tau_{delay} = \underset{n}{\operatorname{argmax}}((f \star g)[n]) * (T_{sample}) \tag{5.3}$$

where T_{sample} is the sample time of the individual signals. Considering the equations above, what is happening is the second series is being shifted relative to the first, at each shift the sum of the product of the newly lined up terms in the series is computed. This sum will be large when the shift (delay) is such that similar structure lines up. This is essentially the same as convolution except for the normalization terms in the denominator. Using this method, the point-on-wave for every cycle of the fundamental frequency wave was calculated. Corresponding to the point-on-wave output, the light output (and its constituent components) was calculated.

In order to calculate the point-on-wave where the distortion was added in each cycle of the fundamental frequency wave, first a standard 'test signal' was defined. One single cycle of the fundamental frequency wave was chosen, where the distortion was added at a known point on the fundamental. This was done by measuring the time difference in samples, between the zero crossing and the peak of the distortion signal. Using this signal, each cycle of the voltage (to which the LED lamp was subjected) was cross-correlated and this process was carried out for a period of 30 s (about 1500 cycles of the fundamental voltage). The phase shift of the distortion signal in a given cycle was thus related to a known signal and the point-on-wave value was obtained.

5.1.6 Operation with high frequency distortion

As shown previously, the behavior of the LED lamps, when operating from a voltage containing high frequency distortion, was significantly different than operation with only background distortion. An example of this is shown in Figure 5.3 which shows the light output from lamp 8 in all three cases. The light output gets reduced when test signal 1 is superimposed on the supply voltage. When test signal 2 is superimposed onto the supply voltage, the light output gets reduced even further. The results are shown for lamp 8, but this behavior was observed in 80% of the lamps that were tested.

Figure 5.3 shows two 'bursts' in light output, observed between cycles 0 to 500 and 1000 to 1500 when the lamp was operated from a voltage supply that contained test signal 2. These bursts were not due to a sudden change in the testing apparatus or external changes (during the

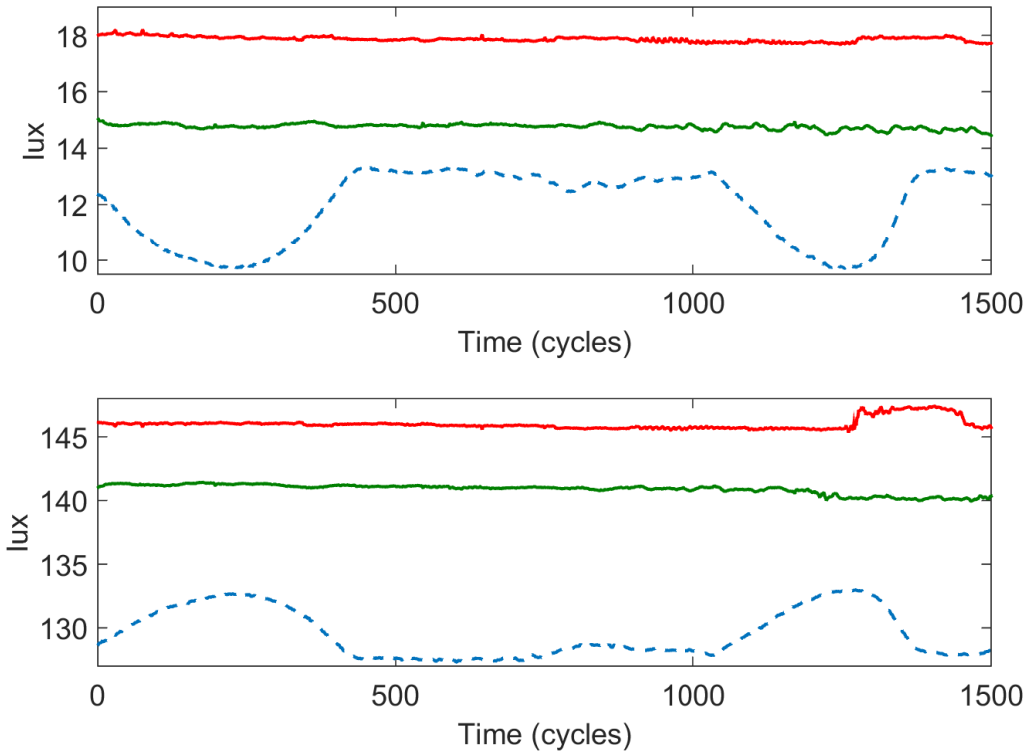

Figure 5.3: Light modulation (top) and average light output (bottom) from lamp 8. The lamp light output when operating from voltage containing background distortion only (solid red), with test signal 1 (dashed green) and with test signal 2 (dashed blue) is indicated in all figures.

test, magnitudes of all input quantities were kept constant). Instead, this change occurred because the light output depends upon more than just the magnitude and frequency of the distortion added to the supply voltage. Similar observations were made with different lamps, and in each case it was observed that for a fixed amplitude of distortion, change of point-on-wave of the distortion along the fundamental wave, had an impact that manifested itself in the form of the 'bursts' mentioned previously. This is analyzed next.

5.1.7 Influence of point-on-wave

Since the light output of an LED is proportional to the amplitude of the current through it, the next step was to determine if there was a change in the input voltage conditions which led to a change in the current input and light output of the LED lamp. It was observed that the 'point-on-

wave' at which test signal 2 appeared on the fundamental wave moved continuously in both lamp 8 and lamp 24. The impact that the point-on-wave of high frequency distortion had on the light intensity of the lamp, is illustrated by showing the lamp voltage, the current and the light output of LED lamp 24 for two instances in time (Figure 5.4), where the second figure was obtained 13 s after the first one.

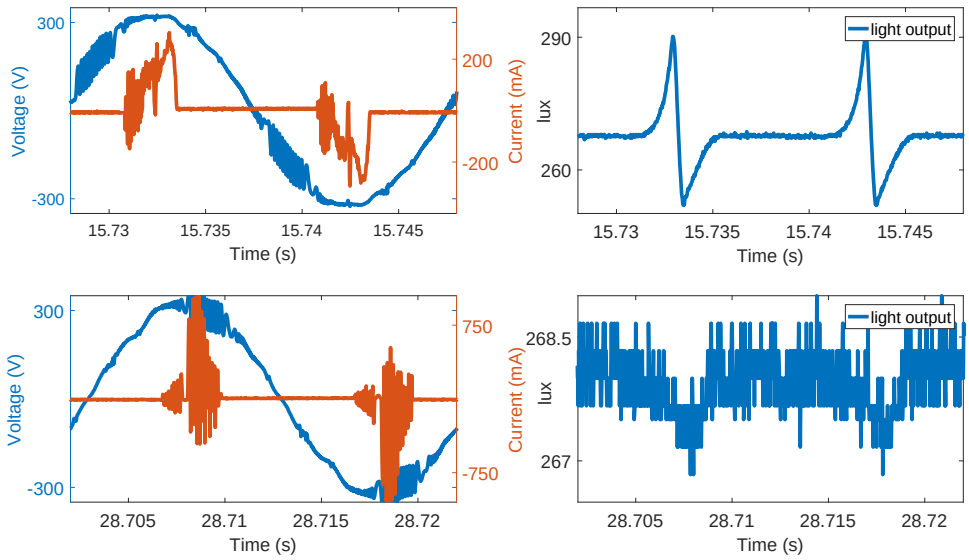

Figure 5.4: One cycle of source voltage, LED input current and light output plotted between 15.728 s and 15.748 s (top left and top right) and 28.702 s and 28.722 s for lamp 24. Test signal 2 was superimposed onto grid voltage. Note the difference in vertical scale for the plot of light modulation in the two cases.

In this case, the LED lamp was subjected to test signal 2 superimposed on the grid voltage. The light output of the lamp was captured over a 30 s time window. Figure 5.4 shows that between 15.728 s and 15.748 s, the distortion signal appears near the zero crossing of the fundamental voltage. Corresponding to this, the light output has an average value of 270 lx and a modulation of 40 lx peak to peak. On the other hand, between 28.702 s and 28.722 s (bottom of Figure 5.4) for the same lamp, the average light output reduces to about 268 lx and the modulation gets reduced to almost 1 lx peak to peak. In contrast to the first case, the distortion appears near the peak of the fundamental wave (on the falling edge) in this case. It is also worth noting that in Figure 5.4, the peak amplitude of the current at 28 s is almost twice as large as its amplitude at 15 s. Evidently, the appearance of distortion at a different point on the fundamental wave causes the value of the current drawn and

the light output from the LED lamp to change.

The method for calculating the point-on-wave of high frequency distortion has been applied to the 30 s measurement windows mentioned earlier, for the lamps shown in Appendix A. As a result, for each 30 s window, 1500 values for point-on-wave were obtained. One value of point-on-wave was calculated for each 20 ms cycle. For each 20 ms cycle the average light output and the modulation of light have been calculated. Instead of plotting these quantities against time, they are plotted against point-on-wave, as will be shown in the forthcoming figures.

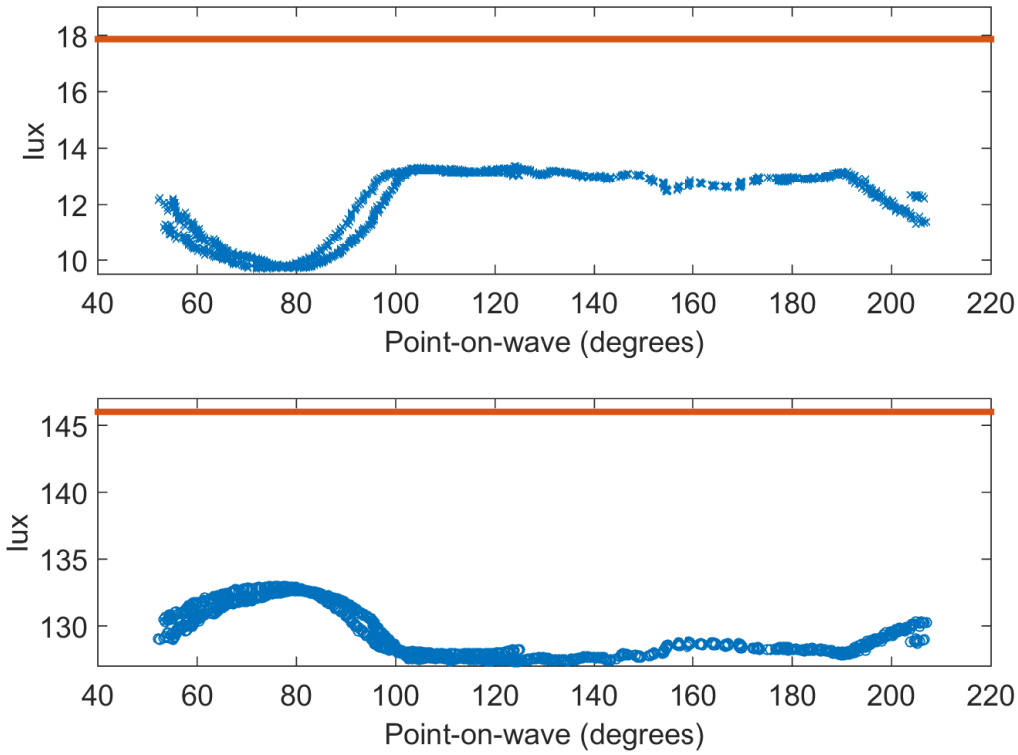

Figure 5.5: Variation of the modulation (top) and average light output (bottom), as a function of the point-on-wave of high frequency distortion, for lamp 8, with test signal 2 (blue markers). The red line indicates the average light output, with background distortion.

Figure 5.5 shows the result for lamp 8. The modulation of light output reaches its lowest value at the point-on-wave where the average light output is at its highest value. The ratio between modulation and average varies between 6.5% and 11.9% while the high-frequency distortion moves through the fundamental waveform. It is also worth noting the in comparison with its value with

background distortion, the light output (average and modulation) has a lower value (see red reference line).

Since the light output is a function of the LED driver utilized in the lamp, each lamp is likely to have a different response to input voltage changes. Hence, it is expected that the characteristics of the point-on-wave curves will be different in each case. This was observed to be the case.

The impact of point-on-wave of high frequency distortion for lamp 31 is shown in Figure 5.6.

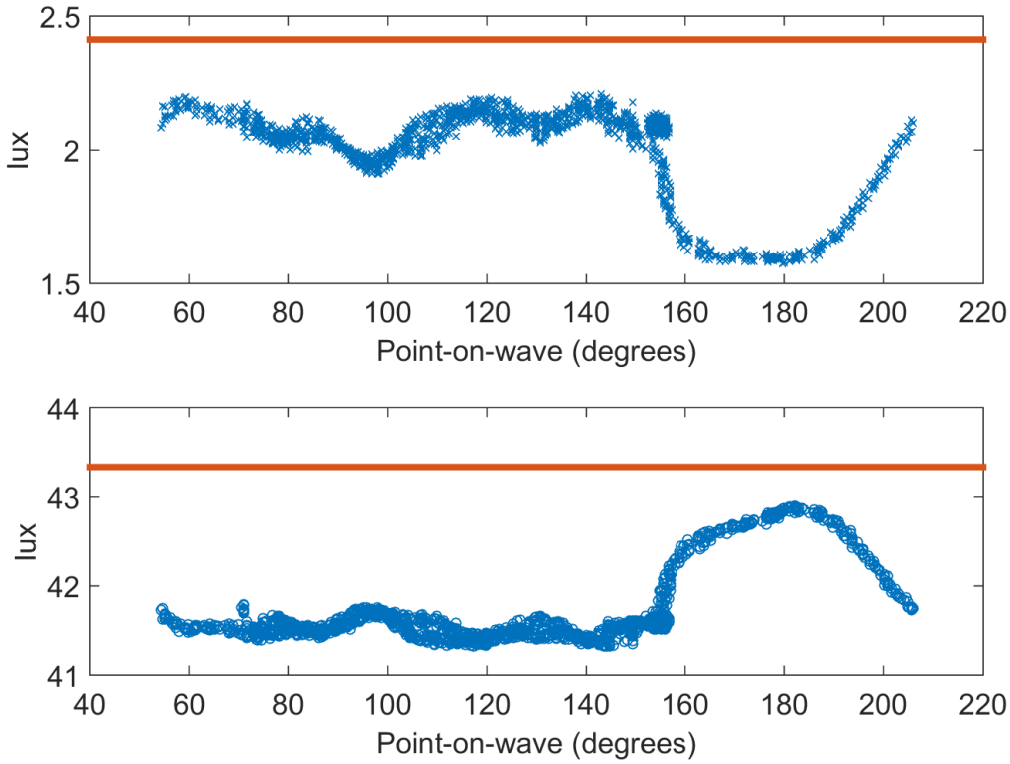

Figure 5.6: Variation of the modulation (top) and average light output (bottom), as a function of the point-on-wave of high frequency distortion, for lamp 31, with test signal 2 (blue markers). The red line indicates the average light output, with background distortion only.

The impact of point-on-wave of high frequency distortion for lamp 3 is shown in Figure 5.6. Figure 5.6 shows that the variation of various components of light output with the point-on-wave follows the same general pattern as in the previous case. However, unlike the previous case, this lamp is more sensitive to changes in point on wave near the zero crossings of the fundamental voltage

waveform. Both average light output and modulation get reduced when high frequency distortion is added. Around certain points-on-wave the average value reduces less but the ripple reduces more. There are however quantitative differences, for example the modulation varies from 5.6% for the case without high frequency distortion to as low as 3.7% for certain points-on-wave with high frequency distortion present. In the case of lamp 8, modulation varies between 12.3% for the case without high frequency distortion to a minimum value of 6.5% with high frequency distortion present. The reduction in average output is at most 17.8% for lamp 8 but at most 3.9% for lamp 31. It is observed that in all these cases, the value of the various components of light changes most for certain values of point-on-wave. The values at which this change occurs are different for each lamp.

The variation of the various components of light output with point-on-wave has been shown for lamp 19 in Figure 5.7. Similar to lamp 31, maximum value of the average light output is obtained when the distortion is near the zero crossing of the fundamental waveform.

It is observed that in all these cases, the value of the two components of light changes most for certain values of point-on-wave. The values at which this change occurs are different for each lamp. As shown, certain lamps are more sensitive to distortion near the zero crossing, while others are more sensitive to voltage distortion near the peaks.

Out of the total of 32 lamps tested, it was observed that supraharmonics cause the light output from the lamp to decrease in 80% of the lamps. In 4 lamps, an increase in light intensity was observed. However, in the case of 4 lamps, it was observed that the lamp did not respond to changes in point-on-wave. This is shown in Figure 5.8. The lamp could not be physically decapsulated without risk of damage to the circuit inside, hence it could not be assessed as to what the topology of the LED driver of these lamps was. Regardless, these lamps came from the same manufacturer. The change in light output from these lamps, in response to supraharmonics, was less as compared to the other lamps. For the sake of brevity, only one out of the four lamps is shown.

5.1.8 Effect of point-on-wave on LED lamp current

The impact of high frequency distortion in voltage on the light output has been discussed in the previous sections. It was shown that not only does high frequency distortion cause the light output of an LED lamp to change, but this change is also affected by the point-on-wave at which the distortion appears. Similarly, the distortion in input voltage also affects the input current drawn by the LED lamp. This relationship is easier to quantify and this is shown in Figure 5.9 for lamp

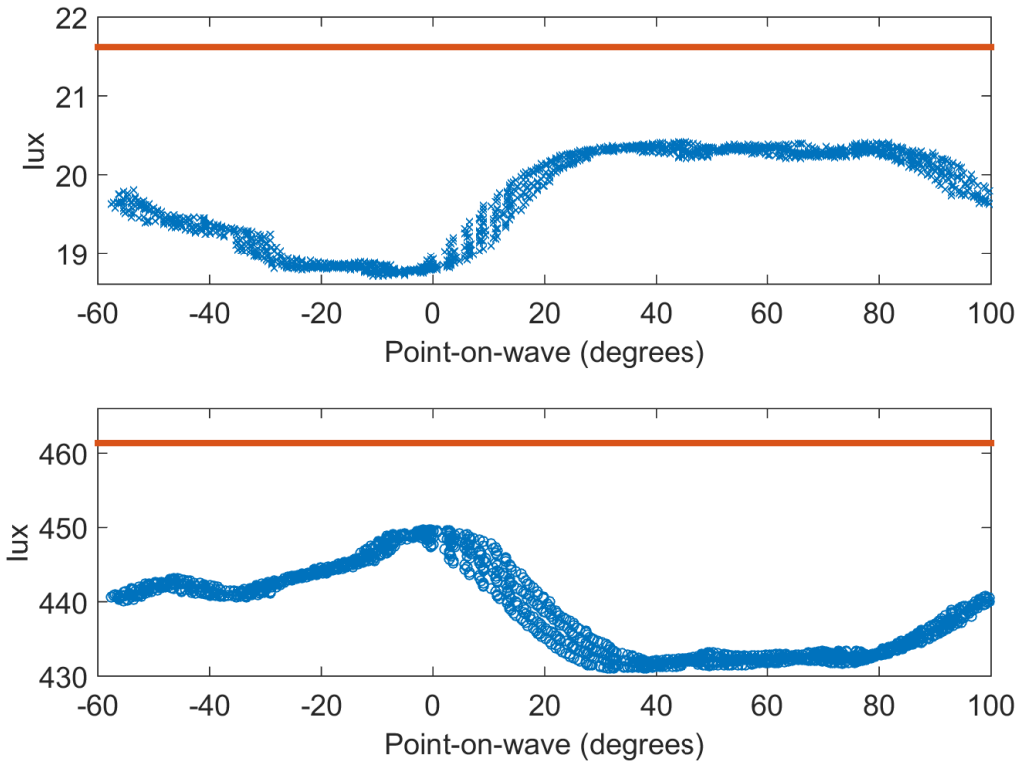

Figure 5.7: Variation of the modulation (top) and average light output (bottom), as a function of the point-on-wave of high frequency distortion, for lamp 19, with test signal 2 (blue markers). The red line indicates the average light output, with background distortion only.

number 24.

Figure 5.9 (top) shows that when the LED lamp is operated from a voltage containing only background distortion, the current waveform begins near the peak value of the voltage with a peak value of about 300 mA; the common behavior of a diode rectifier. The same experiment was then repeated with test signal 2 superimposed onto the fundamental supply frequency. Over a time period of 30 s, with various point-on-wave conditions, it was then observed that the width of the current pulse increases and the peak value of current reaches up to 1500 mA. In the bottom half of Figure 5.9, it can be seen that for particular point-on-wave conditions, the current pulse can start much earlier than the previous value. Also is it possible for the current to flow in the "opposite direction" (for a given voltage, the current can have a negative value due to distortion). This is possibly because the magnitude of the distortion signal can be large enough to forward bias the

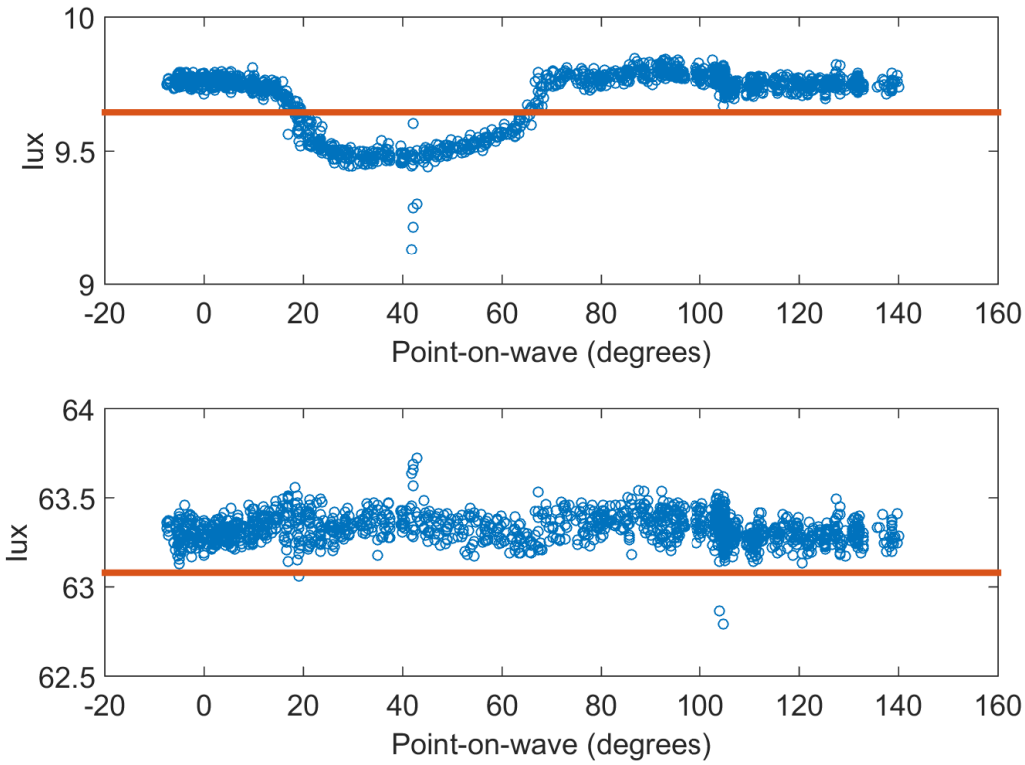

Figure 5.8: Variation of the modulation (top) and average light output (bottom) plotted as a function of point-on-wave where distortion is added, for lamp 27, with test signal 2 superimposed onto grid voltage. The red line indicates the average value of the respective light components, with background distortion.

diodes in the input rectifier stage, much before the 50 Hz component can do this. In this case, due to the presence of the high frequency distortion, the voltage may not fall to the value required to reverse bias the diodes, at quite the same rate as before. As a result, depending on the point on wave condition, the input rectifier stage of the LED driver can either prematurely open or remain open too long (Simulation evidence for this is presented in the next chapter). This is evidenced in Figure 5.9 with the current being drawn at about 200 V instead of the previous value of about 300 V. Further, when the distortion appears at the peak of the voltage wave, it causes the peak value of the current magnitude to also increase to about 1.1 A. At the same time, as was observed before, the magnitude of the light output did not increase with this increase in current drawn. Rather, the magnitude of light output decreased in every case. Compared to incandescent lamps, LED lamps produce a lot less heat. Rather, the heat is generated in the LED driver circuit [51]. It is not

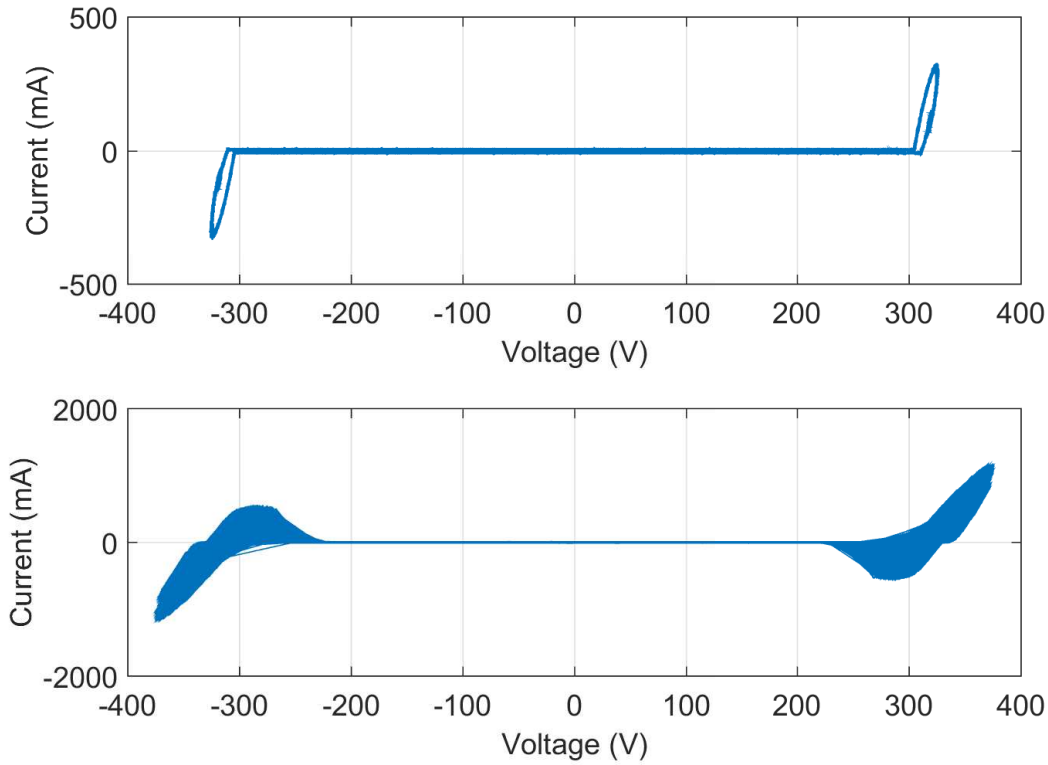

Figure 5.9: LED lamp current plotted against input voltage for a case when the voltage contains only background distortion (top) and test signal 2 (bottom). Samples obtained over a time period of 30 s. Note the difference in vertical scale between the two plots.

immediately apparent whether the excess current drawn by the LED lamps appears as light in the non-visible spectrum or manifests itself as heat.

5.2 Importance of the cross-correlation operator

In this part of the chapter, it was shown that the LED lamps can be very sensitive to point-on-wave of high frequency distortion. The presence of voltage condition where point-on-wave of distortion changes, is thus likely to cause light to flicker. IEC $61000-4-19$ standard recognizes this in its test methodology. However, the tests simply state that for immunity testing, it is alright to 'not have the CW pulses and the fundamental voltage frequency synchronized' to each other. However, there is a complete lack of understanding in literature as to how this point-on-wave impacts LED lamps (or any equipment with a switched mode power supply). This thesis, for the first time, shows

the sensitivity of DC-DC converter circuits to this point-on-wave. The cross-correlation operator is intended to serve as a mathematical aid to identify 'point of maximum sensitivity' for such circuits. It is intended that cross-correlation be utilized as a tool to make these sensitivity experiments reproducible. More importantly, it is intended to be used as a design and development tool in EMC studies for such converters. This section of the thesis is intended to fill this gap in knowledge.

5.3 Impact of converter topology

In this section, the effect of supraharmonics on LED driver circuits is analyzed. It was seen previously that there is a wide variety in the response of LED lamps, to supraharmonics. It was speculated that this variety is due to differences in topology of the LED driver. It was also surmized that maybe certain lamps exhibit immunity to supraharmonics, because of the topology. The inherent assumption being that certain topologies, such as the isolated DC-DC converter topologies could be inherently immune to supraharmonics. However, since the LED driver converter topology could not be immediately determined, this could not be verified in a straightforward manner.

Five commercially available LED driver boards from various manufacturers, various representative power handling capabilities and topologies were chosen for this purpose. Since LED lamps cannot be physically decapsulated without potentially damaging the circuit inside, it was determined that this approach would provide a higher degree of freedom in terms of measurement. Output voltage and current, going into the LED itself could thus be measured and the physical condition of the driver circuit could be monitored. The experimental setup was the same as described before and the experimental procudure was the same. The LED drivers were used to drive discrete LEDs purchased separately.

5.3.1 LED Drivers studied

For the purposes of this study, five LED drivers were chosen to give a sampling of the present topological mix of the LED driver market [16]. The criteria for selection was the achievement of diversity in terms of manufacturers, power capacities and in terms of LED driver topology. The nameplate data of the driver boards used in this study has been detailed in Appendix B.

For the rest of this thesis, each board shall be referred to by the serial number attached to it in Appendix B. The LED load used with each board has been summarized in Appendix C. As a

small note, Appendix B can be used as an indicator of the popularity of the flyback converter in the present LED driver market. In applications below 100 W, these converters are predominant because of the ease of use and control, low bill of material and the galvanic isolation that the converter offers. The details of this converter are discussed in the next chapter.

5.3.2 Impact on light output

The light output from the LEDs is again compared for three cases: (*i*) light output with input voltage containing only distortion that exists in the grid, (*ii*) voltage containing test signal 1 superimposed onto the fundamental frequency; (*iii*) voltage with test signal 2 superimposed. Figure 5.10 shows the results when the tests were carried out with board 1.

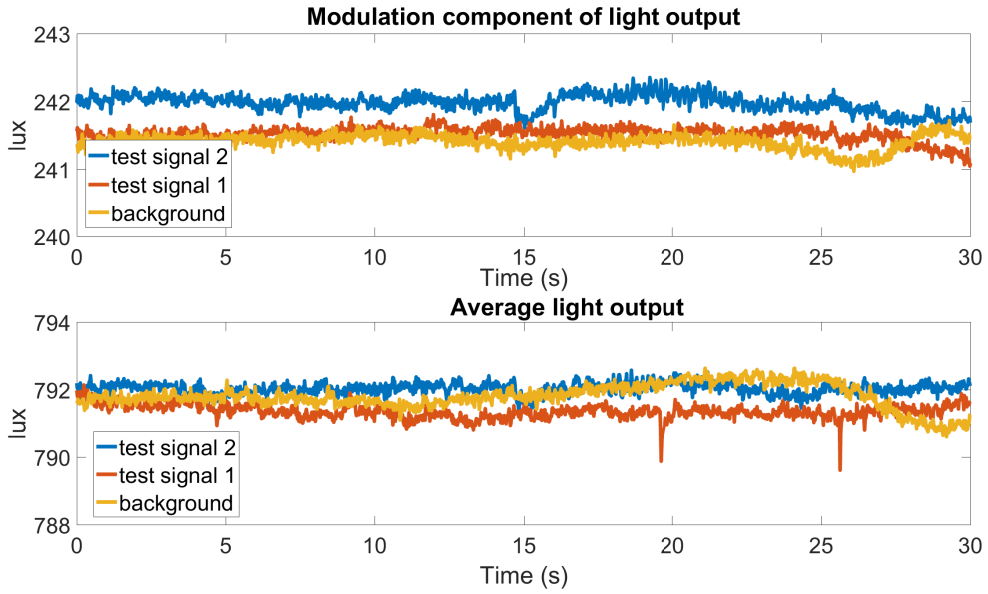

Figure 5.10: Average light output (bottom) and light modulation (top) under three different input voltage conditions for LED driver board 1.

Figure 5.10 shows that the voltage distortion signal applied at the input has minimal effect on both the average light output and the modulation. Board 2 showed identical behavior and hence has not been shown for brevity.

Figure 5.11 shows the results of the same experiment when LED driver board 3 was utilized. It was observed that average light output reduces by about 40% with the introduction of test signal 1 and by about 50% by the introduction of test signal 2 in supply voltage. The same holds for the

modulation of light output.

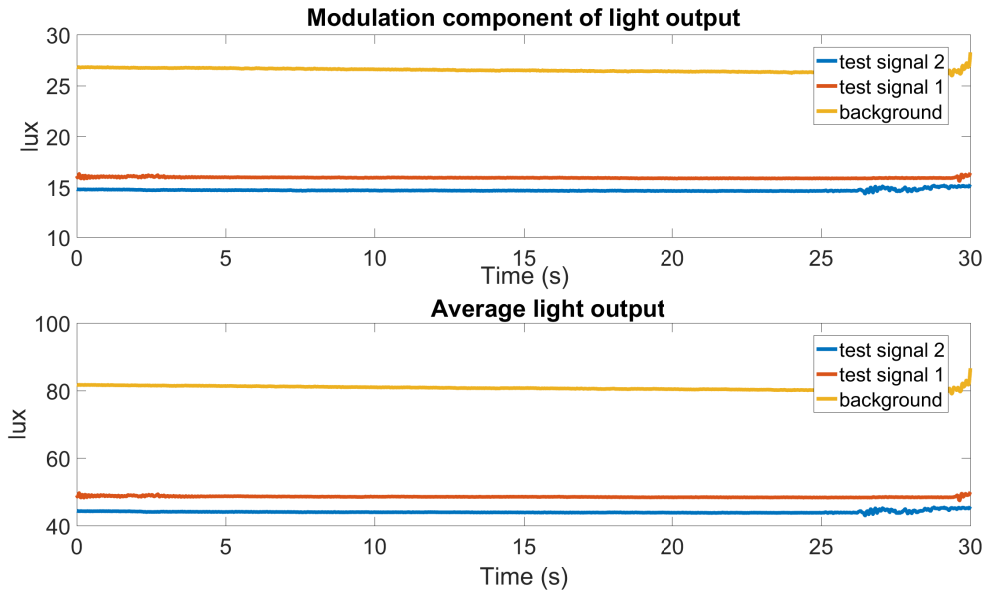

Figure 5.11: Average light output (bottom) and light modulation (top) under three different input voltage conditions for LED driver board 3.

The results for board 4 (Figure 5.12) look similar to the results of board 3 except for one key difference: the average light output and light modulation with test signal 2 show 'bursts' of changing magnitude as were scene with some LED lamps previously, due to change in point-on-wave condition of supraharmonics.

Utilizing LED driver circuits provided the advantage of monitoring LED forward current (this is the output current from the LED driver). Since the light output of an LED is proportional to the amplitude of the current through it, the next step was to determine if the change in the point-on-wave of high frequency distortion led to a change in the current input to the LED. It was observed that the 'point-on-wave' at which test signal 2 appeared on the fundamental wave moved continuously in both cases (board 4 and 5). Plotting the driver input voltage and its output current shows that the output current responds to this shift in point-on-wave position. This is shown in Fig. 5.13 for board 5. It can be seen that the appearance and disappearance of distortion near the peak of the voltage causes the ripple component of the driver output current to change magnitude accordingly. The driver input voltage and output current have been plotted for two instances in time (out of a 30 s window). In one instance, test signal 2 appears near the zero crossing of the

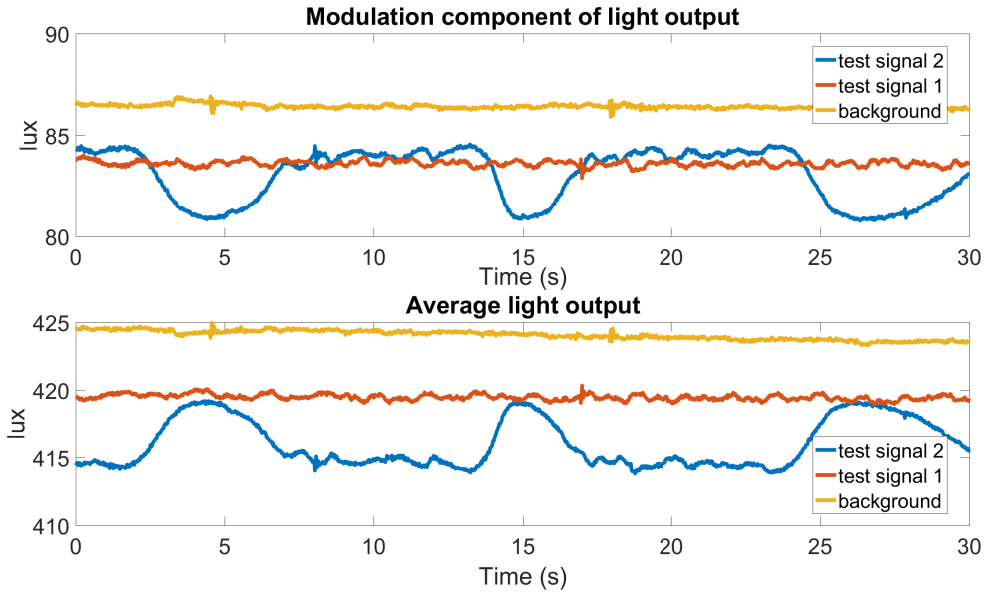

Figure 5.12: Average light output (bottom) and light modulation (top) under three different input voltage conditions for LED driver board 4.

fundamental wave and in the other case, it appears near the peak of the wave. The peak to peak value of the ripple component of the current changes from 50 mA to about 60 mA in response.

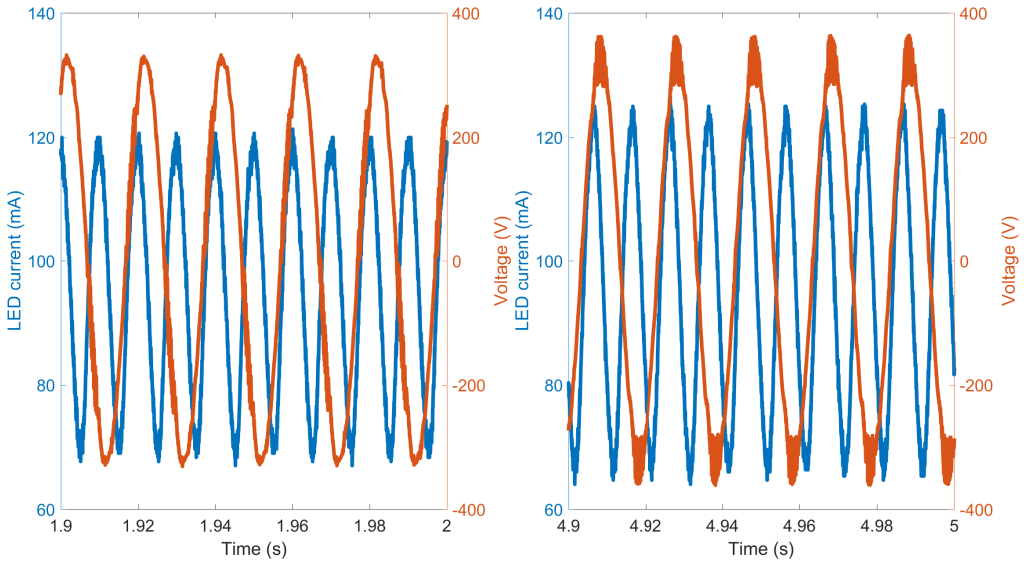

Figure 5.13: Input voltage and output current (to the LED) for LED driver board 5 measured at two different instances of time.

5.3.3 Correlation between light output and LED current

Up until now, the impact of high frequency distortion on light output has been discussed. In Figure 5.11, it was seen that the light output from board 3 undergoes a reduction due to the introduction of test signal 1 in test voltage. This reduction is even more when test signal 2 is superimposed onto the input voltage. This reduction is directly correlated with the reduction in the current through the LED. The average current (cycle by cycle average) through the LED (the output stage of the LED driver) was calculated in each case. For LED driver board 3, these values are shown in Figure 5.14. Figure 5.14 shows that the forward current through the LED and the light output have a direct correlation with each other. Quite like the light output, the forward current through the LED (this is the output from the LED driver) decreases due to the presence of test signal 1 in input voltage. This reduction is larger when test signal 2 is present in the source voltage. This relationship is important and will be utilized in later sections when simulation results are presented. Since simulation cannot show the light output from the LED lamp, the current from the output stage of the LED driver is measured in simulation and used as an indicator of light output.

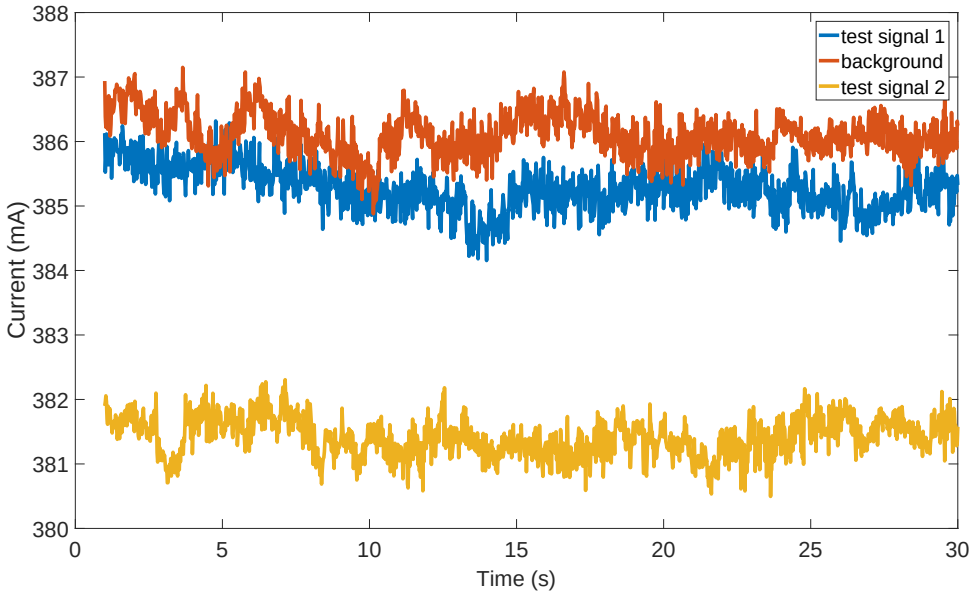

Figure 5.14: Output current from LED driver board 3 under different input voltage conditions.

The output current from LED driver board 4 is shown in Figure 5.15. Note the correlation with Figure 5.11, especially with regards to the effect of point-on-wave of light with test signal 2.

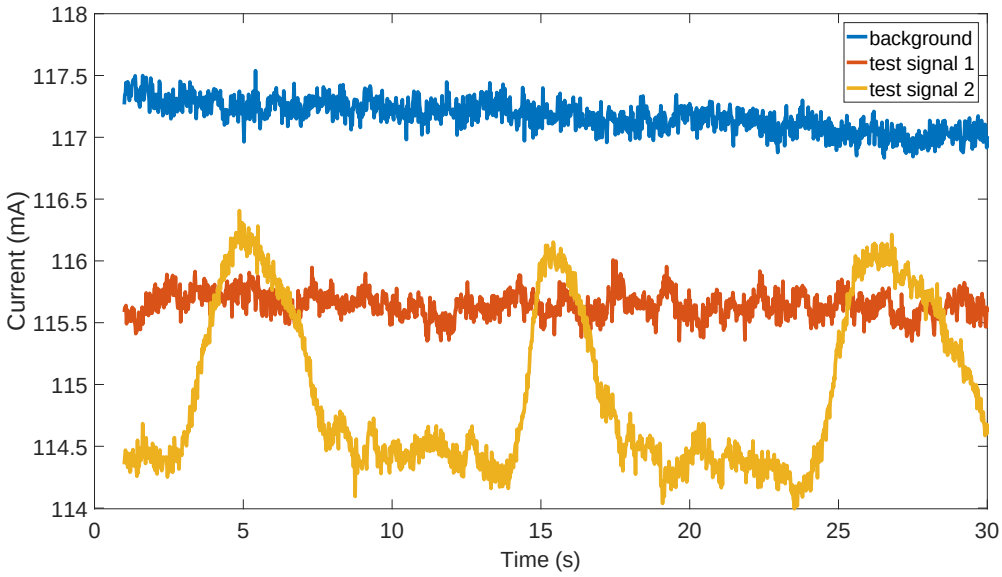

Figure 5.15: Output current from LED driver board 4 under different input voltage conditions.

As a final note, the effect of high frequency distortion on the output current from LED driver board 5 is shown in Figure 5.16. Note the reduction in DC current due to presence of high frequency distortion in the AC input voltage.

5.4 Discussion of experiments

In these experiments, it has been shown that input voltage distortion in the frequency range 2 to 150 kHz can not only cause photometric flicker (and hence percent flicker) to change in magnitude but also cause the average light output to drop, leading to a reduction in the efficiency of the LED driver.

It was observed that the effects are not converter specific, and in fact converters with the same configuration can have completely different behavior. The selection of boards included non-isolated topologies such as the buck and the buck-boost topology as well as the flyback topology which uses a transformer to provide source to load galvanic isolation. In the case of non-isolated topologies, it was observed that input voltage disturbances affect the LED load and the disturbances pass right through. This however, was not anticipated in the case of flyback converter operation. Flyback converters are often the converter of choice in low power applications and the use of primary

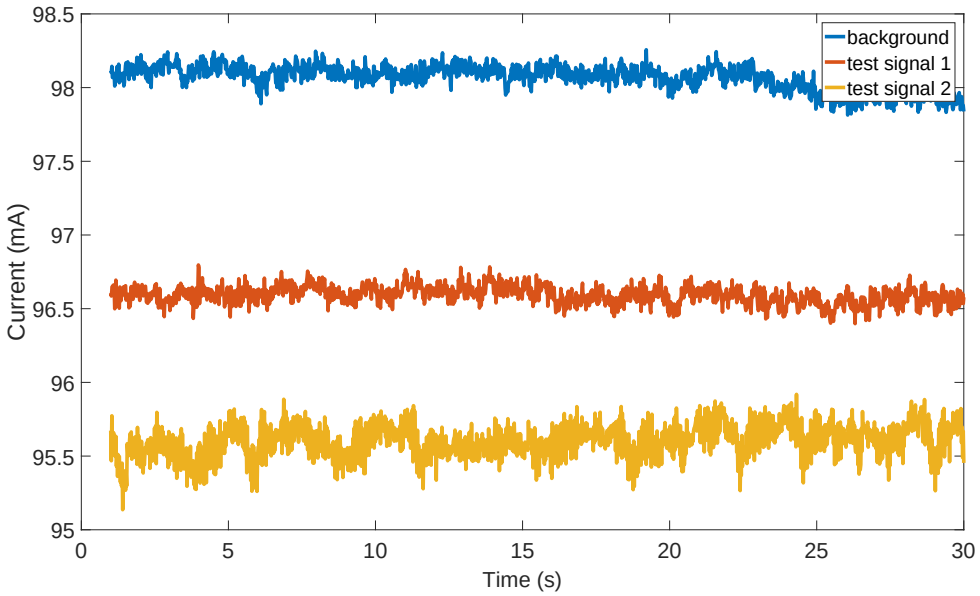

Figure 5.16: Output current from LED driver board 5 under different input voltage conditions.

side regulation and control helps to reduce part count which makes them a popular solution for LED drivers. It was observed that in 2 out of 3 cases tested, the flyback topology does show immunity to input voltage changes. However, in the case of a third driver, light degradation up to 50% was observed. The results of the experimental work show that in the case of DC-DC converter based LED drivers, presence of a transformer between the source and the load does not guarantee that the load will remain isolated from input disturbances. The results show that this phenomenon is rather more involved and requires analysis of converter control mechanisms. Simply changing LED driver topology may not guarantee better performance with regards to EMC.

To verify these results, a detailed simulation of the flyback topology was set up. A popular control scheme for flyback converters, called 'primary side regulation' was examined to understand how this phenomenon of interference with DC-DC converters actually happens. This is detailed in the next chapter.

Chapter 6

Simulation results

In the previous chapters, experimental results with LED lamps and LED drivers were presented. It was seen that conducted disturbances from supraharmonics can cause interference with the DC-DC converter circuit used in an LED lamp, which can ultimately lead to flicker. This has also been observed in the field, both in Europe and in the US. It was shown that this flicker depends upon the point-on-wave of distortion and is not necessarily dependent on LED driver topology. It was shown that LED drivers with the same topology can have completely different EMC characteristics, most likely due to the control methodology utilized. However, it was concluded that the hardware testing has its limitations. Because of limited freedom available in terms of measurement, it could not be assessed what the actual mechanism for this interference (and hence flicker) is. Further, regardless of the number of LED lamps tested, it is very difficult to generalize results to a larger data set. The sheer number of LED driver topologies and control methodologies available, further complicates this. Some of these problems can be overcome by the use of accurate, device level simulations of LED drivers. In this chapter, one such simulation of a very popular LED driver solution has been presented. The laboratory experiments were then repeated in simulation, to verify the empirical observations. The interference mechanism has been explored in detail at the control level. Finally, results of simulation with an actual voltage waveform from the field (which produced flicker) are shown, along with data that points to component degradation in the LED driver due to supraharmonics.

6.1 The theory of LED drivers

Figure 6.1 shows a block diagram of an LED driver. Note that Figure 6.1 is not a generic diagram. Many LED lamps available on the market, do not use a power factor correction (PFC) circuit at their front end. Sometimes, the PFC circuit may be integrated into the rectifier or DC-DC converter stage. Similarly, other lamps may have one or more additional blocks next to the ones shown here.

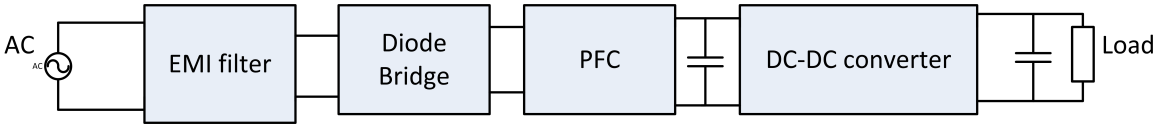

Figure 6.1: Block diagram of an LED driver. Note that load in this case is an array of LEDs.

The broad diversity in currents drawn by LED lamps (likely due to different circuit layouts) can be illustrated by observing the input current waveforms of 4 of the 32 lamps tested. This is shown in Figure 6.2. The lamps shown are lamp 8, 27, 19 and 28.

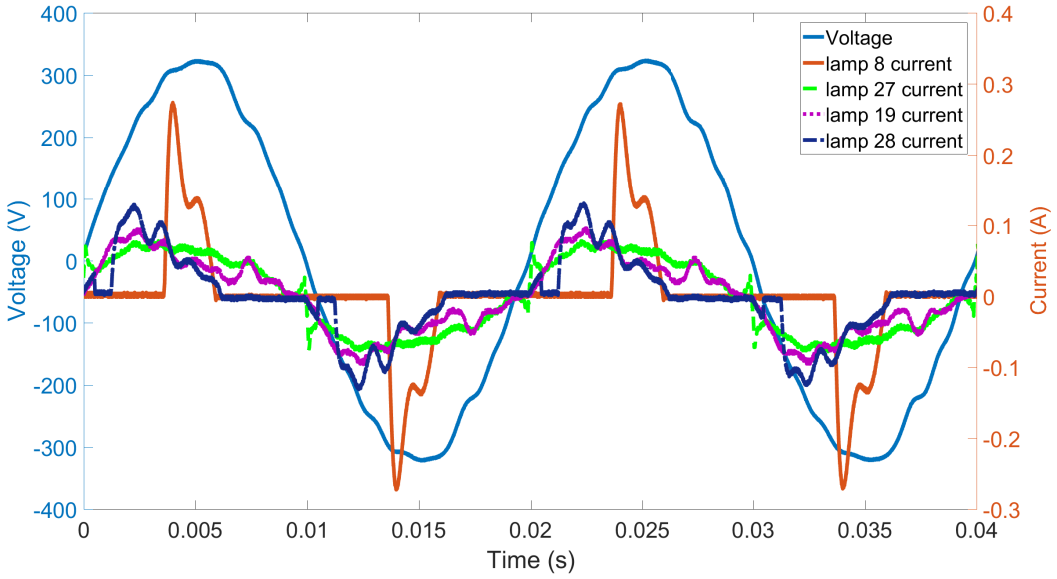

Figure 6.2: Source voltage and input current waveforms for lamps 1 to 4 (from top to bottom).

The brightness of an LED depends upon the forward current through it. Fundamentally, the idea is to provide a constant current to an array of light emitting diodes, in order to maintain a

constant level of illumination. This is accomplished by rectifying the line voltage in the first stage. The most rudimentary circuit that can be used to power LED lamps thereafter is a series resistor. Essentially the idea is to use a resistor in series with the DC voltage, to regulate the current through the LED lamps. This circuit suffers from the following problems:

1. Poor efficiency: Modern day LEDs are designed for nominal operating currents of 350 mA or more. Further, the forward voltage drop of an LED can be 3 V or more. In such conditions, the power that is dissipated in the resistor cannot be ignored [16, 52].

2. Poor regulation: The lack of active switching and control is a big problem with this circuit. The current through the LED has to be controlled to remain constant. The series resistor cannot be used to provide such regulation and control.

These problems are overcome through the use of power electronics based switched mode DC-DC converter circuits. Normally DC-DC converters are designed to stabilize output voltage. However, by adding a shunt resistor in series to the LEDs, the current can be measured by measuring the voltage at the shunt, so that standard techniques of control can be applied. The problem with this technique is that the resistor leads to additional power losses, which designers try to minimize. This technique is generally utilized in the following standard topologies:

1. Buck converter

2. Boost converter

3. Buck-Boost converter

The theory behind the working of these converters can be found in standard text books on power electronics and for a quick reference, the reader may refer to [44, 52]. These topologies are generally referred to as non-isolated converter topologies. There is a conducting path between the source and load and no galvanic isolation. Another category of DC-DC converters utilizes transformers to provide this galvanic isolation. Two popular solutions in this category are:

1. Flyback converter

2. Resonant converter

Based upon literature review and market survey of available LED drivers, it was discovered that flyback converters are by far the most popular solutions for all sorts of applications below 100 W, and also for LED lighting [16]. Thus, the peculiarities, hardware layout and the principles used for controlling these converters are discussed here. The resonant converter is a subject of active research and may end up becoming the solution for the future. This converter is being studied for its low EMI contribution and high power density. The discussion of this converter, since it is not yet a popular commercial solution, is beyond the scope of this thesis.

6.2 The Flyback converter

.

A basic diagram of a flyback converter is shown in Figure 6.3. The flyback converter operates by first storing energy in the primary winding of the flyback transformer when the MOSFET is turned 'ON' [53]. During this period, due to the transformer winding polarities (indicated in the figure), the secondary side winding polarity is such that the diode on the secondary side is reverse biased. As a result, no current flows in the secondary winding of the transformer. During this period, the load current is supplied from the energy stored in the capacitor.

Depending upon the way energy transfer takes place, two types of operating modes can be identified:

- Continuous Conduction Mode (CCM): In CCM, a part of the energy stored in the transformer, remains in the transformer when the next 'ON' period of the MOSFET starts. As a result, the primary current at the start of the 'ON' period has a non-zero value and energy remains stored in any magnetic elements in which current is flowing.

- Discontinuous Conduction Mode (DCM): In DCM, all the energy stored in the transformer during the MOSFET 'ON' period is transferred to the secondary side circuit during the 'OFF' period. As a result, the secondary side linearly reduces to zero from its maximum value during the 'OFF' period of the MOSFET. At the beginning of the next 'ON' period, the primary side current starts from a zero value. Note that there is usually a small delay between the moment the secondary side current reduces to zero and the next 'ON' period of the MOSFET begins.

Flyback converters are typically operated in DCM. This is because DCM offers the following

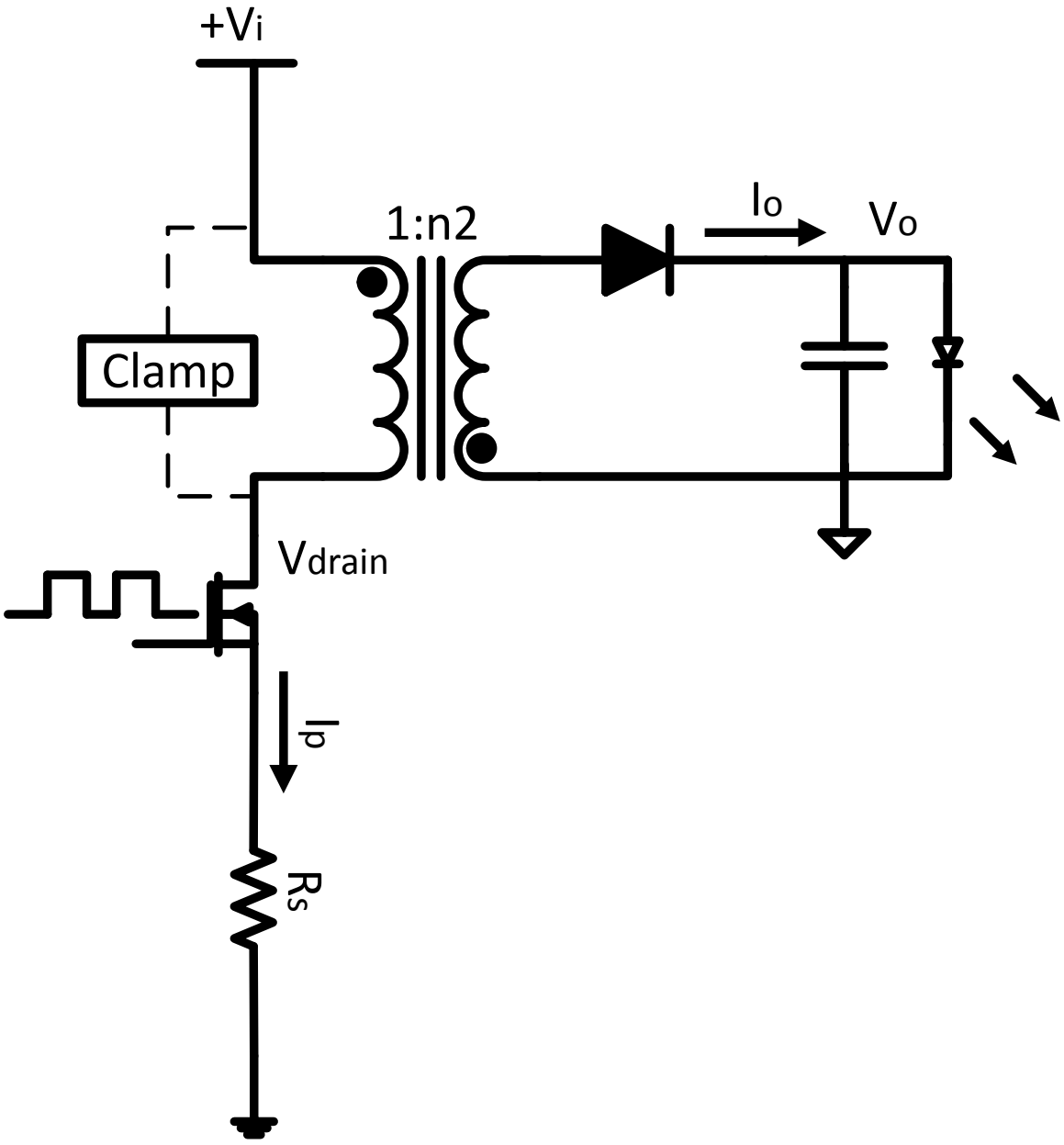

Figure 6.3: Basic diagram of a Flyback converter where Vi is the DC bus voltage on the input of the converter.

advantages:

1. Linear relationship between average input current and voltage, which results in a high power factor.

2. Faster load regulation.

3. Lower value of inductance required.

4. Allows utilization of current mode controllers which are ideal for LED applications.

The one disadvantage of DCM is that since devices have to handle higher peak currents than CCM, some components such as the flyback transformer have to be designed for larger values.

During DCM, when the MOSFET turns 'ON', the primary current starts to rise and reaches a maximum value (Figure 6.4). This maximum value is determined by the controller (described in detail later in this chapter). Once this maximum value is reached, the MOSFET is turned 'OFF'. At this point, the energy stored in the transformer is discharged into the secondary side circuit, which is connected to the LED load. The secondary current starts off at a maximum value and linearly reduces to zero, where it remains until the beginning of the next switching cycle. Since current ripple is much higher than CCM, the transformer inductance value required for this converter is smaller.

In DCM, because of complete discharge of energy, the rms values of the currents are higher. When the MOSFET is turned 'ON', the primary side current increases from zero and reaches a maximum value given by:

$$I_{pmax} = \frac{V_i}{L_p} \times t_{on} \tag{6.1}$$

V_i is the DC link voltage to the converter. In the case of input voltage that is rectified from incoming AC mains, V_i is taken to be the maximum value of the rectified voltage. t_{on} is the conducting interval of the MOSFET. During this period, the reversed biased secondary does not conduct. The load current is supplied by the energy stored in the capacitor. At time $t = t_{on}$, the MOSFET is turned 'OFF'. The secondary current starts from a peak value given by:

$$I_{omax} = n2 * I_{pmax} \tag{6.2}$$

since,

$$L = \frac{\mu N^2 A}{s} \tag{6.3}$$

$$\therefore N = \sqrt{\frac{Ls}{\mu A}} \tag{6.4}$$

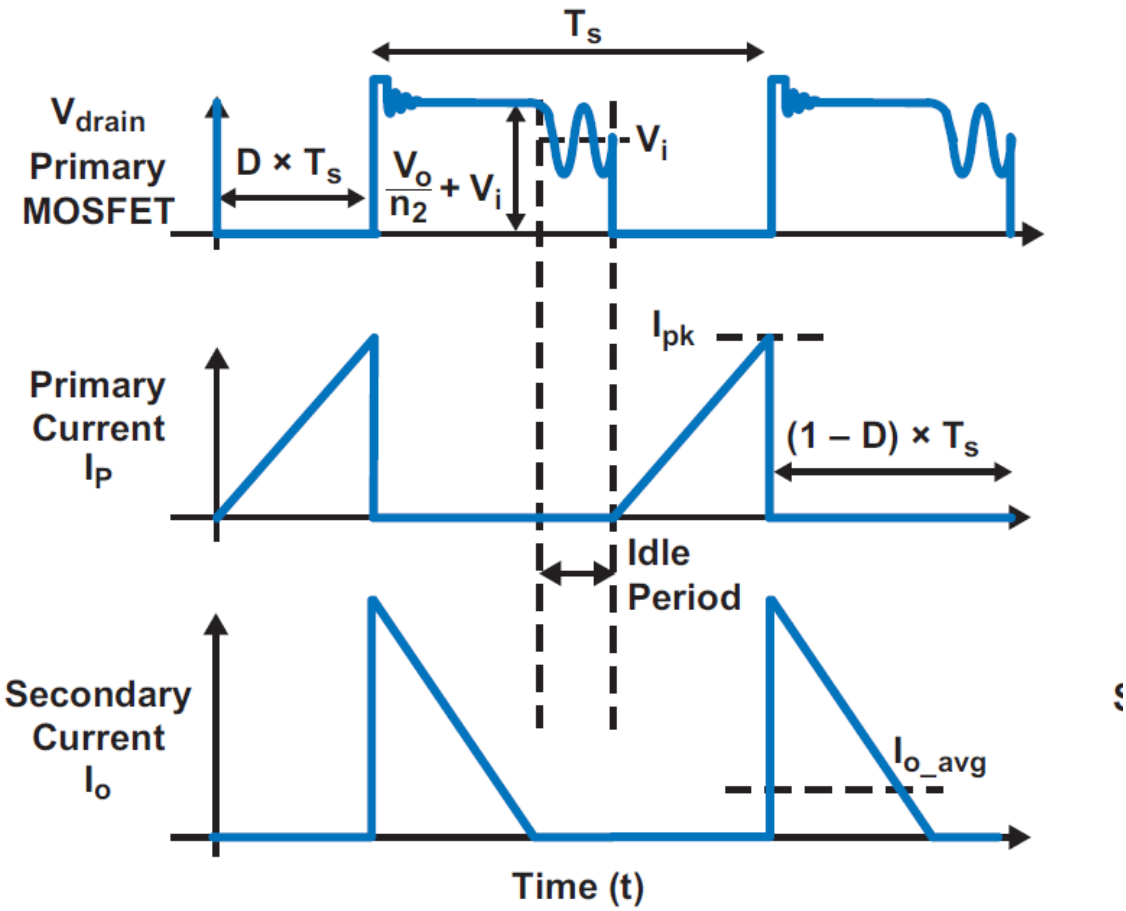

Figure 6.4: Drain voltage at the MOSFET (top), primary current (middle) and secondary (bottom) current in DCM. Note the difference in scale on the vertical axis. [53]

where L (in a simple structure) is the inductance of the coil, N is the number of turns of the coil, A is the cross sectional area of the magnetic core, s is the mean length of the of the magnetic path (the approximate length of the magnetic core that the flux travels), and μ is the permeability of the core. Since the primary and secondary windings are wound on a common magnetic core, equation 6.2 can be rewritten in terms of the winding inductances as:

$$I_{omax} = \sqrt{\frac{L_p}{L_s}} * I_{pmax} \tag{6.5}$$

where L_p and L_s are the inductances of the primary and secondary windings respectively. Assuming that the time at which the secondary circuit discharges completely ($t = t_2$) i.e., the

secondary current goes to zero is known, the average current in the load can be calculated by integrating the secondary side current:

$$I_{avg} = \frac{1}{T_s}\int_0^{T_s} I_o dt = \frac{1}{T_s}\int_{t_{on}}^{t_2} I_o dt \tag{6.6}$$

Since integration gives the area under the curve, in the given case, the integral of the secondary current (average current) is approximated by the area of the triangle ($\frac{1}{2} * base * height$):

$$I_{avg} = \frac{1}{2} I_{omax} \frac{t_2}{T_s} = \frac{1}{2} I_{omax} t_2 f \tag{6.7}$$

where f is the switching frequency and $T_s = \frac{1}{f}$ is the total switching period. For DCM, $t_2 < T_s$. The maximum energy stored in the primary winding of the transformer is:

$$\frac{1}{2} \times L_p \times I_{pmax}^2 = \frac{1}{2} \frac{V_i^2 D^2}{L_p} \tag{6.8}$$

where $D = \frac{t_2}{T_s}$ is the duty cycle of the converter. Since all the energy stored in the flyback transformer is transferred to the load in DCM, the power transferred by the converter to the load during DCM is therefore:

$$P_{DCM} = \frac{1}{2} \frac{V_i^2 D^2}{L_p f} \tag{6.9}$$

The value of the power transferred by the flyback converter to the LED load, thus depends upon input voltage, the 'ON' time of the converter and the value of the inductance.

Assuming that the converter efficiency is 100%, this gives the following relationship between the input voltage and input current of the flyback converter:

$$I_{in} = \frac{1}{2} \frac{V_i D^2}{L_p f} \tag{6.10}$$

Generally, the input DC link voltage is not a stiff DC but rather a pulsating waveform (see Figure 6.14). Based on the above expression, due to the linear nature of the input current and voltage relationship, it is possible to obtain a high power factor from this circuit. In other words, it is possible to force the current drawn by the circuit to follow the input voltage as accurately as possible by a simple design change without the need for an additional power factor correction

circuit. In general, this linear relationship between input voltage and current results in a high input power factor for the converter. An example of this is the implemented simulation. A power factor correction circuit is not employed in this circuit. Yet, the power factor of the designed converter is approximately 0.98. Thus, operation in DCM results in a high power factor for the designed converter.

In real life, the coupling between the primary and secondary is not perfect. There is some leakage inductance in the transformer, due to which part of the energy stored in the primary does not get transferred to the secondary. As a result, during commutation from the primary side to the secondary side, the leakage current tries to charge the parasitic capacitance of the MOSFET. This can result in voltage breakdown of the MOSFET. To prevent this eventuality, usually a snubber and/or a clamp circuit is utilized.

6.3 Flyback converter implementation and control

In actual practice, the flyback converter is a circuit that depends heavily on accurate current and voltage sensing for its operation [54–57]. Traditionally, flyback converter regulation has been achieved by having secondary (output current to the LED) feedback control. This is normally achieved by having error amplifiers and phototransistors on the secondary side circuit to achieve output voltage and current regulation. The main task of this secondary feedback circuit is to transfer the secondary side signals to the primary side so that the controller can modulate the pulse-width. This is how regulation of the output is achieved with change in load.

This method also has its own set of problems, with penalties in terms of the number of components and the size of the printed circuit board (PCB). With the higher part count, the amount of power lost also increases.Further, an optocoupler would be needed for secondary side sensing to maintain galvanic isolation. This device is expensive, prone to failure, and adds substantially to the bill of material (BOM). In many applications, this higher part count, footprint, power consumption and cost are considered unacceptable. To overcome this problem, the method of primary side regulation (PSR) is used today. This circuit eliminates the need for the secondary side feedback circuit by accurate sensing of the secondary side voltage and current from the primary side.

Figure 6.5, shows the block diagram of such a PSR scheme. An auxiliary winding on the transformer is used to monitor the voltage on the secondary side of the circuit.

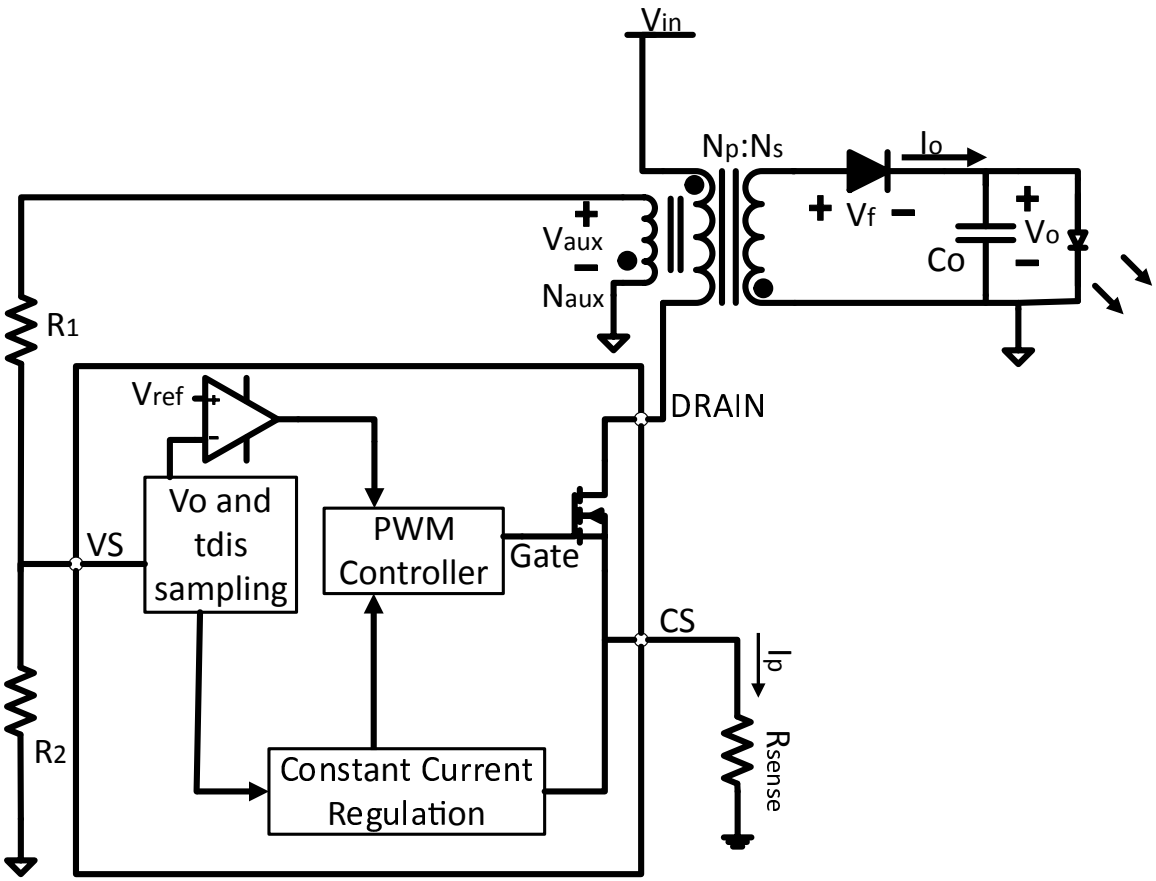

Figure 6.5: Block diagram of flyback converter with PSR.

Once the MOSFET turns 'ON', the current in the primary starts to rise and quickly reaches a peak value in accordance to the formula given in equation 6.1. This energy is stored in the transformer in accordance to equation 6.8. During the MOSFET 'OFF' time (t_{off}), the stored energy is transferred to the load. The output voltage and the forward voltage drop of the diode induce a voltage on the auxiliary winding (V_{aux}) that can be calculated as follows:

$$V_{aux} = \frac{N_{aux}}{N_s}(V_o + V_F) \tag{6.11}$$

where V_o is the output voltage and V_F is the forward breakover voltage of the diode. A sampling circuit on the PSR controller detects a sample of this voltage. With prior knowledge of the diode forward voltage, two pieces of information are obtained by the controller from this voltage sample:

- Output Voltage on the secondary side.
- The discharge time ($t_{dis} = t_2$) of the secondary side circuit.

The controller compares this knowledge of the output voltage against an internal reference voltage (V_{ref}). The operational amplifier thus acts as a voltage-loop error amplifier for amplifying the voltage feedback signal and providing a voltage loop gain for output voltage control. The controller thus establishes a controlled MOSFET on-time to stabilize any deviations in the output voltage. This forms the 'voltage control loop'.

In practice, V_{aux} starts to oscillate when the output current on the secondary side reaches zero. This is because of the $L - C$ circuit formed by the auxiliary transformer inductance and the MOSFET output capacitance. These oscillations continue until the MOSFET turns ON again. The sampling circuit then knows that the time at which V_{aux} starts oscillating is the discharge time of the secondary circuit.

The discharge time signal is provided as input to the 'current control loop'. The PSR controller receives a current waveform from the current sensing resistor (R_{sense}), which generates a voltage (V_{CS} where CS stands for 'current sense') that corresponds to the current flowing in the primary side circuit. This current is used to calculate the total energy stored in the transformer using equation 6.8. Knowledge of the stored energy and secondary side inductance provide the controller with the value of the maximum current on the secondary side (Energy stored energy in an inductor = $\frac{1}{2}Li^2$). This maximum value and the discharge time of the secondary circuit are provided to an integrator which then calculates the average output current value using the formula given in equation 6.7 (repeated here for convenience):

$$I_{avg} = \frac{1}{2} I_{omax} \frac{t_2}{T_s} = \frac{1}{2} I_{omax} t_2 f \tag{6.12}$$

since

$$I_{omax} = \frac{N_p}{N_s} * I_{pmax} \tag{6.13}$$

where N_p and N_s are the number of turns on the primary winding and secondary winding respectively.

$$I_{avg} = \frac{1}{2T_s} \frac{N_p}{N_s} (t_{dis})(I_{pmax}) = \frac{1}{2T} \frac{N_p}{N_s} \frac{V_{cs}}{R_{sense}} (t_{dis}) \tag{6.14}$$

where t_{dis} is the time at which the secondary side current reduces to zero and is thus equal to t_2.

In this manner, the PSR controller obtains an output current feedback signal, indirectly from the current sense resistor. The value of the average output current is regulated by the controller by comparing it with an internal reference signal. Under feedback control, the width of the gating signal is adjusted according to this error control loop. The gating signal dictates the maximum primary side current, which then (on the basis of the above equations) dictates the average output current. Thus, the output of the control scheme is a value of the peak primary side current. The control system thus regulates output current by regulating primary side peak current. The Primary Side Regulation scheme is thus composed of the following important steps:

- Output voltage detection using the auxiliary winding. Generation of a feedback signal by comparing this voltage against an internal reference voltage and using this feedback loop to stabilize deviations from the preset value.
- Calculation of total energy stored in the circuit using peak value of primary current.
- Calculation of average output current using the value of the stored energy and then subsequently using the value of the secondary side discharge time. Using a current regulation loop which then regulates primary side peak current (and hence energy stored in the transformer) and thus controls average output current.

Using the current control loop, the peak primary current value is calculated to regulate the secondary side current. In effect, the switching action of the PSR produces a primary current peak-limiter circuit, since the primary current is constantly being sampled and compared against the set point produced by the PSR controller. Figure 6.6 shows the gating signal, primary and secondary current and auxiliary voltage from an actual PSR implementation which has been described in the next section.

6.4 Software simulation of a Flyback converter with PSR

In order to verify the results obtained experimentally, and to shed some light on the root causes of the observed conducted interference from supraharmonics, a simulation of a flyback converter with PSR was set up in PSpice. The designed converter had the following specifications [18,52]:

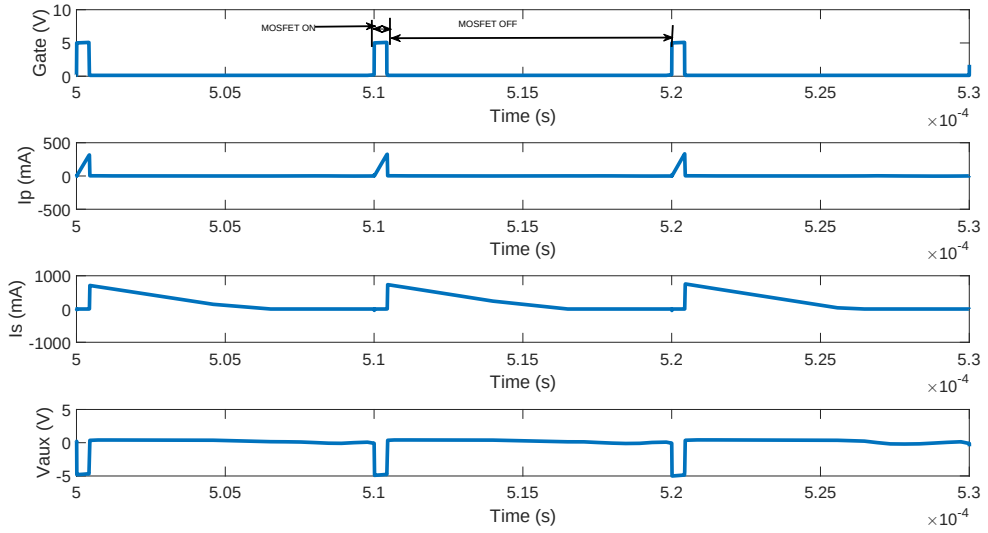

Figure 6.6: Input and Output signal values from a PSR implementation.

1. Input Voltage = 120 V RMS (60 Hz)
2. Output Voltage = 32 V DC
3. Output Current = 350 mA DC
4. Switching frequency = 100 ± 10 kHz
5. Operating mode: Discontinuous current mode (DCM)

The schematic diagram of the simulation is shown in Figure 6.7.

The simulation consists of the following four essential parts:

1. The actual LED driver unit with the current sense resistor.
2. The PI unit which is meant to implement the current control and voltage control loops.
3. The PWM unit.
4. The auxiliary transformer to detect secondary side voltage.

Since the software does not allow for a three winding transformer, the auxiliary winding arrangement was implemented by taking two terminals from the primary winding and applying it to

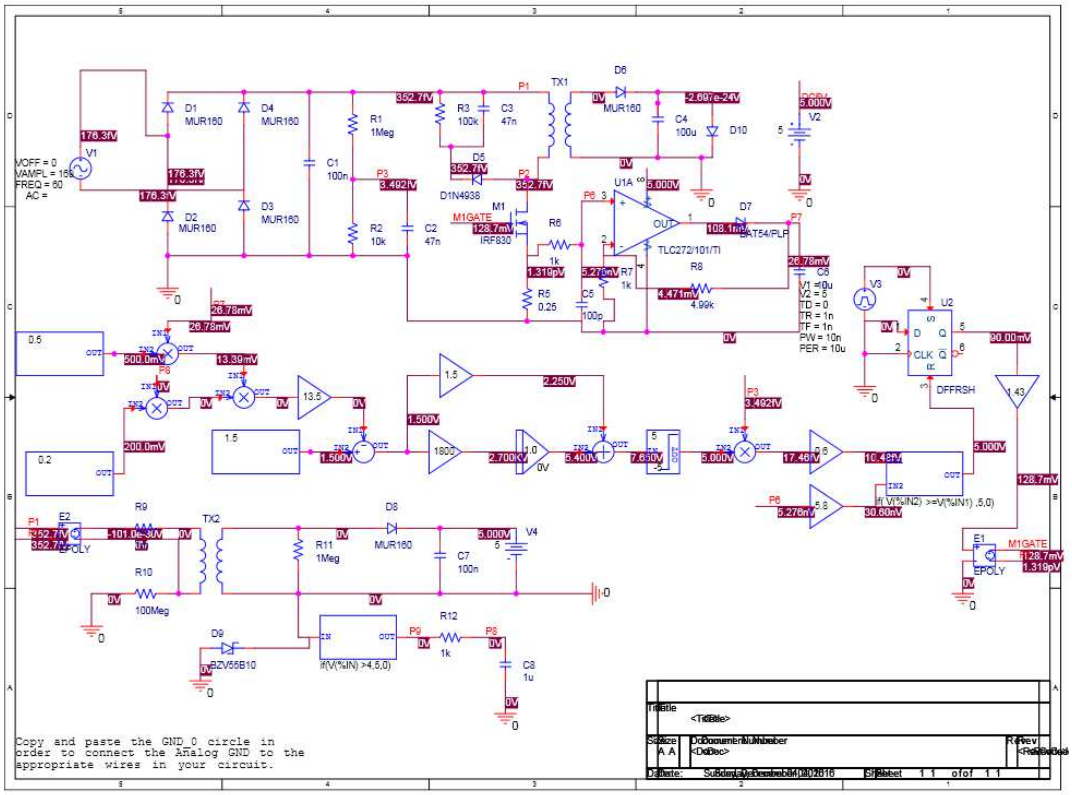

Figure 6.7: Schematic layout of PSpice simulation.

another transformer, which now works as the auxiliary transformer. The secondary side circuit of the converter was recreated to implement the voltage waveform detection logic described previously. As shown in Figure 6.6, this approach works rather well. The only difference is that unlike a physical implementation, the auxiliary voltage V_{aux} does not have any oscillation when the secondary side current decays to zero. This is because unlike a physical circuit, this approximation does not include the L-C loop formed by the MOSFET capacitance and the auxiliary winding.

Analog Behavioral Models (ABM) are used to implement the control logic for the converter. The output of the PID controller i.e., the current and voltage reference values are multiplied by the rectified input voltage waveform to make the reference signal for the PWM. For an LED, since the forward voltage drop is a fixed value, the LED operation comes down to current regulation. The brightness of the LED lamp depends upon this output current. Generally, in case a single or

a group of LEDs starts to malfunction in the LED cluster, the control methodology is designed to maintain a constant current through the new load. The nuances of the control logic depend upon manufacturer but generally in the case of LED lamps, priority is given to output current regulation over voltage regulation. The flowchart of the decision making for the PWM mechanism is shown in Figure 6.8 [18]

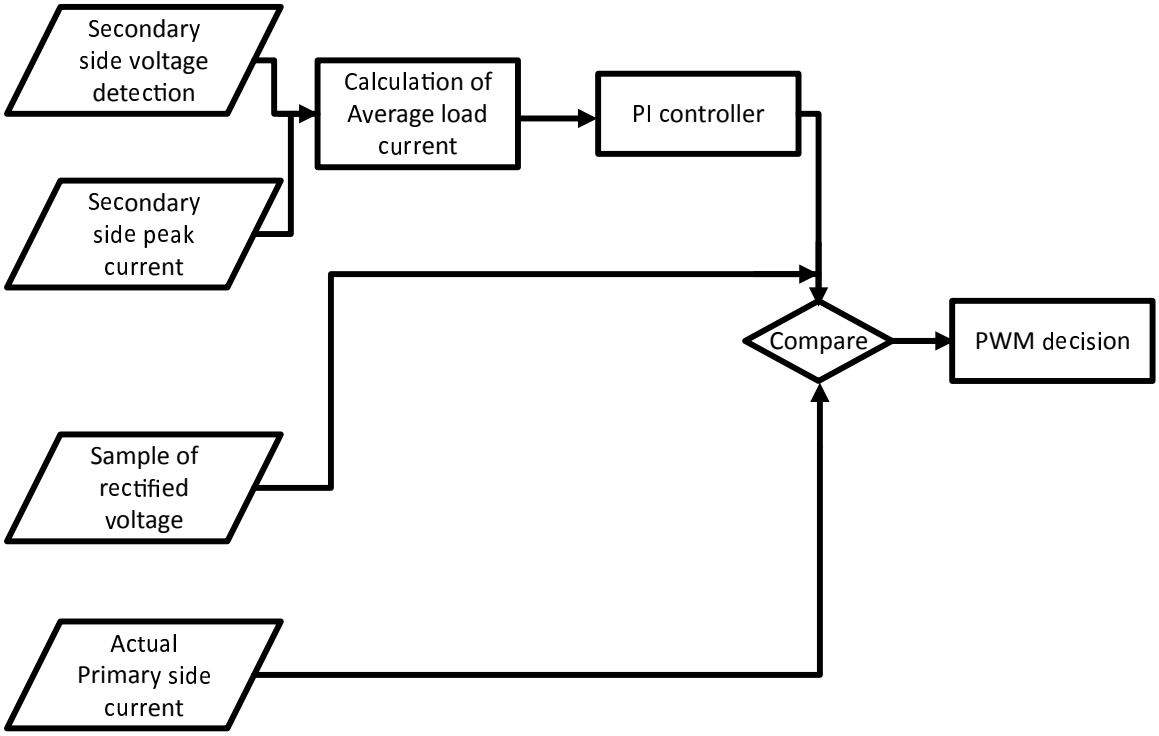

Figure 6.8: Flowchart for decision making process for the PWM mechanism in simulation.

6.5 Simulation Results

The basic results of the simulation in steady state with pure sine wave voltage have been shown in Figure 6.6. The accuracy of the simulation in capturing the actual behavior of a physical LED lamp could only be verified by comparing it against laboratory measurements. Repeating the same experiments with the same test signals as before, the output current (input current for the LED) waveforms from the LED driver are shown in Figure 6.9. Test signal 2 was deliberately not synchronized with the source voltage, to verify the results that were seen with the LED lamps that showed influence of the point-on-wave character of the signal, on the light output. The simulation

was run for a total time of 200 ms with a maximum stepping time of 1 ms.

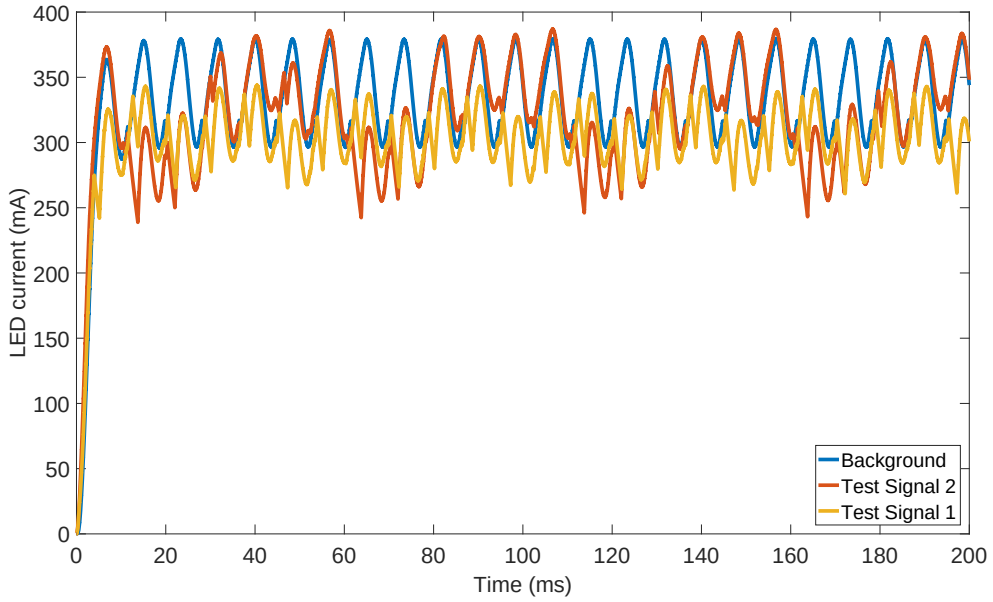

Figure 6.9: Output current from the simulated LED driver under various input voltage conditions.

Figure 6.9 shows that the simulation mirrors laboratory results with remarkable accuracy (shown in Figure 6.10 for comparison). The high frequency input voltage distortion on the AC input causes the output on the DC side i.e. the current output (which the converter is supposed to hold constant), to fluctuate in magnitude. Test signal 1 is present all through out the fundamental voltage wave when it is superimposed onto the fundamental voltage. Test signal 2 though has point-on-wave character and it appears at a given point on the fundamental voltage. The results show that when test signal 1 is superimposed onto the fundamental voltage, output current reduces by about 15%. With the introduction of test signal 2, the output current can reduce by as much as 30% and more importantly, the output current tracks the point-on-wave at which the high frequency distortion appears. Since the output current from the LED driver dictates the LED brightness, the results can be directly correlated with those shown in Figure 6.10. In laboratory experiments, light output from lamp 8 (and indeed most lamps tested) decreased from its nominal value with background distortion, when test signal 1 was superimposed onto the fundamental voltage. With test signal 2, the light output decreases even further and shows dependence on the point-on-wave of high frequency distortion. This was investigated next.

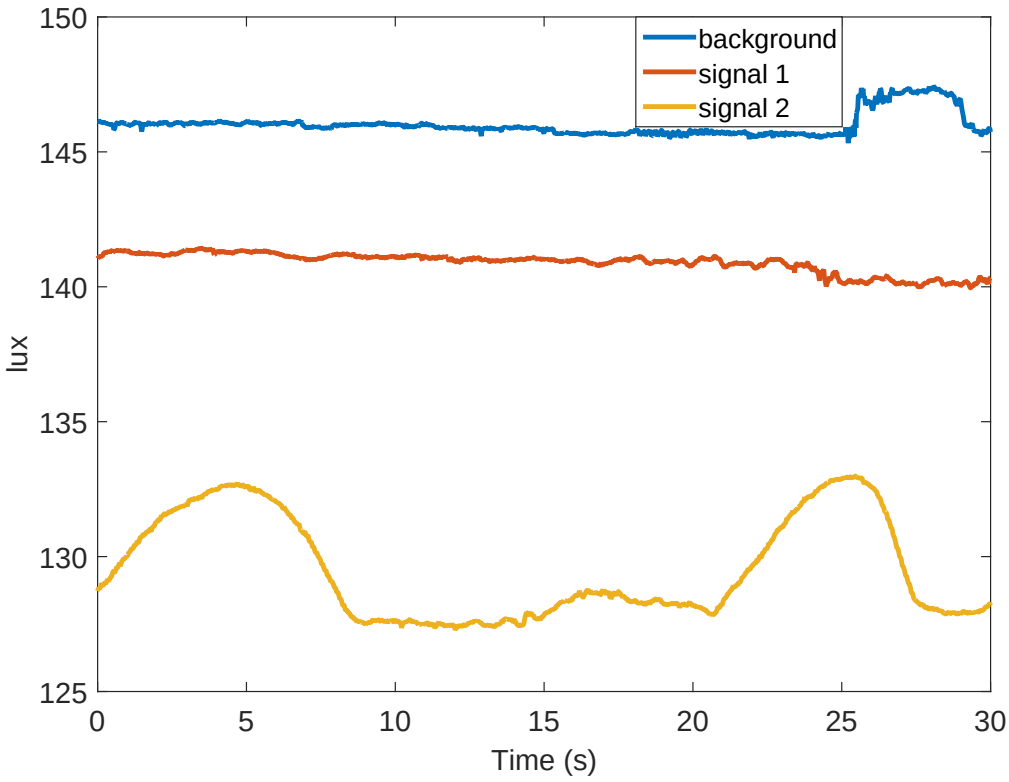

Figure 6.10: Light output from lamp 8 under different voltage conditions (obtained in laboratory tests).

6.5.1 Effects of supraharmonics on the LED driver

Narrowing down the investigation to test signal 2 allowed us to investigate the interference and the point-on-wave character it so often displays. Since the previous graphs only indicate the LED current, the next step was to investigate the primary and secondary currents in the flyback converter, with and without distortion present in the voltage. The current in the primary and the secondary windings of the transformer is shown in Figure 6.11 for a purely sinusoidal voltage and for source voltage containing test signal 2. It was observed that the presence of distortion near the 90°(or 270°for the negative half cycle) point of source voltage causes the MOSFET switch in the primary side of the converter to stay 'ON' longer than it normally does. During this prolonged 'ON' period, the primary winding is exposed to the rectified DC voltage and the primary current is limited by the DC resistance of the primary circuit. In real life, because of the prolonged 'ON' time, the transformer core may get saturated because of the DC voltage.

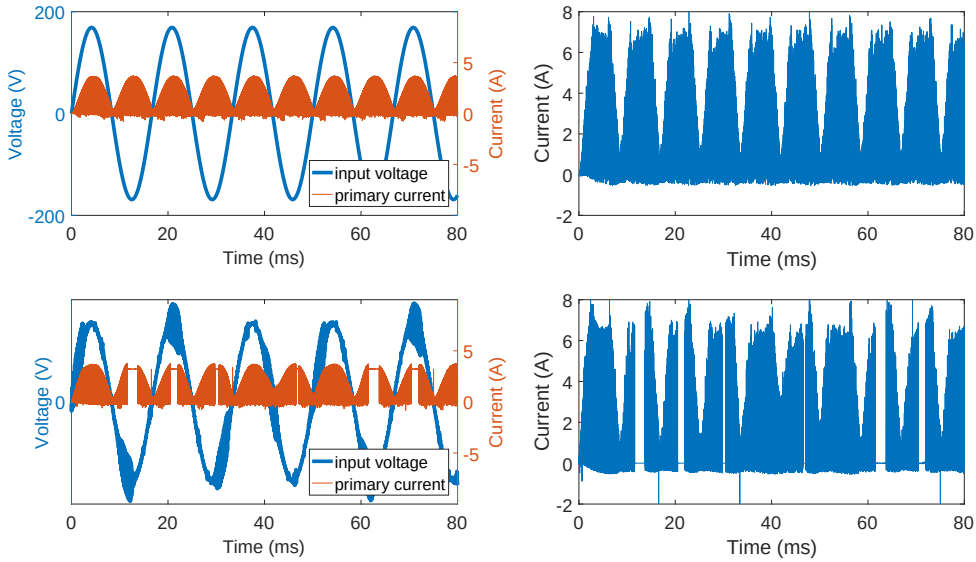

Figure 6.11: Input voltage and primary current (top left) and secondary current (top right) for the simulated LED lamp under ideal voltage conditions. The same quantities have been shown bottom left and bottom right for voltage containing test signal 2.

While the MOSFET remains 'ON', the secondary side does not conduct. During this prolonged 'ON' period of the MOSFET, the load is supplied through the energy stored in the capacitor. This leads the load current to drop as the capacitor discharges more than it normally does. This is in line with the experimental observations, where it was concluded that for certain LED driver topologies, lamp light output response is more pronounced near the peaks (or troughs) of the voltage waveform, while certain others were more sensitive to distortion near the zero crossing of the fundamental voltage wave. In this case, it is observed that the converter is more sensitive to changes in voltage near the peak of the fundamental voltage.

Another important observation from Figure 6.11 is that after every prolonged 'ON' period, the secondary side current value is higher than normal in certain time instances, indicating that the secondary side current decays to zero slower. This indicates that the longer 'ON' time causes more energy to be stored in the transformer, which is then discharged into the secondary during the 'OFF' time.

In order to determine whether the frequencies present in test signal 2, actually appear in the primary or secondary side currents, the spectrum of the currents is presented in Figures 6.12

and 6.13.

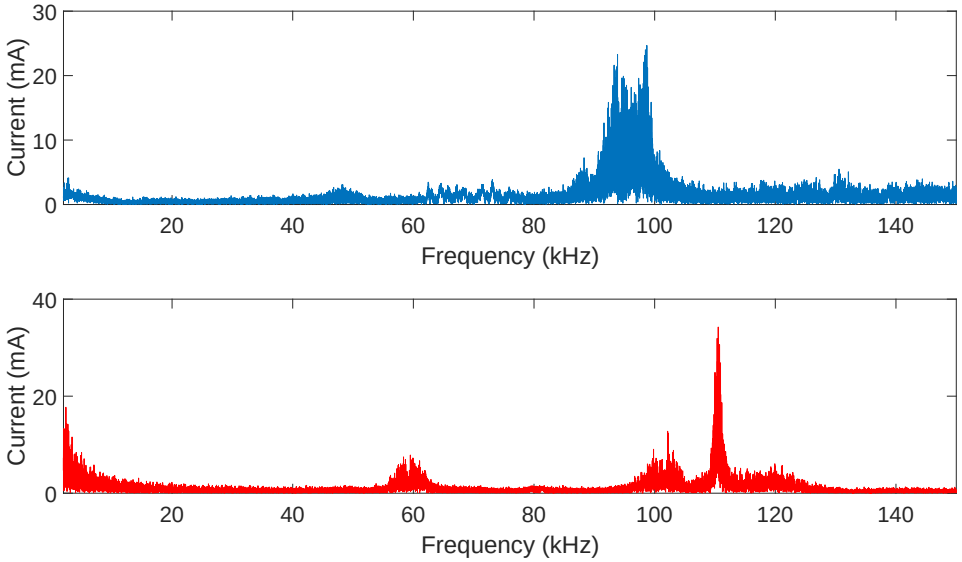

Figure 6.12: Primary current spectrum (top) for the simulated LED lamp under ideal voltage conditions. The same quantity has been shown bottom for voltage containing test signal 2.

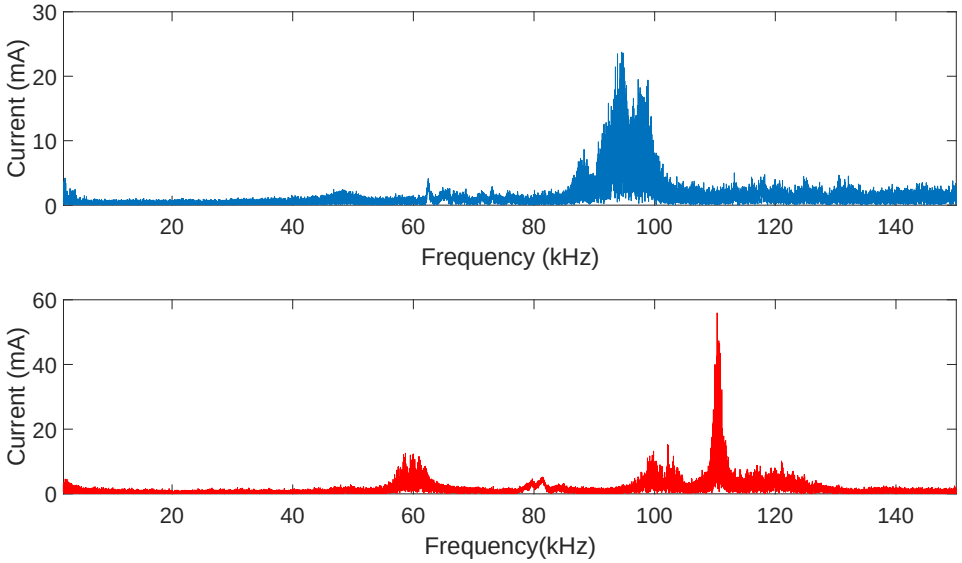

Figure 6.13: Secondary current spectrum (top) for the simulated LED lamp under ideal voltage conditions. The same quantity has been shown bottom for voltage containing test signal 2.

Figures 6.12 and 6.13 show that with a pure sine wave voltage, the converter operates at its minimum switching frequency of 90 kHz. However, with the introduction of test signal 2 into the source voltage, the switching frequency increases to its maximum value of 110 kHz. Further, the amount of current that is drawn in the frequency region of test signal 2 (40 kHz-80 kHz) by the converter is extremely small. This is not really surprising, since the formula for the inductive reactance is:

$$X_L = 2\pi f L \tag{6.15}$$

Hence, the Thevenin equivalent impedance seen by the supraharmonics is so large that it would almost appear to be an open circuit. More importantly, the bigger difference is that with a pure sine wave voltage, the flyback converter draws current at frequencies between 90 and 100 kHz. With test signal 2 a single sharper line is seen at 110 kHz, indicating that the converter spends a lot of time operating at its maximum possible frequency.

Based upon the PWM flowchart shown in Figure 6.8, the longer 'ON' period of the MOSFET is indicative that actual primary side current does not reach its desired set point as outputted by the PI controller (Recall that the controller tries to control primary side peak current to achieve the control objective. The 'ON' signal remains as long as the current does not reach this peak value determined by the controller.). Evidence from the primary and secondary currents clearly shows that the MOSFET remains 'ON' so long as the distortion remains near the peak of the primary voltage. The only conclusion that can be drawn from these two facts is that during the time that distortion is present near the input voltage peak, the expected value (current set point from the PI controller) of the current is higher than normal. This becomes more evident when the rectified voltage waveforms are observed in Figure 6.14

It is seen in Figure 6.14 that test signal 2 causes the peak values of the rectified voltage to be much higher than they normally would be. The converter uses this rectified voltage to generate the PWM signal as seen in Figure 6.8. Hence a higher rectified voltage value would lead the controller to command a higher current from the source. However, the LED driver does not draw current that corresponds to this high voltage peak produced by the supraharmonics. As a result, the PI controller generates a high current set point, which in reality never materializes because the Thevenin impedance of the transformer is simply too high corresponding to that frequency.

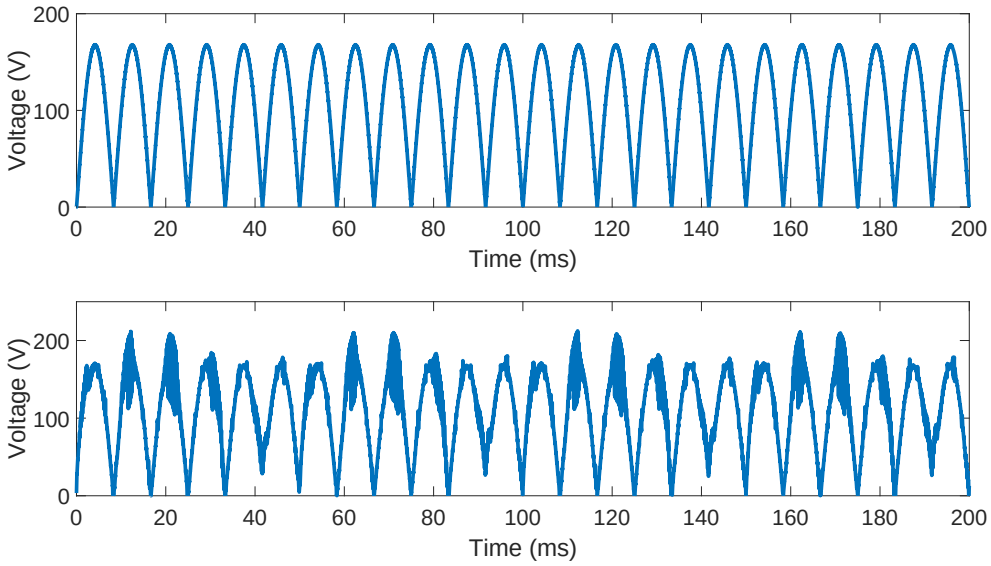

Figure 6.14: Rectified voltage (top) for the simulated LED lamp under ideal voltage conditions. The same quantity has been shown bottom for voltage containing test signal 2. Note the difference in vertical scale.

When the distortion appears anywhere else on the voltage waveform, the natural rise (or fall) of the primary side current takes care of the problem. When the distortion in input voltage appears at the peak, the converter simply draws the maximum possible current on the primary side as long as the distortion remains superimposed onto the DC voltage. As soon as the supraharmonics disappear, the converter resumes normal operation.

One interesting aspect of this interference with the working of the converter is the effect that it has on the load. When normal operation resumes after the prolonged 'OFF' period of the MOSFET, the capacitor has discharged more than normal. Excessive energy stored in the transformer must be dissipated in the secondary side. At the same time, the average load current is less than its normal value. According to equation 6.7, the average load current is:

$$I_{avg} = \frac{1}{2} I_{omax} \frac{t_2}{T_s} = \frac{1}{2} I_{omax} t_2 f \tag{6.16}$$

Due to the excess energy stored in the transformer, the discharge time of the secondary side (t_2) increases. This is observed in Figure 6.15, where the higher value of t_2 can be seen near the 40 ms and 50 ms mark. When the value of the current does not increase fast enough in successive samples,

the converter can then compensate by reducing the value of T_s i.e., the switching period. This leads to an increase in switching frequency as was observed earlier. This implies that higher energy is delivered to the capacitor at a higher frequency. There is a strong likelihood that degradation of the capacitor may result due to dissipation of energy in the series resistance of the capacitor. The instantaneous power in the capacitor was measured in simulation and is shown in Figure 6.15. The graphs indicate the energy delivered by the capacitor to the load. The part of the plots below the zero point are indicative of energy being delivered to the capacitor from the source during each 'off' period of the MOSFET. The straight vertical lines below the zero point in the bottom plot are indicative of the higher energy being delivered to the capacitor due to the prolonged opening of the MOSFET switch due to high frequency distortion.

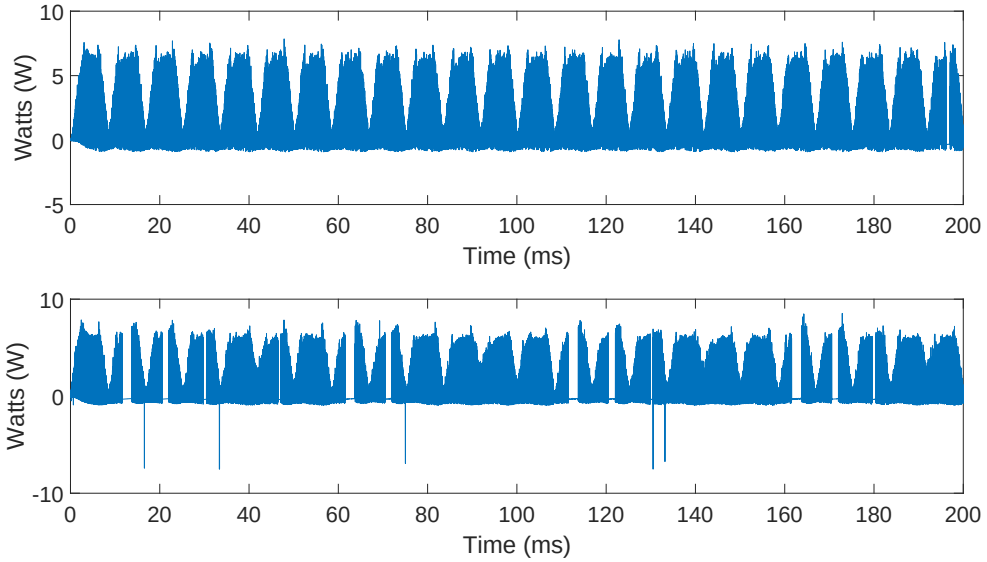

Figure 6.15: Instantaneous capacitor power (top) for the simulated LED lamp under ideal voltage conditions. The same quantity has been shown bottom for voltage containing test signal 2.

6.5.2 Summary of the interference mechanism

The best way to understand how the interference mechanism with flyback converters with PSR controllers works, is by the following summary sequence of events:

1. The appearance of supraharmonics near the peak of the rectified voltage causes the primary side current setpoint to be too high.

2. The current does not rise to the expected value and hence the MOSFET 'OFF' command is delayed until the condition is met.

3. The primary side circuit remains 'ON' for longer than necessary, storing a higher amount of energy. At the same time the secondary side current remains zero. The capacitor discharges more than normal to maintain constant load current. Average load current value dips.

4. When the MOSFET finally turns 'OFF', the controller senses lower than normal load current and an increased the discharge time of the secondary (to dissipate the higher stored energy). Part of the stored energy goes to recharge the capacitor and part of it goes to the load. The average current value starts to increase.

5. Since the capacitor discharges more than normal, this causes a higher amount of energy being delivered to the capacitor. The lower value of the average current in the load causes the converter to increase switching frequency until average load current comes back up to the desired value.

6.5.2.1 Interference in real life

The simulation results showed that the change in rectified DC voltage causes interference with the converter. Although, each manufacturer has its own way of applying the control logic and/or schemes, almost all these schemes utilize rectified line voltage at least in part to set the bias of the control circuit [55,56]. This value is also used in all comparator circuits thereafter. Hence, the unrealistically high value of primary side current generated by the controller does actually happen in physical LED circuits also (this is also evidenced by experimental data). This is partly also the cause of the point-on-wave characteristics of light output. For a distortion signal such as test signal 1, the sustained nature of noise will simply cause the value of the output current (and hence light) to drop since the voltage fluctuations move faster than the physical circuit can react.

6.5.3 Possible solutions

The interference that occurs with LED lamps from supraharmonics has been detailed here. The next question is: 'how do we solve this problem?'. Two solutions can be thought of for this:

- Hardware changes.

- Changes in control methodology.

An ideal hardware change would be the utilization of a filter at the front end of the circuit to allow only the lower frequencies to pass through. Generally, any method that increases part count will be deemed unsuitable (recall that PSR was adopted for its lower footprint, part count and bill of material). The most elegant solution will likely involve some sort of change in switching methodology. One of the possible solutions is the utilization of a 'Phase locked loop'. This seems, at least on paper, to be an ideal solution, given its utilization of a low pass filter (this can be implemented digitally) that would likely eliminate interference from supraharmonics. The underlying motivation in all such changes will be to eliminate the effect of higher frequencies on control. The analysis and design of such a system is out of the scope of this thesis.

Chapter 7

Conclusions and Discussion

7.1 Main findings and discussion

Based upon the work done in this project and presented in the various parts of this report, the following findings are obtained:

1. LED lamps produce light by driving a constant current through a light emitting diode. The light output of an LED is proportional to the forward current flowing through it. In an ideal case, an LED lamp produces constant light output, i.e. no components in light spectrum other than a DC component. However, for 27 out of the 32 lamps tested, the light output contained a modulation component at 100 Hz. Out of these 27 lamps, 24 lamps contained frequency components at 100 Hz and at multiples of 100 Hz in the light output spectrum. With conventional incandescent lamps, the presence of frequency components at multiples of 100 Hz was not observed. These findings have also been reported in literature.

2. The modulation produced by majority of LED lamps has been found to be higher than the modulation produced by incandescent lamps. This modulation, also referred to as 'photometric flicker' remains the subject of considerable interest in the research community, due to its impacts on human health.

3. From the laboratory experiments, it became clear that LED lamps are impacted by high frequency voltage distortion. The most predominant effect that was observed with distorted voltage was the reduction in average light output with lamps.

4. High frequency voltage distortion also impacts photometric flicker and under certain conditions, causes slow variations in light output which can be perceived by human observers. This has also been confirmed by field observations, both in the US and Europe.

5. Flicker with LED lamps, and especially with high frequency distortion is a subject that has not received the attention it deserves from the lighting community or from the power quality community. The available mathematical tools to quantify flicker actually do not take into account the nuances of this technology, which is very different from incandescent lamps.

6. Even before distortion was added to the supply voltage, it was observed that the LED lamp input current was severely distorted. Input current THD and modulation of light output were found to have a roughly inverse relationship. Given certain mathematical bounds, LED lamps were found to fall into three categories: lamps with low input current THD and high light modulation, lamps with high input THD but low modulation in light output and lamps with both low THD and low modulation.

7. Most LED lamps used in domestic applications are dimmable and are used in conjunction with dimmers. It was observed that the dimmers are sensitive to the presence of distortion in supply voltage. The high frequencies cause the solid state switches to maloperate, and the lamp starts blinking and even turns off during an entire half cycle. Clearly, dimmer design needs to be reassessed and reevaluated to take into account the nature of supply voltage.

8. It was observed that light variations due to the presence of high frequency distortion in supply voltage, depend on the point-on-wave at which the distortion appears. For certain points-on-wave, the reduction in light output is less as compared to others. Point-on-wave also influences the input current drawn by the lamp. Relative motion between the distortion signal and the fundamental voltage causes the input current to increase in width and peak amplitude.

9. Light variations from LED lamps do not depend upon converter topology or the presence of a transformer to provide galvanic isolation. It was observed that LED drivers of similar topology can behave completely different.

10. In the case of flyback converters with primary side regulation, it was observed that presence of high frequency distortion in rectified DC voltage interfered with the controller and caused the light output to drop. The mechanism was explored in thorough detail and it was theorized

that the resulting energy imbalance may place undue stress on the output capacitor of the circuit and cause it to deteriorate faster than normal and ultimately fail.

7.2 Future work

The following areas for future investigation and research have been identified based upon the work done in this project:

1. The response of the LED lamp to other power quality events such as voltage sags needs to be carefully investigated. The influence of the point-on-wave of the sag also needs to be taken into account. This is based upon the observation that high frequency changes in AC input voltage of the LED lamp can produce variations in light output.

2. The control schemes employed by LED lamps need to be re-examined in the light of the findings of this work. Solutions to prevent interference from conducted disturbances need to be considered at both the hardware level and in control scheme. Ideally, the latter will be more desirable as it will not add to the bill of material of the LED lamp or its footprint.

3. A systematic study, utilizing a thermally isolated chamber, is required to study the impact of supraharmonics on circuit components. The aim of such a study would be to ultimately determine thermal degradation and/or failure of the LED driver circuit.

Appendices

Appendix A Relevant data of LED lamps tested

Sr. No.	Power (Watts)	Illumination (Lumens)
1	0.9	50
2	2	120
3	4.5	230
4	5.5	345
5	6	470
6	6	470
7	10	810
8	11	810
9	1.2	60
10	1.5	79
11	1.8	180
12	1	40
13	2	140
14	3.6	400
15	3	240
16	4	250
17	5	350
18	7	470
19	10	800
20	1 (blue)	3
21	1 (red)	3
22	2	136
23	6	470
24	11	810
25	3.6	230
26	6	470
27	11	1055
28	3	136
29	3	136
30	7	300
31	8	470
32	12	806

Appendix B Nameplate data of LED drivers tested

No	**Power Capacity**	**Topology**
1	14W	Flyback
2	3.5W	Flyback
3	8W	Flyback
4	5W	Buck-boost
5	9W	Buck

Appendix C Load used with LED driver boards

Board no.	LED forward voltage	LED rated current	Configuration
1	2.8 V	440 mA	6 LEDs in series. 2 strips in parallel.
2	6 V	440 mA	2 LEDs in series.
3	2.8 V	440 mA	6 LEDs in series.
4	16 V	100 mA	3 LEDs in series
5	16 V	105 mA	5 LEDs in series

Bibliography

[1] "Testing and measurement techniques test for immunity to conducted, differential mode disturbances and signaling in the frequency range 2 kHz to 150 kHz at a.c. power ports," *EN 61000-4-19*, 2014.

[2] M. Klatt, J. Meyer, P. Schegner, A. Koch, J. Myrzik, T. Darda, and G. Eberl, "Emission levels above 2 kHz; laboratory results and survey measurements in public low voltage grids," in *Electricity Distribution (CIRED 2013), 22nd International Conference and Exhibition on*, June 2013, pp. 1–4.

[3] E. O. A. Larsson, M. H. J. Bollen, M. G. Wahlberg, C. M. Lundmark, and S. K. Ronnberg, "Measurements of high-frequency (2-150 kHz) distortion in low-voltage networks," *IEEE Transactions on Power Delivery*, vol. 25, no. 3, pp. 1749–1757, July 2010.

[4] G. Chicco, A. Russo, and F. Spertino, "Supraharmonics: Concepts and experimental results on photovoltaic systems," in *2015 International School on Nonsinusoidal Currents and Compensation (ISNCC)*, June 2015, pp. 1–6.

[5] E. O. A. Larsson, "On high-frequency distortion in low-voltage power systems," Doctoral Thesis, Luleå University of Technology, 2011.

[6] S. K. Ronnberg, "Emission and interaction from domestic installations in the low voltage electricity network, up to 150 kHz," Doctoral Thesis, Luleå University of Technology, 2013.

[7] C. M. Lundmark, "The zone concept: design of low-voltage installations considering the spread of high frequency harmonics," Doctoral Thesis, Luleå University of Technology, 2010.

[8] A. D. Familua, A. O. Qatarey, P. A. J. V. Rensburg, and L. Cheng, "Error pattern/behavior of noise in in-house CENELEC A-Band PLC channel," in *Power Line Communications and Its Applications (ISPLC), 2012 16th IEEE International Symposium on*, March 2012, pp. 114–119.

[9] A. Emleh, A. S. de Beer, H. C. Ferreira, and A. J. H. Vinck, "The impact of the CFL lamps on the power-line communications channel," in *Power Line Communications and Its Applications (ISPLC), 2013 17th IEEE International Symposium on*, March 2013, pp. 225–229.

[10] S. K. Ronnberg, M. H. J. Bollen, and M. Wahlberg, "Interaction between narrowband power-line communication and end-user equipment," *IEEE Transactions on Power Delivery*, vol. 26, no. 3, pp. 2034–2039, July 2011.

[11] S. Ronnberg, M. Wahlberg, M. Bollen, A. Larsson, and M. Lundmark, "Measurements of interaction between equipment in the frequency range 9 to 95 kHz," in *Electricity Distribution - Part 1, 2009. CIRED 2009. 20th International Conference and Exhibition on*, June 2009, pp. 1–4.

[12] S. Ronnberg and M. Bollen, "Measurements of primary and secondary emission in the supra-harmonic frequency range 2 to 150 kHz," in *Electricity Distribution (CIRED 2015), 23rd International Conference and Exhibition on*, June 2015.

[13] "Study report on electromagnetic interference between electrical equipment / systems in the frequency range below 150 kHz," *CENELEC*, p. SC205A/ Sec0260/, April 2010.

[14] R. Lenk and C. Lenk, *Practical Lighting Design with LEDs*. Wiley-IEEE Press, 2011. [Online]. Available: http://ieeexplore.ieee.org/xpl/articleDetails.jsp?arnumber=5751739

[15] L. Yu and J. Yang, "The topologies of white LED lamps' power drivers," in *2009 3rd International Conference on Power Electronics Systems and Applications (PESA)*, May 2009, pp. 1–6.

[16] H. van der Broeck, G. Sauerlander, and M. Wendt, "Power driver topologies and control schemes for LEDs," in *APEC 07 - Twenty-Second Annual IEEE Applied Power Electronics Conference and Exposition*, Feb 2007, pp. 1319–1325.

[17] "Casting the light: Illuminating the opportunities in 2023's led luminaire market," https://portal.luxresearchinc.com/research/report_excerpt/15808, accessed: 2013-12-25.

[18] N. N. Tran, "Designing and implementing a micro-controller based primary-side sensing flyback converter for LEDs driver," p. 94, 2014. [Online]. Available: http://search.proquest.com/docview/1630056440?accountid=27917

[19] A. M. Blanco, R. Stiegler, and J. Meyer, "Power quality disturbances caused by modern lighting equipment (CFL and LED)," in *PowerTech (POWERTECH), 2013 IEEE Grenoble*, June 2013, pp. 1–6.

[20] S. K. Ronnberg, M. Wahlberg, and M. H. J. Bollen, "Harmonic emission before and after changing to LED lamps-field measurements for an urban area," in *Harmonics and Quality of Power (ICHQP), 2012 IEEE 15th International Conference on*, June 2012, pp. 552–557.

[21] M. Bollen, M. Olofsson, A. Larsson, S. Ronnberg, and M. Lundmark, "Standards for supra-harmonics (2 to 150 kHz)," *IEEE Electromagnetic Compatibility Magazine*, vol. 3, no. 1, pp. 114–119, 2014.

[22] G. Singh and E. R. Collins, "Influence of auxiliary winding resonance on the harmonic behavior of single phase capacitor motors," in *PES General Meeting — Conference Exposition, 2014 IEEE*, July 2014, pp. 1–5.

[23] E. R. Collins, J. R. Shirley, and J. C. Fox, "An experimental investigation of third harmonic current distortion in single-phase induction motors," in *Harmonics and Quality of Power, 2008. ICHQP 2008. 13th International Conference on*, Sept 2008, pp. 1–7.

[24] M. Pikkarainen, S. Vehmasvaara, B. A. Siddiqui, P. Pakonen, and P. Verho, "Interference of touch dimmer lamps due to plc and other high frequency signals," in *Electric Power Quality and Supply Reliability Conference (PQ), 2012*, June 2012, pp. 1–6.

[25] E. O. A. Larsson and M. H. J. Bollen, "Emission and immunity of equipment in the frequency range 2 to 150 khz," in *2009 IEEE Bucharest PowerTech*, June 2009, pp. 1–5.

[26] "Signalling on low-voltage electrical installations in the frequency range 3 kHz to 148.5 kHz. general requirements, frequency bands and electromagnetic disturbances," *EN 50065-1*, 2011.

[27] "Electromagnetic compatibility (EMC) - part 3: Limits - section 8: Signalling on low-voltage electrical installations - emission levels, frequency bands and electromagnetic disturbance levels," *EN 61000-3-8*, 1997.

[28] "Voltage characteristics of electricity supplied by public distribution systems," *EN 50160*, 1999.

[29] "Limits and methods of measurement of radio disturbance characteristics of electrical lighting and similar equipment," *CISPR 15:2013*, 2013.

[30] "Electromagnetic compatibility (EMC) part 4-30, testing and measurement techniques - power quality measurement methods," *EN 61000-4-30*, 2015.

[31] "Electromagnetic compatibility (EMC) - part 4-7: Testing and measurement techniques - general guide on harmonics and interharmonics measurements and instrumentation, for power supply systems and equipment connected thereto," *IEC 61000-4-7:2002*, 2002.

[32] M. Klatt, J. Meyer, P. Schegner, R. Wolf, and B. Wittenberg, "Filter for the measurement of supraharmonics in public low voltage networks," in *2015 IEEE International Symposium on Electromagnetic Compatibility (EMC)*, Aug 2015, pp. 108–113.

[33] S. R. A. Gil-de Castro, A. Larsson and M. Bollen, "LED lamps under different EMC environments," in *International Conference and Exhibition on Electricity Distribution (CIRED), 2015, Lyon, France*, 2015, pp. 1–6.

[34] E. O. A. Larsson, "High frequency distortion in power grids due to electronic equipment," Licentiate Thesis, Luleå University of Technology, 2006.

[35] "Model s4 hagner universal photometer/radiometer model s4," http://www.hagner.se/combination-instruments-1/model-s4/, accessed: 2016.

[36] M. Poplawski and N. Miller, "Exploring flicker in solid-state lighting: What you might find, and how to deal with it," in *Illuminating Engineering Society Annual Conference*, Nov. 2011.

[37] ——, "Flicker in solid-state lighting: Measurement techniques, and proposed reporting and application criteria," in *CIE-France*, April 2013.

[38] R. S. Fisher, G. Harding, G. Erba, G. L. Barkley, and A. Wilkins, "Photic and pattern-induced seizures: Expert consensus of the epilepsy foundation of america working group," *Epilepsia*, vol. 46, no. 9, pp. 1426–1441, 2005.

[39] A. J. Wilkins, I. Nimmo-Smith, A. I. Slater, and L.Bedocs, "Fluoroscent lighting, headaches and eyestrain," *Lighting Research and Technology*, vol. 21, no. 1, p. 11, 1989.

[40] "Recommended practice for lighting industrial facilities." *IES RP-7, Illuminating Society, New York*, 2001.

[41] J. A. Veitch and S. L. McColl, "Modulation of fluorescent light: Flicker rate and light source effects on visual performance and visual comfort," *Lighting Research and Technology*, vol. 27, no. 4, p. 243, 1995.

[42] D. M. Fenton and R. Penney, "The effects of fluorescent and incandescent lighting on the repetitive behaviors of autistic and intellectually handicapped children," *Journal of Intellectual and Development Disability*, vol. 11, no. 3, pp. 137–141, 1985.

[43] A. Wilkins, J. Veitch, and B. Lehman, "LED lighting flicker and potential health concerns: IEEE standard PAR1789 update," in *Energy Conversion Congress and Exposition (ECCE), 2010 IEEE*, Sept 2010, pp. 171–178.

[44] M. H. Rashid, *Power Electronics - Circuits, Devices and Applications*, 3rd ed. Prentice Hall.

[45] S. Z. Djokic, J. V. Milanovic, and S. M. Rowland, "Advanced voltage sag characterisation ii: point on wave," *IET Generation, Transmission Distribution*, vol. 1, no. 1, pp. 146–154, January 2007.

[46] E. R. Collins and F. Zapardiel, "An experimental assessment of AC contactor behavior during voltage sags," in *Industrial Electronics, 1997. ISIE '97., Proceedings of the IEEE International Symposium on*, vol. 2, Jul 1997, pp. 439–444 vol.2.

[47] M. H. J. Bollen, "Voltage recovery after unbalanced and balanced voltage dips in three-phase systems," *IEEE Transactions on Power Delivery*, vol. 18, no. 4, pp. 1376–1381, Oct 2003.

[48] Y. Liu and V. Vittal, "Distribution side mitigation strategy for fault induced delayed voltage recovery," in *2014 IEEE PES General Meeting — Conference Exposition*, July 2014, pp. 1–5.

[49] M. H. Bollen, *Understanding Power Quality Problems:Voltage Sags and Interruptions*. Wiley-IEEE Press, 2000. [Online]. Available: http://ieeexplore.ieee.org/xpl/articleDetails.jsp?arnumber=5271123

[50] "Cross correlation," http://paulbourke.net/miscellaneous/correlate/, accessed: August 1996.

[51] A. M. S. Uddin, H. Shareef and M. A. Hannan, "Harmonics and thermal characteristics of low wattage led lamps," in *PRZEGLD ELEKTROTECHNICZNY (Electrical Review)*, vol. 88, no. 11a, 2012, pp. 266–271.

[52] S. Ang and A. Oliva, *Power-Switching Converters*, 3rd ed. Taylor and Francis, 2011.

[53] J. Picard, "Under the hood of flyback SMPS designs," http://www.ti.com/lit/ml/slup254/, 2010.

[54] S. Chen, E. Lan, and L. Lin, "Implementation of the primary-side regulation in flyback converters," http://www.eetimes.com/document.asp?doc_id=1278807, accessed: 2016.

[55] "UCC28722 constant-voltage, constant-current controller with primary-side regulation, BJT drive," http://www.ti.com/lit/ds/symlink/ucc28722.pdf, 2015.

[56] "Design guideline for primary side regulated (PSR) flyback converter using FAN103 and FSEZ13X7," https://www.fairchildsemi.com/application-notes/AN/AN-8033.pdf, 2016.

[57] L. Dinwoodie, "Design review: Isolated 50 watt flyback converter using the UCC3809 primary side controller and the UC3965 precision reference and error amplifier," http://www.ti.com/lit/an/slua086/slua086.pdf, 1999.